



January 2012

Experimental Investigation Of Fatigue Behavior Of Carbon Fiber Composites Using Fully-Reversed Four-Point Bending Test

Ali Amiri

Follow this and additional works at: <https://commons.und.edu/theses>

Recommended Citation

Amiri, Ali, "Experimental Investigation Of Fatigue Behavior Of Carbon Fiber Composites Using Fully-Reversed Four-Point Bending Test" (2012). *Theses and Dissertations*. 1331.
<https://commons.und.edu/theses/1331>

This Thesis is brought to you for free and open access by the Theses, Dissertations, and Senior Projects at UND Scholarly Commons. It has been accepted for inclusion in Theses and Dissertations by an authorized administrator of UND Scholarly Commons. For more information, please contact zeinebyousif@library.und.edu.

**EXPERIMENTAL INVESTIGATION OF FATIGUE BEHAVIOR OF CARBON
FIBER COMPOSITES USING FULLY-REVERSED FOUR-POINT BENDING
TEST**

by

Ali Amiri
Bachelor of Science, Shiraz University, Shiraz, Iran 2003

A Thesis

Submitted to the Graduate Faculty

of the

University of North Dakota

In partial fulfillment of the requirements

for the degree of

Master of Science

Grand Forks, North Dakota
December
2012

Copyright 2012 Ali Amiri

This thesis, submitted by Ali Amiri, in partial fulfillment of the requirements for the Degree of Master of Science from the University of North Dakota, has been read by the Faculty Advisory Committee under whom the work has been done and is hereby approved.

Dr. Matthew Cavalli

Dr. Bishu Bandyopadhyay

Dr. Marcellin Zahui

This thesis meets the standards for appearance, conforms to the style and format requirements of the Graduate School of the University of North Dakota, and is hereby approved.

Dr. Wayne Swisher
Dean of the Graduate School

Date

Title Experimental Investigation of Fatigue Behavior of Carbon Fiber
 Composites Using Fully-Reversed Four-Point Bending Test

Department Mechanical Engineering

Degree Master of Science

In presenting this thesis in partial fulfillment of the requirements for a graduate degree from the University of North Dakota, I agree that the library of this University shall make it freely available for inspection. I further agree that permission for extensive copying for scholarly purposes may be granted by the professor who supervised my thesis work or, in his absence, by the chairperson of the department or the dean of the Graduate School. It is understood that any copying or publication or other use of this thesis or part thereof for financial gain shall not be allowed without my written permission. It is also understood that due recognition shall be given to me and to the University of North Dakota in any scholarly use which may be made of any material in my thesis.

Ali Amiri
11/11/2012

TABLE OF CONTENTS

LIST OF FIGURES	viii
LIST OF TABLES	xii
ACKNOWLEDGMENTS	xiii
ABSTRACT	xiv
CHAPTER	
I. INTRODUCTION	1
Applications	2
Purpose of Fatigue Testing	4
Fatigue in Composites.....	5
Fatigue Damage in Composites	6
Different Fatigue Test Setups	9
Three-Point Bending Setup with Rotating Supports.....	10
Four-Point Bending Setup.....	12
Clamped Four-Point Bending Test	13
Clamped Three-Point Bending Setup	13
Effect of Friction on Hysteresis Loops from Three-Point Bending Tests	14

	Fully-reversed Bending Test of Carbon Fiber Reinforced Epoxy Composite Strands	15
	Strength Measurement of Optical Fibers by Bending.....	17
	Conclusion	20
II.	MATERIALS AND METHODS.....	22
	Material	22
	Sample preparation	22
	Hand lay-up method.....	23
	VARTM Method.....	26
	Determination of Fiber Volume Fraction (V_f)	29
	Testing Methods.....	31
	Static test.....	31
	Fatigue Test.....	33
	Fatigue Test Apparatus	35
III.	RESULTS AND DISCUSSION	38
	Static Test.....	38
	Static Test with Regular Four-Point Bending Fixture – $(0^\circ/90^\circ)_{15}$ samples.....	38
	Static Test with Clamped Four-Point Bending Fixture – $(0^\circ/90^\circ)_{15}$ samples.....	39
	Static test Four-Point Bending – $(\pm 45^\circ)_{15}$ Fibers.....	42
	Fatigue Test.....	48

Four-Point Fatigue Test – (0°/90°) ₁₅ samples.....	48
Discussion of Fatigue Results for (0°/90°) ₁₅ Samples	51
Predicting Fatigue Life of Composite Samples	53
Post-Fatigue Tests of (0/90) ₁₅ Samples.....	59
Four-Point Fatigue Test – (±45°) ₁₅ samples	60
Discussion of Fatigue Results for (±45°) ₁₅ Samples.....	61
Post-Fatigue Tests of (±45°) ₁₅ Samples	63
IV. SUMMARY AND CONCLUSION	67
APPENDICES	70
REFERENCES	76

LIST OF FIGURES

Figure	Page
1. Schematic S-N curve, average stress (σ_a) versus cycles to failure (N_f) [30-32].	6
2. Degeradation of composite strength by wear-out.	7
3. Transverse force and moment diagrams for three point and four point bending setups [48].	10
4. Bending fatigue test mechanism used by Couillard <i>et al.</i> in [30].	16
5. Schematic of fiber bending mechanism used by Matthewson <i>et al.</i> [52].	17
6. Schematic drawing of fatigue bending machine used in [27, 55].	19
7. Fabric structure used for this study.	22
8. Hand lay-up setup for the first plate.	23
9. Surface of first plate after curing under vacuum at room temperature for 24 hours.	24
10. Hand lay-up set up for second plate. A piece of plywood was placed over the stack of material and under the vacuum bag.	24
11. Dry spots on surface of second plate made using the hand lay-up process.	25
12. Hand lay-up setup for third plate.	25
13. Dry spots on surface of third plate made using hand lay-up process.	26
14. (a) VARTM infusion process. (b) Components of VARTM set up.	27

15.	Composite plates (a) during and (b) after resin transfer process.	28
16.	Sample geometry for $(0^\circ/90^\circ)_{15}$ fibers in accordance with ASTM D6272-02.	28
17.	Cross section of composite material as square packed array.	29
18.	Static four-point bending fixture.....	32
19.	Schematic of static and fatigue test setup.	32
20.	Fatigue fixture designed and manufactured to perform fully-reversed four-point bending test. All dimensions are in mm.	34
21.	Different components of four-point fatigue bending fixture.	35
22.	Stress- strain curves for four-point bending tests for $(0^\circ/90^\circ)_{15}$ samples.	39
23.	Static test setup with clamped four-point bending fixture.	40
24.	Comparison of stress-strain values measured with two types of four-point bending setup for $(0^\circ/90^\circ)_{15}$ samples.	41
25.	Different stress-displacement curves for the simulation of clamping and regular three-point bending fixtures in [47].	42
26.	Geometrical limitation of four-point bending test fixture for $(\pm 45^\circ)_{15}$ samples.	43
27.	Stress-strain curves for four-point bending tests for $(\pm 45^\circ)_{15}$ samples.	44
28.	Average stress-strain curves for $(0/90)_{15}$ and $(\pm 45)_{15}$ samples.	46
29.	Stress-strain curves for $(0/90)$ and (± 45) samples from [80].	47
30.	Stress – displacement curves for static flexural tests from [57].	48
31.	Fatigue test apparatus and four-point bending test fixture.....	49
32.	a) Sample of sine wave applied (b) corresponding deformation at same cycle.	49

33.	S-N data for CFRP samples with $(0^\circ/90^\circ)_{15}$ layup.	51
34.	S-N diagram for $(0/90)$ laminates with 5.0 GPa CFRP from [55].	52
35.	S-N diagram for $(0/90)_3$ at room temperature in [56].	53
36.	Loss in flexural modulus vs. lives of $(0^\circ/90^\circ)_{15}$ samples (linear Scale).	55
37.	Loss in flexural modulus vs. lives of $(0^\circ/90^\circ)_{15}$ samples (log scale).	56
38.	Loss of applied bending moment through 10^6 cycles versus number of cycles for $(0/90)_{15}$ samples (linear scale) in [57].	57
39.	Loss of applied bending moment through 10^6 cycles versus number of cycles for $(0/90)_{15}$ samples (logarithmic scale) in [57].	58
40.	Post-fatigue results of static four-point bending test for $(0/90)_{15}$ Samples.	59
41.	Average of results before fatigue tests and after fatigue tests for samples 1, 3 and 4 of $(0/90)_{15}$	60
42.	Variation in flexural modulus vs. lives of $(\pm 45^\circ)_{15}$ samples (linear scale).	62
43.	Variation in flexural modulus vs. lives of $(\pm 45^\circ)_{15}$ samples (Logarithmic scale).	62
44.	Post-fatigue results of static four-point bending test for Sample no. 8.	64
45.	Post-fatigue results of static four-point bending test for Sample no. 9.	64
46.	Post-fatigue results of static four-point bending test for Sample no. 10.	65
47.	Direct comparison of the average values of stress-strain for samples tested before fatigue, and samples after 1.7×10^6 cycles of fatigue loading.	65
48.	Fatigue fixture, drawing of part 5.	71
49.	Fatigue fixture, drawing of parts 2 and 3.	72
50.	Fatigue fixture, drawing of part 4.	73

51.	Fatigue fixture, drawing of part 1.	74
52.	Fatigue fixture, assembly drawing.....	75

LIST OF TABLES

Table	Page
1. Selected properties of bulk and fibrous materials [1, 2].	2
2. Composite plate lay-ups, materials used and curing details.	28
3. Result of burn-off test.	31
4. Specifications of four-point bending test.	35
5. Fatigue test data log sheet for $(0^\circ/90^\circ)_{15}$ and $(\pm 45^\circ)_{15}$ samples.	37
6. Measured mechanical properties of $(0^\circ/90^\circ)_{15}$ samples.	39
7. Force, displacement and stress values for clamped and regular four-point bending fixture.	40
8. Measured mechanical properties of $(\pm 45^\circ)_{15}$ samples.	44
9. Fatigue lives for CFRP samples with $(0^\circ/90^\circ)_{15}$ layup.	50
10. Values of Constant A in Equation 15.	56
11. Fatigue lives for CFRP samples with $(\pm 45^\circ)_{15}$ layup.	60

ACKNOWLEDGMENTS

I would like to express my sincere gratitude to all individuals from whom I received support and encouragement over past three years. Dr. Matthew Cavalli has been a knowledgeable graduate advisor, a supportive teacher and a great mentor to me. His steadfast encouragement, motivation and guidance made this a thoughtful and rewarding journey. I would like to thank Dr. Marcellin Zahui and Dr. Bishu Bandyopadhyay for accepting to be on my thesis committee. With their valuable advice and comments I moved from an idea to a completed study. Thanks to Dr. George Bible and Dr. Brian Tande for helping me gain better insight into this study. Special thanks to ME department research specialists, Gary Dubuque and Jay Evenstad without whom it would not have been possible to complete this research. I would also thank my friend, ME department graduate student, Tanveer Chawla, for sharing his valuable information and experience on composite materials.

Last but not least, I want to thank my amazing parents, Nazanin Sadeghi and Gholamreza Amiri whom always valued education and with their selfless love taught me the way of life, hard work, perseverance, humility, honesty and integrity. I am grateful that omnipresent God gave me the strength and provided me with the opportunity to complete this study.

To my parents,
for their endless love, support and encouragement.

ABSTRACT

Carbon fiber reinforced polymers (CFRP) have become an increasingly notable material for use in structural engineering applications. Some of their advantages include high strength-to-weight ratio, high stiffness-to-weight ratio, and good moldability. Prediction of the fatigue life of composite laminates has been the subject of various studies due to the cyclic loading experienced in many applications. Both theoretical studies and experimental tests have been performed to estimate the endurance limit and fatigue life of composite plates. One of the main methods to predict fatigue life is the four-point bending test. In most previous works, the tests have been done in one direction (load ratio, $R, > 0$). In the current work, we have designed and manufactured a special fixture to perform a fully reversed bending test ($R = -1$). Static four-point bending tests were carried out on three $(0^\circ/90^\circ)_{15}$ and $(\pm 45^\circ)_{15}$ samples to measure the mechanical properties of CFRP. Testing was displacement-controlled at the rate of 10 mm/min until failure. In $(0^\circ/90^\circ)_{15}$ samples, all failed by cracking/buckling on the compressive side of the sample. While in $(\pm 45^\circ)_{15}$ all three tests, no visual fracture or failure of the samples was observed. 3.4 times higher stresses were reached during four-point static bending test of $(0^\circ/90^\circ)_{15}$ samples compared to $(\pm 45^\circ)_{15}$. Same trend was seen in literature for similar tests. Four-point bending fatigue tests were carried out on $(0^\circ/90^\circ)_{15}$ sample with stress ratio, $R = -1$ and frequency of 5 Hz. Applied maximum stresses were approximately 45%, 56%, 67%, 72% and 76% of the measured yield stress for $(0^\circ/90^\circ)_{15}$ samples. There was visible cracking through the thickness of the samples. The expected downward trend in

fatigue life with increasing maximum applied stress was observed in S-N curves of samples. There appears to be a threshold for ‘infinite’ life, defined as 1.7 million cycles in the current work, at a maximum stress of about 200 MPa. The decay in flexural modulus of the beam as it goes under cyclic loading was calculated and it was seen that flexural modulus shows an exponential decay which can be expressed as: $E = E_0 e^{-AN}$. Four-point bending fatigue tests were carried out on three $(\pm 45^\circ)_{15}$ samples with stress ratio, $R = -1$ and frequency of 5 Hz. Maximum applied stress was 85% of the measured yield stress of $(\pm 45^\circ)_{15}$ samples. None of the samples failed, nor any sign of crack was seen. Tests were stopped once the number of cycles passed 1.7×10^6 . In general, current study provided additional insight into the fatigue and static behavior of polymer composites and effect of fiber orientation in their mechanical behavior.

CHAPTER I

INTRODUCTION

Composite materials are one of the four basic categories of structural materials and typically are made by different combinations of the other three: metals, polymers and ceramics. The properties of composite materials are intended to be superior compared to the properties of the constituent materials performing individually [1, 2]. In structural applications, a composite material usually consists of a reinforcement which is stiffer and stronger than the less stiff surrounding material called the matrix. The properties of the composite depend on many factors including the properties, geometry and distribution of its phases [1-3].

Some of the properties that can be optimized by utilizing composites include strength, stiffness, resistance to corrosion and wear, thermal conductivity, density and fatigue life. The objective of composite material usage is to improve one or more of the aforementioned properties to perform a specific task [1]. The anisotropic and heterogeneous character of composite materials provide many degrees of freedom for optimizing the material [2].

Many materials are much stronger in fiber, rather than bulk, form [1, 3]. A. A. Griffith [4] measured properties of glass fibers and glass rods and compared the results of tensile tests with different diameters. He found that as the fibers got thinner they got stronger. He related these results to a reduced probability of production of surface cracks. Based on another study [5] it is believed that carbon nanotubes are the stiffest and

strongest reinforcement materials known [1]. Advanced composite materials are typically made from carbon, silicon carbide, boron and aramid polymer reinforcement. As seen in Table 1, higher modulus, higher strength and lower density are the main advantages of advanced fibers [1, 2]. Carbon nanotubes are the strongest of the bulk and fibrous materials mentioned.

Table 1. Selected properties of bulk and fibrous materials [1, 2].

Material	Tensile Strength (MPa)	Tensile Modulus (GPa)	Density (g/cm ³)
Bulk Materials			
6061 T6 Aluminum	310	69	2.71
4340 Steel	1030	200	7.83
Polyvinylchloride	40	3.1	1.44
Silicon Carbide	.4	400	3.4
Aluminum Oxide	.5	380	3.8
Fibers			
E-Glass	3448	72	2.54
S-Glass	4278	228	2.49
AS4 Carbon Fibers	4278	228	1.79
T300 Carbon Fibers	3750	231	1.76
Kevlar 29 aramid	3620	83	1.44
Polyethylene	3340	124	.97
Boron	3400	400	2.52
Carbon Nanotubes	30000	1000	1.9

Applications

Due to mechanical and structural advantages, carbon fiber reinforced polymers (CFRP) have become increasingly notable materials used in many engineering applications from aerospace to infrastructure to alternative energy. Metals, such as aluminum and steel, used to be the main materials for manufacturing racing cars. In the early 1980's, Formula 1 initiated a revolution that today had become its hallmark:

manufacturing car chassis out of carbon fiber (CF) composites. These days, almost all parts of racing car chassis, suspension systems, wings and engine covers are built out of carbon fiber composites. The main advantages of CF composites are [6, 7] :

- great weight and part saving,
- high strength,
- high stiffness,
- parts consolidation,
- design flexibility,
- corrosion resistance, and
- complex shape manufacturing.

Recent developments in carbon fiber research have reduced the costs and enhanced the understanding of CF composites. As a result, the feasibility of using CF composites has been increased in many industries including the automotive industry [8].

Due to the aforementioned advantages, carbon fiber composites have found a lot of use in high-end sports equipment such as hockey sticks and race bicycles. New, advanced materials have enormous impact on society and sports. Advanced products and materials generate new sports and affect existing sports. These customized products create external tools for athletes to use to enhance their ability to perform [9]. As an example, carbon fiber composite comprise the legs of Oscar Pistorius, the “Blade Runner”, who had double below-knee amputation and competed in the 400 meter dash in the London Summer 2012 Olympics. The carbon fiber composite spring blades weigh only 500 g are capable of holding up to 150 kg of weight [10]. They are stiff enough to support the whole weight of an athlete, flexible enough to enable him to run, and store

and release compressive energy to make it possible for the athlete to achieve his best performance.

Composite materials have been used in commercial airplanes for decades. The application of composite materials has been developed from small scale in past decades to large structures today. Typical examples of widespread applications of composites in commercial aircraft are the Boeing 777 and 787, and Airbus A340 and A350 [7]. These aircraft have replaced main parts in wings and fuselage with CFRP and the weight fraction of carbon composites in some air craft is up to 50% [11-13].

Purpose of Fatigue Testing

In all of the aforementioned applications, improved performance, increased lifetime and reduced manufacturing costs are of high importance. Therefore, studying and improving of static, fatigue and fracture behavior of composite materials is critical to the successful execution of an effective structural design. Extensive studies have been carried out to study the fatigue behavior of composite materials under cyclic loading [14-18] and predict their life and failure [19-24]. The main purposes of fatigue testing can be summarized as [25]:

- To estimate load (stress), strain, deflection amplitude and cycle life-to-failure,
- To compare fatigue properties of two or more materials or components,
- To obtain practical design data relevant to specific service applications,
- To study the mechanism of stiffness degradation and ultimate failure,
- To ensure that fatigue life is greater than required, and/or replacement life is identified, and/or

- To compare materials under standard loading conditions as a basis of material development or material selection.

Fatigue in Composites

With the increase of industrial and structural applications of composite materials such as aircraft, automobiles, power plants and sports where the material is exposed to multiaxial/biaxial loading conditions, extreme temperatures, vibrations, impacts, etc., understanding the behavior of the materials under such environments and loading conditions has become a matter of great importance [26]. Materials in engineering applications are subjected to long-term loading and often go through repeated loading and unloading conditions (fatigue). Most materials, when subjected to fatigue loading, are likely to fail after certain of cycles. An important aspect of structural design is to understand a material's behavior under fatigue loading. The machines and devices designed for service under such loads need to be similarly characterized [27-29]. Fatigue is defined as the process of progressive localized permanent structural change that occurs in a material subjected to variable stresses and strains. Fatigue might end in cracking (damage accumulation) or complete failure after a certain number of cycles. The number of cycles of stress or strain that the material undergoes before failure is referred to as the fatigue, or service life. The service life depends on the applied stress level, loading frequency, and other factors [25]. This behavior is typically collected in the form of an S-N curve, shown schematically in Figure 1 [30-32].

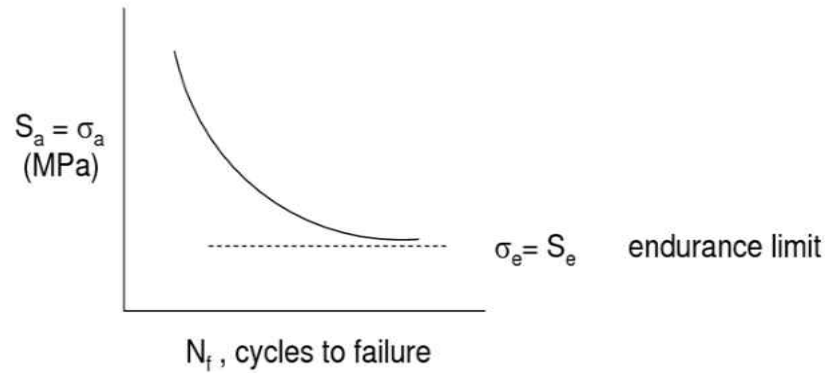


Figure 1. Schematic S-N curve, average stress (σ_a) versus cycles to failure (N_f) [30-32].

For some materials, as shown in Figure 1, a stress exists below which fatigue failure is not likely to occur (endurance limit). However, an endurance limit has not been observed in most composites. As a result of the inhomogeneous and anisotropic nature of composite materials, their fatigue behavior is more complicated than for more homogeneous and nominally isotropic materials such as metals. Composite fatigue failure modes include combinations of damage such as matrix failure, fiber cracking, debonding, delamination and ply failure [30, 31].

Fatigue Damage in Composites

Because of their inhomogeneous and anisotropic nature, failure in composite materials does not happen by propagating a single crack, but by damage accumulation throughout the material. The mechanisms of damage accumulation include fiber breakage, matrix breakage, debonding, transverse-ply cracking, and delamination. Sometimes these mechanisms occur independently and sometimes interactively. They are highly affected by material properties and testing variables [25].

Most composites sustain damage at low levels of stress in monotonic loading or early life during fatigue loading. The damage is distributed over the stressed area and usually reduces the stiffness of the composite. This phenomenon, as shown in Figure 2,

also known as wear-out, is usually accompanied by a slight increase in strength at early stages of cyclic loading. Damage accumulation in some regions of composites might be so large that the residual load in that region reaches the same level as the maximum stress in the fatigue cycle and, as a result, failure occurs [25].

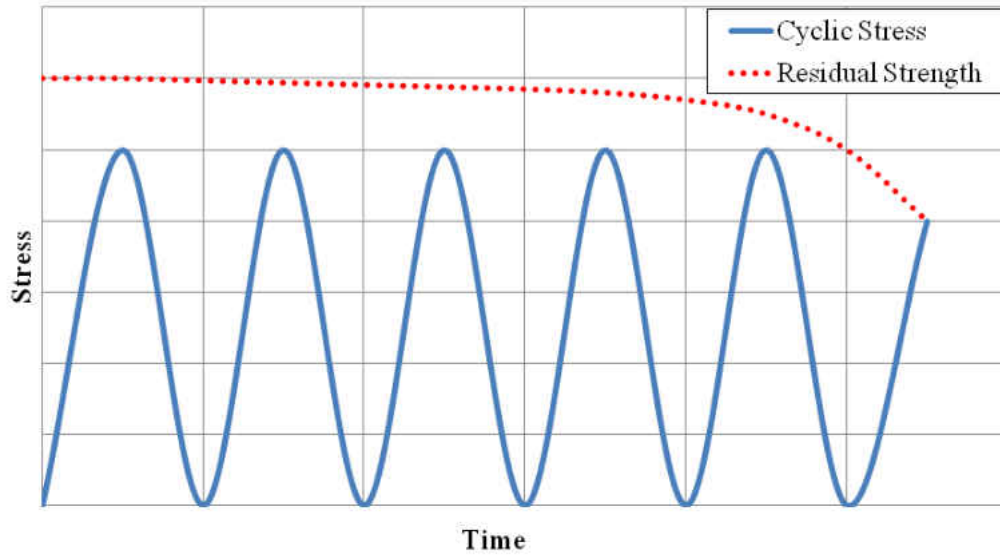


Figure 2. Degeradation of composite strength by wear-out.

In 1972, Owen and Howe studied damage accumulation in chopped glass reinforced plastic under tensile and fatigue loading [33]. They found that cyclic loading will create more intensive resin cracking than monotonic loading and, as a result of resin cracking, the tensile strength will be reduced. Also, accumulation of fatigue damage is non-linear and independent of the amount of stress. They suggested a cumulative damage rule:

$$\Delta = \sum \left[B \left(\frac{n}{N} \right) - C \left(\frac{n}{N} \right)^2 \right] \quad (1)$$

where n is number of cycles experienced by the composite at a stress level which will cause failure after N cycles, B and C are constants, and $\Delta = 1$ at failure. They predicted residual strength after fatigue loading of chopped strand mat polyester laminates by means of modification of this rule. They found that the different damage mechanisms accumulate damage at different rates [33]. As a result, different damage models can have various results for different damage mechanisms. Similarly, Chen and Harris showed that multiple damage mechanisms are responsible for changes in the mechanical properties and eventual failure of CFRP during cyclic loading [34].

Poursartip *et al.* [35, 36] developed the mechanics of fatigue damage of carbon fiber composite laminates. They derived a general differential formulation for damage accumulation. They assumed that the rate of damage accumulation, dD/dN , depends on the current level of damage, the load ratio and the stress amplitude. This relation can be expressed as:

$$\frac{dD}{dN} = f(\Delta\sigma, R, D) \quad (2)$$

where, $\Delta\sigma$ is the stress amplitude, R is ratio $\left(\frac{\sigma_{min}}{\sigma_{max}}\right)$ and D is the current level of damage. Because the function f is unknown, they used changes in the elastic modulus to monitor the damage. By integration from D_i to D_f , they were able to predict the life, N_f . The final relation can be expressed as:

$$f(\Delta\sigma, R, D) = \frac{1}{g'(g^{-1}(E/E_0))} \frac{1}{E_0} \frac{dE}{dN} \quad (3)$$

where g is the relation between the current elastic modulus, E , and the undamaged elastic modulus, E_0 , and g' is the derivative of g with respect to D . To find the parameters in their proposed model, they conducted series of tests for a range of values of $\Delta\sigma$ at

constant E/E_0 and R , for a range of R at constant $\Delta\sigma$ and E/E_0 , and for a range of E/E_0 at constant $\Delta\sigma$ and R . To analyze their experimental results using their damage model, they used the same method O'Brien derived [37]. O'Brien derived a simple rule of mixtures analysis and, with the help of plate theory, predicted the stiffness decrease caused by delamination. He also verified his model with sets of experimental tests and found excellent agreement. Poursartip *et al.* observed that, under load control, the damage growth rate was independent of the current damage present. Also, their experiments showed that the damage growth rate is a power function of the range of applied stress and the mean stress. At very high stresses the failure behavior tends to be static failure and at very low stresses there is a threshold stress for damage growth. In addition, they applied their damage model to predict life under constant stress amplitude at different mean stresses and found reasonable agreement. However, life predictions for various and random loading were less satisfactory. They concluded that their damage model can be used to predict the S-N curve for different R-ratios [36].

Different Fatigue Test Setups

Bending tests are widely used to study the fatigue behavior of structural materials, especially composite materials [38-46]. Generally, bending tests have some advantages over uniaxial tension-compression tests including: (i) in-service load conditions often include bending components, (ii) the danger of Euler buckling is removed, and (iii) the forces required to achieve the required stresses are typically much lower than for uniaxial loading [47]. Different three-point and four-point bending test configurations have been designed and used to model the fatigue loading conditions in variety of studies, to obtain flexural strength and flexural moduli, and to verify different fatigue damage models and

predict fatigue life. The loading conditions in bending tests are valuable for validation of damage models. These setups can impose both tension and compression in the specimen at different locations. As a result, these setups can be used to validate (i) a static damage model that includes both tensile and compressive damage, (ii) a fatigue damage model that includes combinations of tension-tension and a compression-compression. Transverse force and moment diagrams for 3- and 4-point bending setups are illustrated in Figure 3 [48].

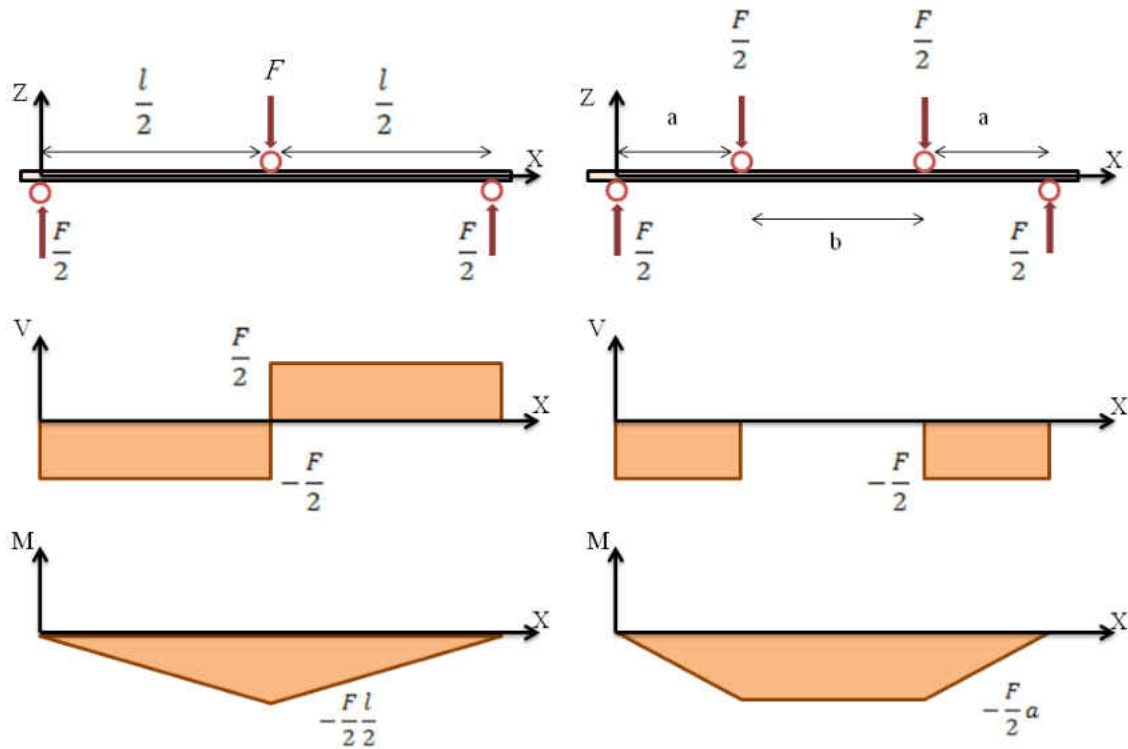


Figure 3. Transverse force and moment diagrams for three point and four point bending setups [48].

Three-Point Bending Setup with Rotating Supports

Debaere *et al.* studied a standard three-point bending setup for thin composite laminates [49]. They conducted fully-reversed bending experiments with a three-point bending setup designed to investigate if this setup can be used for validation of a combination of damage models for thin composite laminates in static or fatigue loading

conditions. The material used for this study was carbon fiber-reinforced polyphenylene sulphide (PPS with commercial name of CETEX). The carbon PPS plates were fabricated by hot pressing and test samples (160mm x 30mm) were cut by a diamond saw. The stacking sequence used for the study was $[(0^\circ, 90^\circ)]_{4s}$, where $(0^\circ, 90^\circ)$ represent one layer of fabric. The resulting maximum stress can be calculated as [48-50]:

$$\sigma_{xx} = \frac{M_{MAX} \frac{h}{2}}{I_{xx}} \quad (4)$$

where I_{xx} is the moment of inertia and h is height of the beam. Above the neutral axis, material is in compression and below the neutral axis it is in tension. The maximum bending moment can be written as:

$$M_{MAX} = \frac{Fl}{4} \quad (5)$$

Debaere *et al.* carried out fatigue tests at the speed of 300 mm/min and all the specimens broke at approximately 20 mm displacement at a corresponding stress of 625 MPa. Comparing a rotating support setup with a single-sided setup, for equal displacements, lower forces are reached with rotating outer supports, and higher bending stiffnesses and ultimate loads were reached with the use of single-sided setup without rotating supports. During the fatigue tests, large mid-span displacements were reached which limited the test frequency. Friction on the supports caused extra difficulties in interpreting hysteresis loops [49].

Debaere *et al.* used ABAQUS to perform a finite element simulation of regular and fully-reversed three-point bending setups. Simulation of the three-point bending setup has some difficulties. As seen in Figure 3, there is a transverse force, V , over the entire beam equal to $F/2$, and the bending moment grows linearly till the maximum value

which is at the center of the beam. To model these loads, the rotating supports should be modeled because they cannot be modeled by equivalent loads and boundary conditions. Modeling the rotating supports needs contact conditions with the friction coefficient of carbon PSS and steel. The simulation needed too much computation time due to modeling the effect of friction on the rotating supports [49].

Four-Point Bending Setup

De Baere *et al.* [47], studied a modified jig design for a bending setup that may be used for the validation of damage models. In this study they considered a four-point bending setup with rotating supports to carry out fatigue tests. Compared to three-point bending setup, a four-point bending setup has more interesting loading conditions. As seen in Figure 3, the area between two loading supports has constant bending moment of [47, 48, 50]:

$$M_{MAX} = \frac{Fa}{2} \quad (6)$$

And there is no transverse force in the mid-section. Therefore, finite element modeling seemed to be easier compared to three-point bending setup since only the area between the two indenting rollers must be modeled. However, they faced some problems during the experimental assessment of the setup. Because of the geometrical limitations of the setup, for load span of 40 mm and 50 mm the samples could not be bent to fracture. For a 30 mm load span, the setup seemed to work, but still the mid-span displacements were relatively large for low loads, limiting the test frequency. Also, these large mid-span displacements caused another problem: the applied loads were no longer vertical, instead they are perpendicular to the bent surface of the specimen, creating normal forces in the

samples. As a result, the authors recommended that the whole setup be modeled in finite element software and non-linear calculations be carried out [49].

Clamped Four-Point Bending Test

To reach higher forces, De Baere *et al.* [47], proposed a modified four-point bending setup with clamping of the specimen ends. Although higher loads were reached for lower displacement, another problem was encountered: the specimen failed at the clamped ends. The stress (load) that was reached for mid-span displacement of 8.3mm was 1830 MPa (2636 N), compared to 625 MPa (900 N) stress for 20 mm displacement with the setup used in the previous study [49]. The same material and same sample geometry as [49] were used for these tests.

Clamped Three-Point Bending Setup

De Baere *et al.* used the same concept to fabricate a clamped three-point bending setup. In order to prevent the two clamped ends from any inward motions, a small piece of aluminum was placed between two grips [47]. It was observed that the results of tests from this setup were highly reproducible. Also, for low displacements, higher forces were reached. The loads were four times higher for less than half the displacement compared to three-point bending setup. The force at failure was measured to be 3.6 kN, which is notably lower than failure force in uni-axial tensile test (52.6 kN for the specimen having the same cross-section geometry). It was observed that during fatigue testing, after few hundred cycles, the indenter lost contact for a certain period. Further investigations revealed this loss of the contact is due to slipping of specimen out of the grips due to high membrane stresses. To determine how much of the bending force is due to bending and how much is because of membrane stresses, a finite element simulation using ABAQUS

was performed. The finite element analysis results revealed that, although simple one dimensional beam theory simulation can be used to validate fatigue damage models, a three dimensional simulation is also necessary. Also, sample slipping in the end grips has some influence on the measured loads [47].

Effect of Friction on Hysteresis Loops from Three-Point Bending Tests

Van Paepegem *et al.* studied the effect of friction between the tested material and the supports of the bending setup on stiffness degradation and energy dissipation [51]. This was achieved by comparing three-point bending fatigue tests to static bending tests with different support conditions. They performed a displacement-controlled fatigue test on the same material as the previous study with different stacking orders. The deflection was limited to 10 mm and three different support conditions were tested: (1) contact specimen-Teflon[®] sheet, (2) contact specimen-bare steel and (3) contact specimen-emery paper. The shape of the hysteresis loop can be changed by changing the friction at the supports. The effect was observed to be less at lower displacements. To verify the effect of friction on hysteresis loops, the finite element code SAMCEF was applied to simulate the setup with different friction coefficient between carbon fibers and supports [51].

The results of the work of Van Paepegem *et al.* revealed that the shape of the hysteresis loop is significantly affected by friction at the supports. This effect is higher when larger displacements are present. Therefore, the energy dissipation and stiffness degradation of the closed hysteresis loop cannot be a valid reference and the information from hysteresis loops from bending test should be interpreted very carefully [51].

In conclusion, single-sided bending had the advantages of being easily modeled but during the fatigue tests there was a loss of contact between the indenter and the

sample after few thousand cycles which resulted in impact of the indenter and corrupted fatigue data. Fully-reversed bending setup does not have such a disadvantage; however, the finite element simulation required long calculation time because of the support rotation. Also, large displacement of the mid-span limited the frequency of the tests.

A four-point bending setup had the advantage of easy modeling, but still the deflections were large for relatively low loads. Adding membrane stresses by clamping the specimen at the ends on the four-point bending setup resulted in smaller displacements, but samples failed near the clamps due to high membrane stresses.

Adding clamps to the end of specimen on three point-bending setup resulted in almost four times larger failure forces for less than half of the displacement compared to regular three-point bending tests. This implies that clamped three-point bending test is preferred over unclamped three-point bending.

Based on the study of Van Paepegem *et al.*, information from hysteresis loops in bending must be considered very carefully. Although stiffness degradation and micromechanical damage growth are typical fatigue mechanisms for fiber-reinforced composites, they cannot be directly related with the recorded force-displacement hysteresis curves of three-point bending tests, because of the effect of friction of samples with supports [47-51].

Fully-reversed Bending Test of Carbon Fiber Reinforced Epoxy Composite Strands

Couillard *et al.* characterized bending fatigue behavior of unidirectional carbon fiber / epoxy composites using a fully-reversed bending test [30]. Composite strands with a cross-sectional diameter of 0.5 mm and fiber volume fraction of 0.43 were tested under fully-reversed bending fatigue test at frequency of 3 Hz. The fatigue damage

accumulation and the different modes of failure were investigated with the help of optical microscopy and SEM (Scanning Electron Microscopy). Figure 4 shows the bending fatigue test mechanism that they used to apply continuous bending moment at a frequency of 3 Hz. The load cell attached to the bottom grip was monitoring the bending moment as a function of time. The maximum curvature reached was 0.09 mm^{-1} which corresponds to maximum theoretical strain of 2.25% whilst the failure strain of the composite strand was mentioned to be 2.5%. The lifetime of the samples in this study was defined as a number of cycles required for a drop in the value of the initial bending moment. This drop was measured at three levels of moment loss, $B/B_0 = 0.75, 0.6$ and 0.4 . Where B_0 is initial bending moment and B is measured moment.

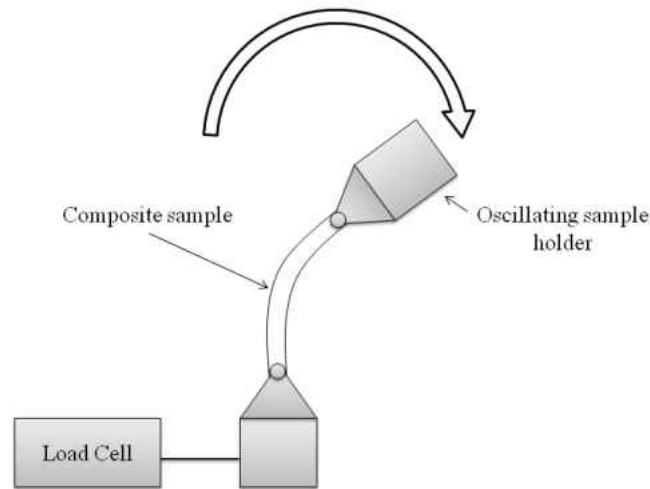


Figure 4. Bending fatigue test mechanism used by Couillard *et al.* in [30]

They expressed the fatigue lifetime as:

$$t = e^{\frac{(B-B_0)}{(B_0K)}} \quad (7)$$

where t is time, B is measured bending moment, B_0 is initial bending moment, K is a constant which they found it to be -0.039 . The failure mechanism that Couillard *et al.* observed was mixed. It was primarily fiber breakage and matrix cracking. By increasing the number of bending cycles, there was crack growth in the matrix and along fiber interfaces [30].

Strength Measurement of Optical Fibers by Bending

In 1986, Matthewson *et al.* [52] utilized a bending technique to measure the strength of glass fibers. They also presented an analysis to determine the effective tested length as a function of statistical parameters that describe the fracture properties of the fiber. They used the mechanism shown in Figure 5. The two face plates are brought together by a computer-controlled stepper motor until fiber fracture is sensed by an acoustic detector. The fiber is clamped to the guide plate.

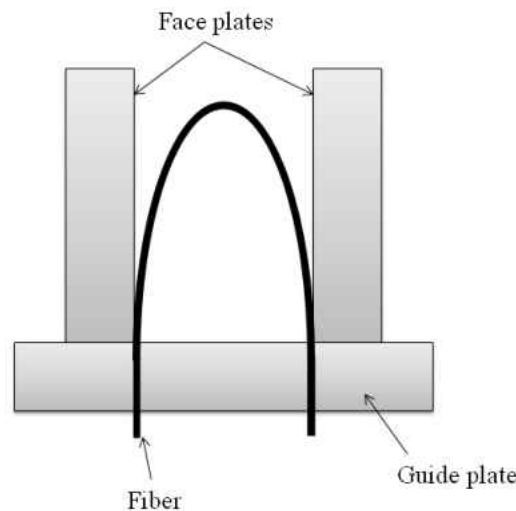


Figure 5. Schematic of fiber bending mechanism used by Matthewson *et al.* [52].

The test provided failure force of the fiber which could be used to calculate failure stress of the fiber. As a result, they found this test to be very effective and recommended

it useful and to be used parallel with tensile test to determine the glass fiber strength [52]. Inspired by Mathewson *et al.*, Nelson *et al.* [53] modified conventional a four-point bending apparatus to measure the strength of thin composite beams. Experimental results with their modified device had good agreement with the theoretical values.

In [54], Ferry *et al.* designed a special apparatus to adapt on a uniaxial tensile machine and generate a multiaxial stress state. The device was designed to apply both four-point bending and torsion loads glass fiber / epoxy composite samples. The aim of the study was to investigate the fatigue behavior under mixed-mode conditions. A charge-coupled device (CCD) camera was used to monitor the damage progress in the samples. They found that the type of damage and initiation of failure depends on value of R as well as ratio of force/torque in mixed-mode testing. Three different failure mechanisms were observed: delamination, fiber failure and cracking.

Tomita *et al.* [55] studied bending fatigue behavior and fracture mechanism of Long carbon fibers with 3.5, 4.5, 5.0 and 5.5 GPa in average tensile stress reinforced epoxy laminates. They studied PAN based long carbon fibers and epoxy resin and manufactured carbon/epoxy laminates using hot-press method. They used a Schenk-type fatigue machine, Figure 6, to perform bending fatigue tests with cyclic stress ratio, $R=-1$ and frequency of 30 Hz. They also measured the generated heat during fatigue testing using an infrared thermo-graphy. They found out that the fatigue limit of cross-ply laminated was influenced by compressive stress of 0° layers and heat generation during fatigue testing. For the 3.5, 4.5 and 5.5 GPa CFRP composites the fatigue limit was related to the compressive stress of 0° layers in the laminates. For quasi-isotropic

laminates, ($0^\circ/45^\circ/90^\circ$), the fatigue limit was related to the compressive stress of the 0° layers in the laminates and failure mechanism was delamination during fatigue test.

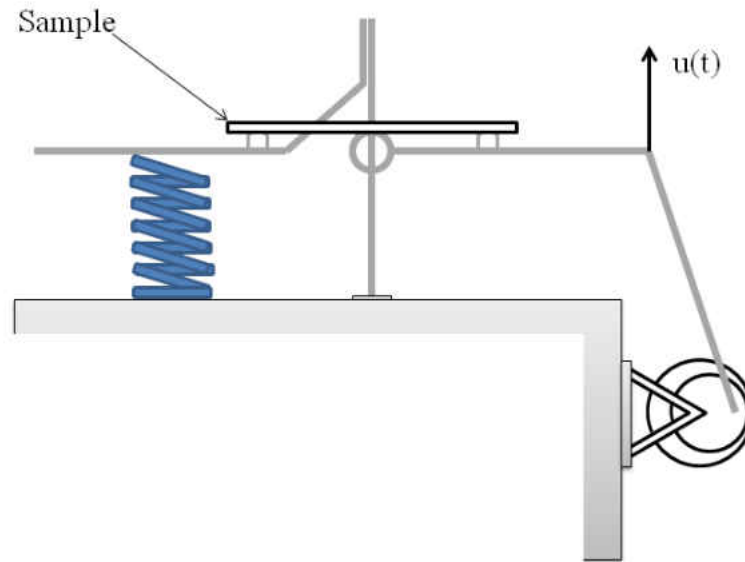


Figure 6. Schematic drawing of fatigue bending machine used in [27, 55].

In another study, Kawai *et al.* [56] performed load-controlled on-axis fatigue tests at room temperature and high temperature (100°C) on cross-ply and unidirectional carbon/epoxy laminates manufactured by the autoclave forming technique. They also observed that the S-N relationship for the cross-ply laminate is almost parallel to the result on the unidirectional laminates, and concluded that the fatigue strength of the cross-ply laminate is determined by the fatigue strength of the axial plies and the difference between the S-N relationships for the cross-ply and unidirectional laminates is characterized by their different magnitudes of static strength.

Using classical lamination theory, they developed a simple fatigue failure model for cross-ply laminates as:

$$N_f = \frac{1}{\left(\frac{\sigma_{max}}{\frac{\alpha X}{K}}\right)^n}$$

where N_f is the fatigue life of cross-ply laminates, σ_{max} is the fatigue stress, X is the reference strength of unidirectional laminate, α/k is a scale factor and n is material constant.

To validate their proposed fatigue model, they used their experimental data. The fatigue strength of the cross-ply laminates was successfully predicted using proposed fatigue model.

Belingardi *et al.* [57] used the same mechanism of bending fatigue test as [56] to study fatigue stiffness and degradation in cross-ply and angle-ply carbon-glass/epoxy laminates. Tensile and flexural static tests and displacement-controlled bending fatigue tests were carried out with the stress ratio of $R=0.1$. They observed linear stress-strain curves for cross-ply laminates in static tensile and flexural tests while for angle-ply specimens these curves were non-linear. Also, they observed different damage mechanisms for the two specimens. Their results will be discussed more in Chapter III of this thesis.

Conclusion

As there is uprising need and interest for carbon fiber composite materials, they have been subject of many recent studies. One important aspect of study of CFRP is to investigate their fatigue behavior under different loading conditions. Because of the aforementioned advantages of bending tests over tensile and compression tests, different setups for bending tests have been proposed and have been used to study and investigate fatigue life of CFRP under bending tests. Several proposed bending fatigue fixtures and

their advantages and disadvantages were reviewed in this chapter. There has been very limited number of previous research has been done on four-point bending test of CFRP composites with stress ratio, $R = -1$. Based on the literature review and results of previous studies, fatigue behavior of cross-ply and angle-ply CFRP composites with has been studied and the methods and results are discussed in the following chapters of this thesis.

CHAPTER II

MATERIALS AND METHODS

To obtain the desired results from this research, an experimental method was set up to study the behavior of carbon fiber reinforced plastics under cyclic bending loads.

Material

The material used for this study was biaxial woven carbon fibers obtained from TenCate Advanced Composites located in Morgan Hills, California. The fabric is 2x2 twill weave as shown in Figure 7. The matrix material was low reactive, intermediate viscose polyester resin, POLYLITE[®], provided by Reichhold Chemicals located in Durham, North Carolina.

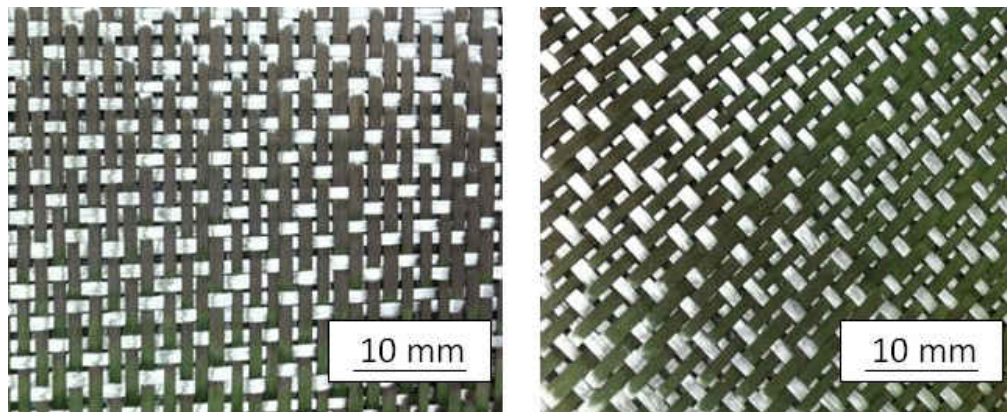


Figure 7. Fabric structure used for this study.

Sample preparation

To prepare the samples needed for this study, two methods of laminate fabrication were used. Three plates were made by means of a hand lay-up method but each was rejected because of flaws resulting from the process. Ultimately, Vacuum Assisted Resin

Transfer Molding (VARTM) was selected for its repeatability and sample quality. Both methods are explained below.

Hand lay-up method

15 layers of biaxial carbon fibers, 2.6 mm thick, 300 mm x 300 mm were built up successively on the mold surface and worked by hand to fabricate the plate [58]. Figure 8 shows a schematic of the stacking order. The smooth work surface was waxed before applying components; one layer of peel ply was applied on the work surface. Layers of carbon fibers were stacked on top of each other and resin was applied to each layer by means of a hand roller. A void roller was used to drive out any possible air bubbles between plies. Special care was taken to avoid any warpage in fiber orientations. Another layer of peel ply was applied on top, and a layer of breather on top of all materials. Vacuum bagging was placed over the stack of material and the working surface with the help of tacky tape. The plate was placed under vacuum with the help of a vacuum pump for 24 hours at room temperature at 23 °C.

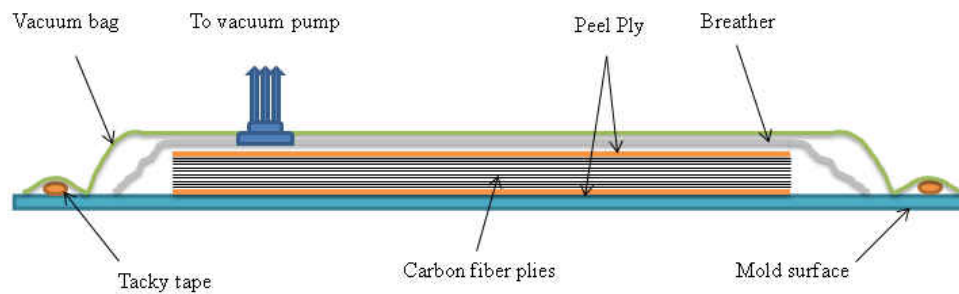


Figure 8. Hand lay-up setup for the first plate.

The resulting plate is shown in the Figure 9. There were several flaws in the plate. As seen in the picture, the top surface had wrinkles due to the pressure of vacuum bagging with dry spots on the wrinkles and on the bottom surface of the plate. The

thickness of the plate also was uneven. To remove the vacuum bagging wrinkle effect, a different setup, shown in Figure 10, was used. Half inch thick plywood was placed over the pile of material under vacuum bagging. The same process was used as the first plate with same amount of cure time.



Figure 9. Surface of first plate after curing under vacuum at room temperature for 24 hours.

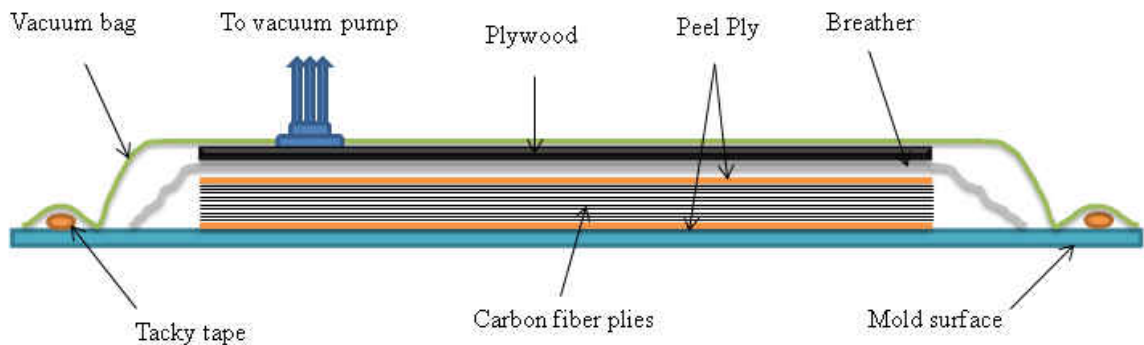


Figure 10. Hand lay-up set up for second plate. A piece of plywood was placed over the stack of material and under the vacuum bag.

The plywood was effective in removing the wrinkles on the surface and to some extent reduced the thickness variation in the plate, but still there were some dry spots both on the top and bottom of the plate. Figure 11 shows the top surface of the second plate made.

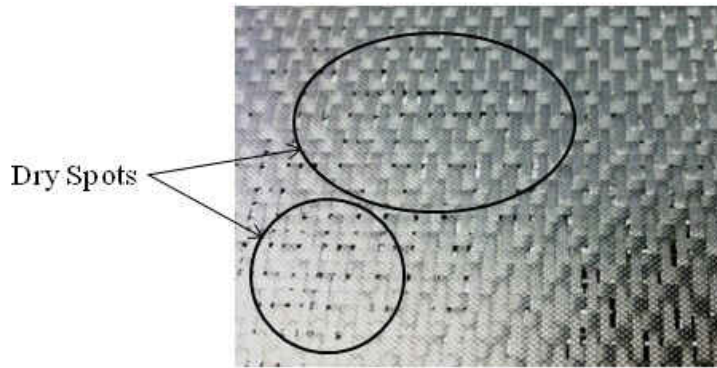


Figure 11. Dry spots on surface of second plate made using the hand lay-up process.

The next plate was fabricated with the same process; this time a different type of breather was used on the top and bottom of the carbon fiber plies. Also, the working surface was sprayed three times with rubberized undercoating spray in 10 hours intervals to achieve a better and smoother work surface in order to reduce the dry spots on the plate surface. The same process and material as the second plate were applied, and for this plate some heavy weights were placed over the vacuum bagging during 24 hours of room temperature curing to improve the consistency in the thickness of the plate. Figure 12 shows a schematic of the set up. The result was better compared to previous two plates, but, as seen in Figure 13, there are some dry spots on the surface. Moreover, the thickness of the plate was not constant.

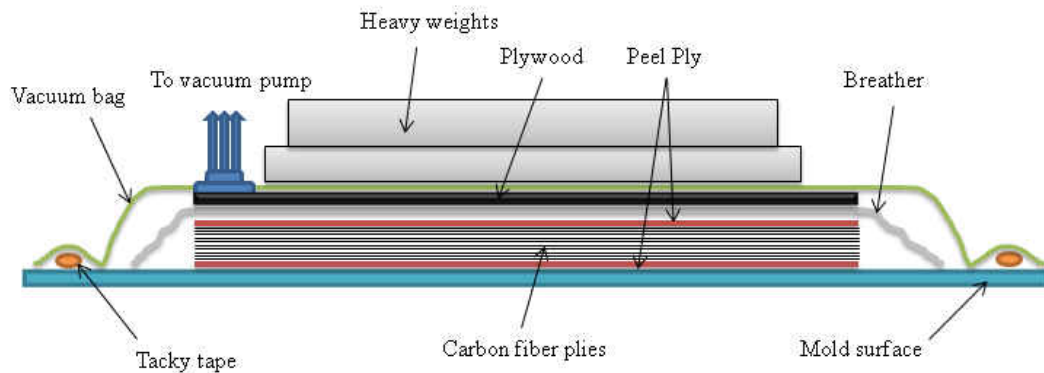


Figure 12. Hand lay-up setup for third plate.

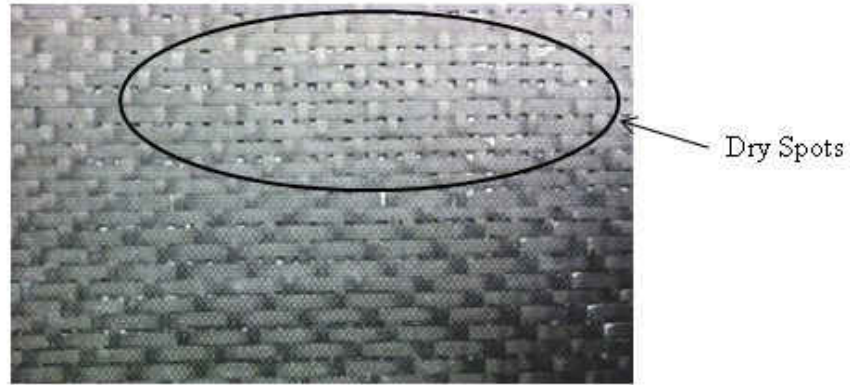
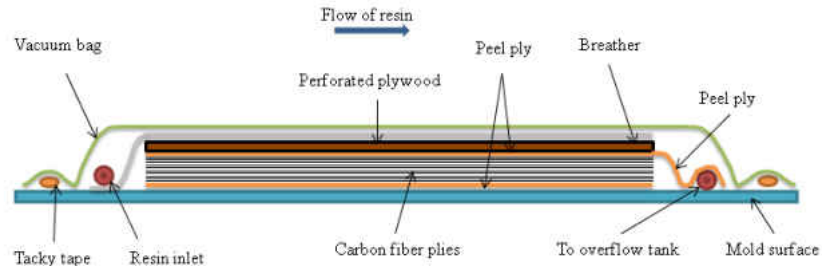


Figure 13. Dry spots on surface of third plate made using hand lay-up process.

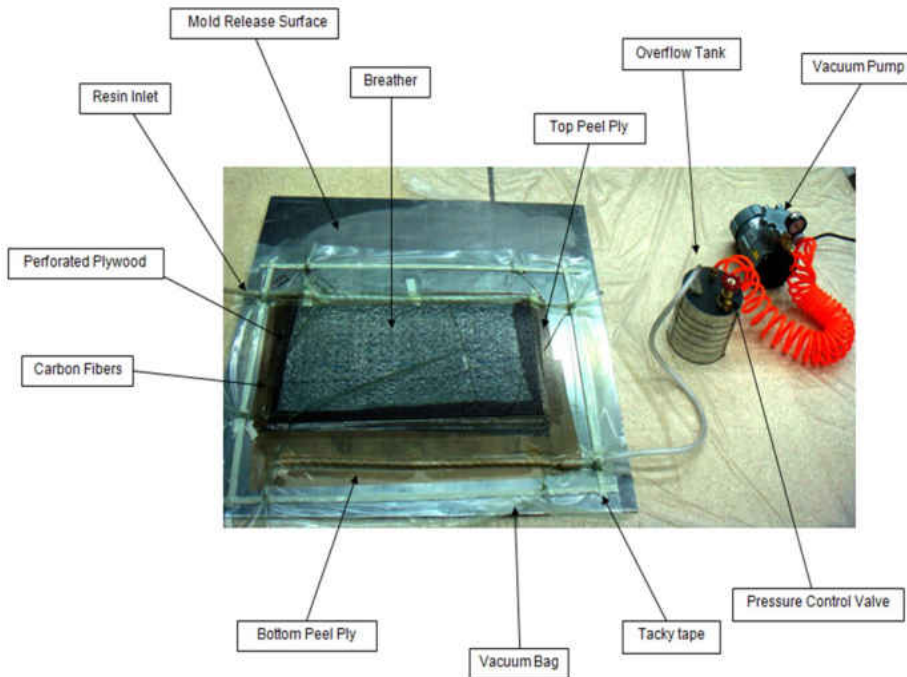
VARTM Method

To achieve better quality, the next plate was fabricated using vacuum assisted resin transfer molding (VARTM). VARTM has been used to manufacture composites for more than 50 years, and it continues to be developed [59]. It is a very effective method to manufacture complex-shaped parts with lower tooling costs; VARTM will reduce the void content of the composite and improve the quality of the part [60, 61]. In this process, the reinforcement is assembled in a mold and is sealed inside a vacuum bag. The resin is transferred into the part through a resin inlet under ambient pressure. Figure 14 shows a schematic setup for the VARTM process and different components of the setup that was used to fabricate the composite plates for this study. The work surface was waxed and one layer of peel ply was placed on the work surface. Fifteen layers of carbon fiber with dimensions of 600 mm x 300 mm were stacked up on each other, two layers of peel ply were placed on top, a 600 mm x 300 mm perforated plywood and one layer of breather was placed on top of all materials. Finally, a vacuum bag was applied. Carbon fibers were aligned along the 0° direction to fabricate $(0^\circ/90^\circ)_{15}$ specimens, and were rotated at 45° to fabricate $(\pm 45^\circ)_{15}$ plates. After putting the vacuum bag over the material and mold

surface, the vacuum pump was started; when the vacuum pressure of -80 kPa was reached the resin inlet was opened to let the resin flow into the material. Once the flow of resin was seen in the overflow tank, the inlet flow was stopped and the pressure was lowered to -60 kPa. After 20 minutes and initial gelling of the resin, the plates were left under vacuum and cured at room temperature for 24 hours and then post-cured at 40°C for 16 hours. The final thicknesses of plates were 3.98 ± 0.15 mm for $(0^\circ/90^\circ)_{15}$ and 3.71 ± 0.15 mm for $(\pm 45^\circ)_{15}$ plates, respectively.



(a)



(b)

Figure 14. (a) VARTM infusion process. (b) Components of VARTM set up.

Plate layup and curing details are given in Table 2.

Table 2. Composite plate lay-ups, materials used and curing details.

Lay-up	Method	Details
Biaxial Carbon Plies $(0^\circ/90^\circ)_{15}$	VARTM	Curing: 24 hours at room temperature
Biaxial Carbon Plies $(\pm 45^\circ)_{15}$		Post curing: 16 hours at 40 °C

Figure 15 shows the VARTM process during and after resin transfer. Test samples were cut by diamond saw from the manufactured plates in accordance with ASTM D6272-02 [62] as shown in Figure 16.

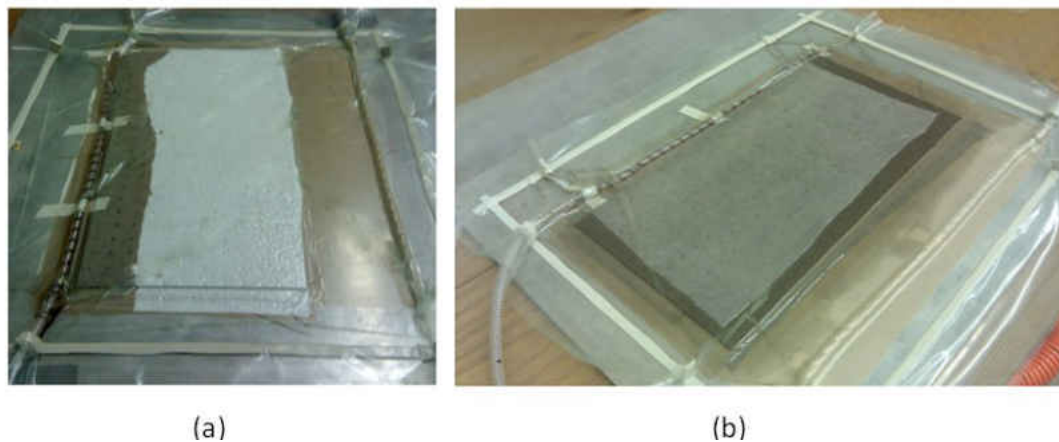


Figure 15. Composite plates (a) during and (b) after resin transfer process.

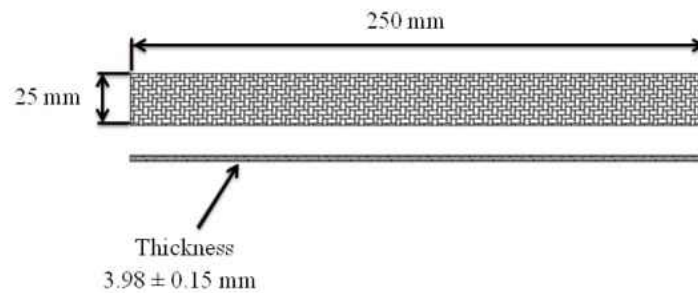


Figure 16. Sample geometry for $(0^\circ/90^\circ)_{15}$ fibers in accordance with ASTM D6272-02.

Determination of Fiber Volume Fraction (V_f)

In fiber reinforced composite materials, the distribution of fibers throughout the matrix follows a repeating pattern. Although there are random arrangements of fibers, the cross-section of the material can be approximated as a square packed array. As seen in Figure 17, the cross-section of the fibers is a fraction of total cross section and is a measure of volume of fibers relative to the total volume of composite. This parameter is called fiber volume fraction, V_f [63, 64].

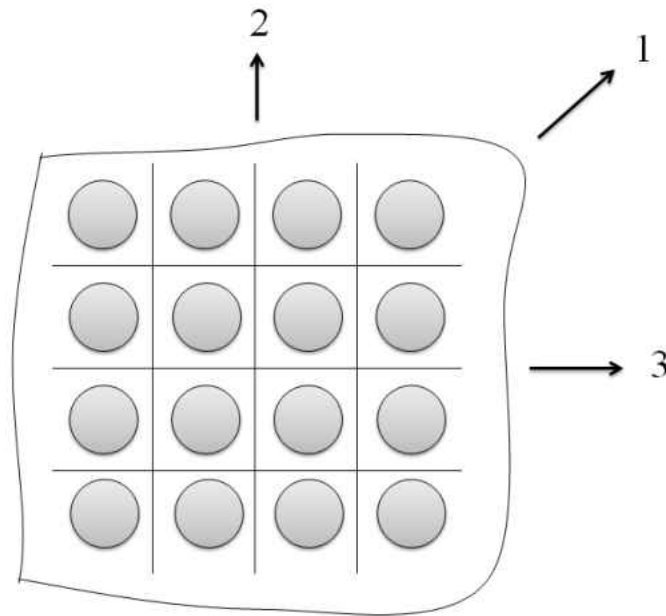


Figure 17. Cross section of composite material as square packed array.

The fiber volume fraction affects the material's mechanical properties, hence, it is important to measure and determine V_f for each material tested [65]. There are several procedures to measure the fiber volume fraction in composite materials: 1) resin removal method, 2) thickness measurement method and 3) burn-off test. In the resin removal method, the mass of a test specimen is measured before and after removal of resin and therefore the volume fraction of the fibers is calculated. Combustion, nitric acid digestion and digestion in a sulfuric acid/hydrogen peroxide mixture are some ways to remove the

matrix from the composite samples. In the thickness measurement method, the thickness of the composite is measured over the entire surface of the composite. By using a known value of mass per unit area and density of the fibers, the fiber volume fraction of the composite is calculated [66]. To determine fiber volume fraction for the composite samples for this study, a burn-off test was conducted in accordance with ASTM D2548-68 [67]. The ASTM D2548-68 burning method is a simple and useful way of determining fiber volume fraction of composite materials. In the case of composites with matrix fillers, the method shows some limitations. There is no standard procedure to separate filler material from fibers and resin to determine V_f [68].

To measure the fiber volume fraction, ceramic crucibles, electric furnace capable of maintaining a temperature of 400°C or more and weighing scale with accuracy of 0.001 g were used. Ceramic crucibles were heated to 500°C for 10 minutes then they were cooled down to room temperature and their weight was measured and recorded. Three samples were cut from each plate and the weight of samples and crucibles were recorded. The crucible and specimen were placed in the furnace at temperature of 460°C for at least 6 hours until all resin was gone. After cooling down to room temperature, the weights of the fibers and crucibles were recorded.

To calculate the fiber volume fraction, the following equations were used [1, 2, 69]:

$$M_c = M_r + M_m$$

where M_c is the mass of the composite sample, M_r is mass of reinforcement (carbon fibers) and M_m is the mass of matrix.

$$V_r = \frac{M_r}{\rho_r}$$

where V_r is the volume of reinforcement (carbon fibers) and ρ_r is the density of reinforcement (carbon fibers).

$$V_m = \frac{M_m}{\rho_m}$$

where V_m is the volume of matrix and ρ_m is the density of matrix.

$$V_f = \frac{V_r}{V_c}$$

where V_f is volume fraction of carbon fibers.

$$W_f = \frac{M_f}{M_c}$$

where W_f is weight fraction of carbon fibers. Table 3 shows the result of the burn-off tests.

Table 3. Result of burn-off test.

Sample	M_m (g)	M_r (g)	$V_m(\text{Cm}^3)$	$V_r(\text{Cm}^3)$	$W_f(\%)$	$V_f(\%)$
$(0^\circ/90^\circ)_{15}$	0.84 ± 0.13	1.61 ± 0.23	0.71 ± 0.11	0.63 ± 0.01	66 ± 0.75	47 ± 0.85
$(\pm 45^\circ)_{15}$	1.05 ± 0.02	2.13 ± 0.02	0.89 ± 0.02	0.84 ± 0.01	67 ± 0.55	49 ± 0.63

Testing Methods

Static test

Four-point static bending tests were conducted to determine the yield and ultimate strength of the samples. The tests were done using a Shimadzu AG-IS 50 kN universal test machine with a crosshead motion rate of 10 mm/min. Three samples from each plate were chosen and run in the four-point bending static test fixture shown in Figure 18.

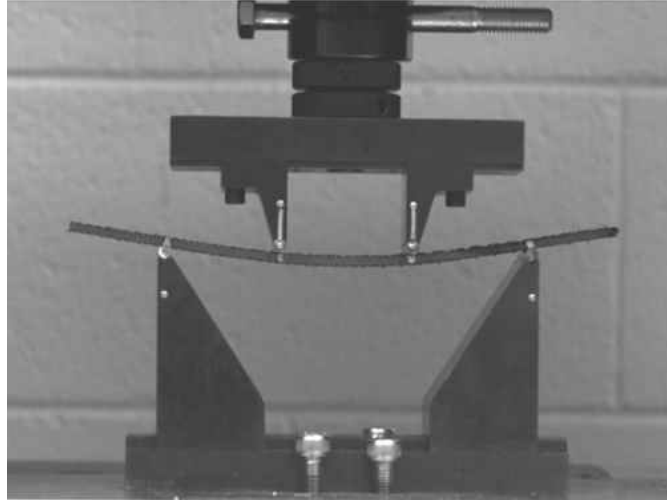


Figure 18. Static four-point bending fixture.

The tests were performed in accordance with ASTM D6272-02 [62]. A schematic of the test configuration is shown in Figure 19. The distance between the two support noses, L , was 170 mm and the distance between loading supports was 60 mm. The radii of the loading and support noses were 3.2 mm. By having such a setup, the support span-to-depth ratio (L/h) was 42:1 and the overhang was 40 mm on each side of the support span. The instantaneous force and the crosshead displacement were measured at 0.5 second intervals.

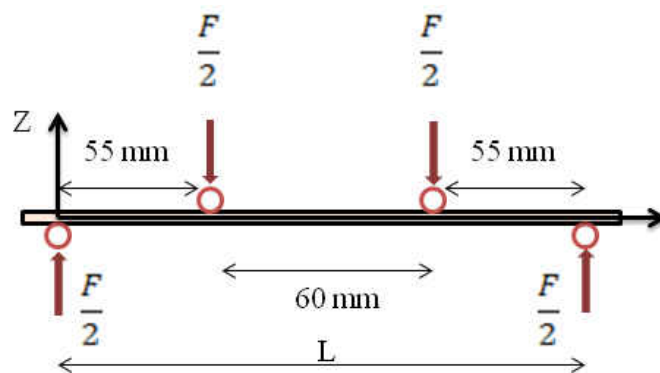


Figure 19. Schematic of static and fatigue test setup.

The flexural modulus was calculated as [62, 70]:

$$E_B = \frac{0.21L^3m}{bd^3} \quad (8)$$

where E_B is flexural modulus (GPa), L is the support span (mm), b is the width of the beam (mm), d is the depth of the beam (mm) and m is the slope of the tangent line to the initial straight part of the load-deflection curve for tested samples. To calculate the strain, the following equation was used [62]:

$$\varepsilon = \frac{4.7 Dd}{L^2} \quad (9)$$

where ε is strain in the outer fiber (mm/mm) at deflection D (mm) of the center of the beam. The maximum strain occurs at the mid-span when deflection of the center of the beam is at its maximum value.

Fatigue Test

There have been different setups for four-point bending tests in the literature [39, 40, 44, 45, 47, 49, 54, 71-74]. During the fatigue testing, after a few thousand cycles, specimens can show permanent deflection. If the test is performed under displacement-control, when the displacement is smaller than the amount of permanent deformation there is a loss of contact with the indenter; in the next cycle, the indenter will impact on the surface of the specimen, resulting in impact damage which leads to corrupted fatigue data. One solution can be performing the test as a load-controlled test, and then there is no problem of loss of contact. Load-controlled bending tests require more accurate PID controllers and lead to more convergence problems. Another solution can be keeping the permanent deformation at zero. This can be achieved by performing fully-reversed bending. In a fully-reversed bending test, each side of the sample is loaded in compression and tension; therefore, this test can be used to validate tension-compression

fatigue damage models [49]. To perform a fully-reversed bending test, a special fixture was designed and manufactured as shown in Figure 20.

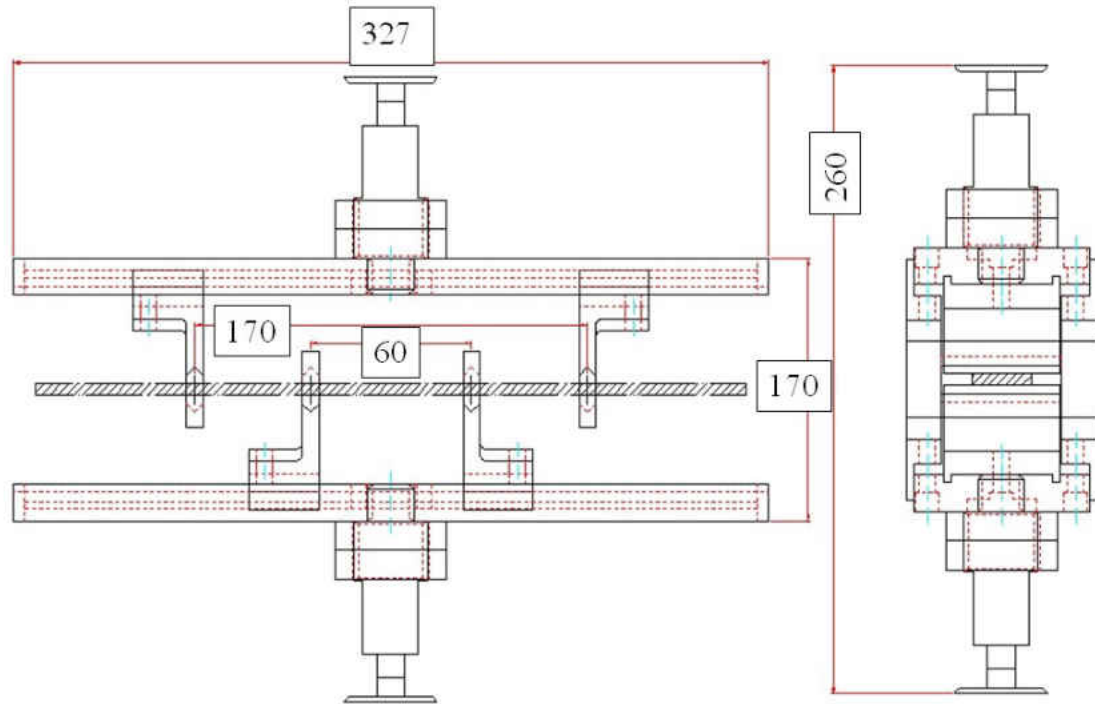


Figure 20. Fatigue fixture designed and manufactured to perform fully-reversed four-point bending test. All dimensions are in mm.

The fixture consists of two rectangular bars that hold the upper and lower anvils and can be attached to the fatigue machine by two flanges at the upper and lower ends. The specimen will be clamped between two nested anvils and will be grabbed by two cylindrical rollers with radius of 3.2 mm to reduce the friction as well as allowing the specimen to rotate at supports. Specification of fixture is shown in Table 4.

Table 4. Specifications of four-point bending test.

Maximum capacity	kN	7
Maximum load/support span	mm	350
Minimum load/support span	mm	20
Maximum thickness of specimen	mm	9
Maximum width of specimen	mm	50
Maximum deflection	mm	17
Material		Al 6061
Total weight	kg	3.3

Different components of the four-point bending fixture are shown in Figure 21.

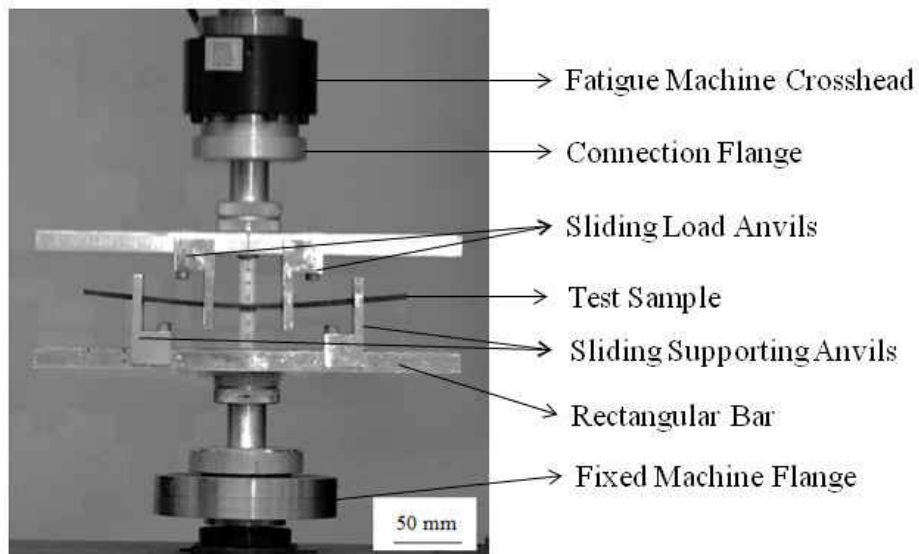


Figure 21. Different components of four-point fatigue bending fixture.

Fatigue Test Apparatus

Fatigue testing was conducted using a Bose Electroforce[®] 3510 test system. The machine has a load range of ± 7.5 kN and a displacement range of ± 25 mm. The machine is operated and controlled through WinTest[®] 4.1 software. The use of high frequency in

fatigue testing of composite laminates can generate heat in tested specimens and therefore affect the fatigue results [75-77]. Also, in testing of composite materials, it is necessary to carry out fatigue tests at a constant rate of stress application [78, 79]. Therefore, a sine waveform at a frequency of 5 Hz was generated. All tests were done with stress ratio, $R = -1$. In the WinTest[®] software, a limit action was defined as maximum displacement of 15 mm so the system could sense specimen failure or unwanted rapid motion of the crosshead due to a large stiffness decrease in specimen.

Electroforce[®] test instruments are equipped with TuneIQ[®] control optimization software, which improves the closed loop system performance of testing instrument. TuneIQ is used to adjust proportional integral derivative control loop settings and tune the parameters of linear motor of the machine based on the type of the specimen. This is to make sure the waveform produced by machine's crosshead, is what we asked. When waveform used in the tests is defined, TuneIQ will use the waveform parameters to impose noise signals on a low and high frequency sine wave. Acquired data during this process will be analyzed and based on that the parameters of machine's linear motor will be defined. It is required to tune machine for each load before doing the actual fatigue test. The same sample cannot be used both for tuning and the actual fatigue test, because during the tuning process, specimen won't be exposed to load conditions further than waveform amplitude, but the frequency of the tuning process will be up to 200 Hz. This level of excitation will affect some mechanical properties and as a result, will affect fatigue life of the used sample.

Four-point bending fatigue tests were carried out with maximum stresses of approximately 45%, 56%, 67%, 72% and 76% of the measured yield stress for $(0^\circ/90^\circ)_{15}$

samples and 53%, 60%, 73%, 80% and 85% of measured yield stress for $(\pm 45^\circ)_{15}$ samples. Tables 5 and 6 show geometrical properties of $(0^\circ/90^\circ)_{15}$ and $(\pm 45^\circ)_{15}$ samples respectively. Samples were clamped in the fixture with 50 Nm torque on all bolts. Accurate measurements by a digital caliper were conducted to make sure that samples and the fixture are in perfect geometrical symmetry.

Table 5. Fatigue test data log sheet for $(0^\circ/90^\circ)_{15}$ and $(\pm 45^\circ)_{15}$ samples.

Sample	Lay-up	Thickness (mm)	Width (mm)
14	$(0^\circ/90^\circ)_{15}$	4.02 ± 0.02	24.71 ± 0.02
2	$(0^\circ/90^\circ)_{15}$	3.98 ± 0.03	25.08 ± 0.15
1	$(0^\circ/90^\circ)_{15}$	3.98 ± 0.01	24.60 ± 0.17
3	$(0^\circ/90^\circ)_{15}$	3.99 ± 0.03	24.89 ± 0.01
4	$(0^\circ/90^\circ)_{15}$	4.03 ± 0.08	24.55 ± 0.00
6	$(0^\circ/90^\circ)_{15}$	3.96 ± 0.02	24.78 ± 0.03
11	$(0^\circ/90^\circ)_{15}$	3.98 ± 0.05	24.99 ± 0.03
12	$(0^\circ/90^\circ)_{15}$	3.97 ± 0.01	24.93 ± 0.03
8	$(0^\circ/90^\circ)_{15}$	3.98 ± 0.01	24.95 ± 0.09
9	$(0^\circ/90^\circ)_{15}$	3.96 ± 0.04	24.90 ± 0.02
10	$(0^\circ/90^\circ)_{15}$	3.89 ± 0.05	24.90 ± 0.03
5	$(0^\circ/90^\circ)_{15}$	3.98 ± 0.04	24.85 ± 0.05
13	$(0^\circ/90^\circ)_{15}$	4.01 ± 0.04	24.91 ± 0.04
15	$(0^\circ/90^\circ)_{15}$	4.00 ± 0.02	24.73 ± 0.04
3	$(\pm 45^\circ)_{15}$	3.69 ± 0.01	27.38 ± 0.23
5	$(\pm 45^\circ)_{15}$	3.65 ± 0.04	24.64 ± 0.05
4	$(\pm 45^\circ)_{15}$	3.59 ± 0.02	24.88 ± 0.03
12	$(\pm 45^\circ)_{15}$	3.77 ± 0.02	24.78 ± 0.03
7	$(\pm 45^\circ)_{15}$	3.74 ± 0.02	24.86 ± 0.03
6	$(\pm 45^\circ)_{15}$	3.73 ± 0.00	24.85 ± 0.13
1	$(\pm 45^\circ)_{15}$	3.70 ± 0.01	24.82 ± 0.06
14	$(\pm 45^\circ)_{15}$	3.73 ± 0.02	24.82 ± 0.06
2	$(\pm 45^\circ)_{15}$	3.74 ± 0.01	24.82 ± 0.03
11	$(\pm 45^\circ)_{15}$	3.73 ± 0.00	24.68 ± 0.08
12	$(\pm 45^\circ)_{15}$	3.71 ± 0.01	24.86 ± 0.06
7	$(\pm 45^\circ)_{15}$	3.71 ± 0.04	24.87 ± 0.05
8	$(\pm 45^\circ)_{15}$	3.69 ± 0.01	24.82 ± 0.03
9	$(\pm 45^\circ)_{15}$	3.68 ± 0.01	24.82 ± 0.18
10	$(\pm 45^\circ)_{15}$	3.71 ± 0.01	24.78 ± 0.00

CHAPTER III

RESULTS AND DISCUSSION

Static Test

Static Test with Regular Four-Point Bending Fixture – (0°/90°)₁₅ samples

Static four-point bending tests were carried out on three (0°/90°)₁₅ to measure the mechanical properties of CFRP. Testing was displacement-controlled at the rate of 10 mm/min until failure. In all cases, samples failed by cracking/buckling on the compressive side of the sample.

The maximum stress in outer fiber of the samples was calculated using :

$$\sigma_{max} = \frac{3F(L - L_i)}{2bd^2} \quad (10)$$

where F is the maximum load (N), L is support span (mm), L_i is the load span (mm), b is the width of the beam (mm) and d is the depth of the beam (mm). For this setup L - L_i = 55 mm, so Equation 10 becomes:

$$\sigma_{max} = \frac{82.5F}{bd^2} \quad (11)$$

Tables 6 shows the measured and calculated mechanical properties of (0°/90°)₁₅ samples based on static tests. The flexural modulus is calculated from Equation 8. Stress – deformation curves for the three tested samples are plotted in Figure 22. Strain is calculated from Equation 9.

Table 6. Measured mechanical properties of $(0^\circ/90^\circ)_{15}$ samples.

Property	Measured average	CV ^a (%)
Maximum load (N)	747	1.8
Maximum stress (MPa)	314	3.1
Maximum strain (%)	0.58	5.7
Flexural Modulus (GPa)	75	1.5

^a CV = coefficient of variation = (standard deviation / average) x 100 %

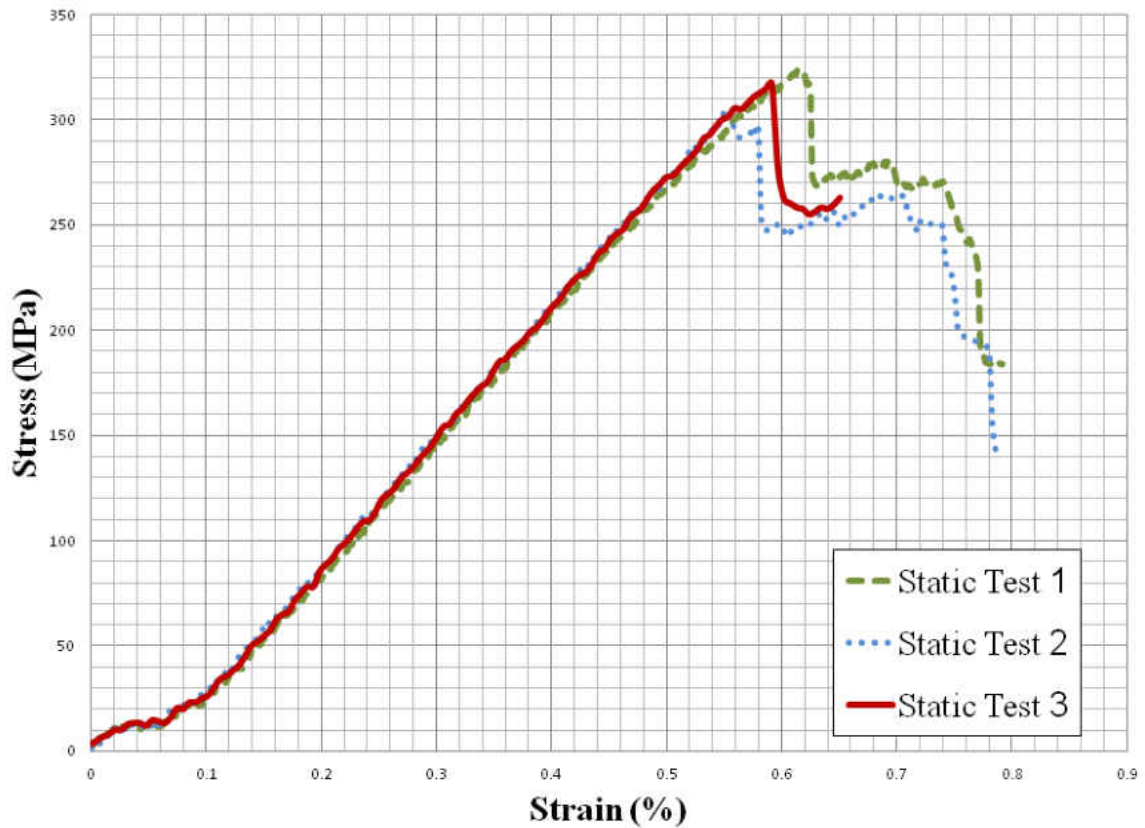


Figure 22. Stress- strain curves for four-point bending tests for $(0^\circ/90^\circ)_{15}$ samples.

Static Test with Clamped Four-Point Bending Fixture – $(0^\circ/90^\circ)_{15}$ samples

To compare the stresses occurring during fatigue tests with stresses observed during static testing, two samples from the $(0^\circ/90^\circ)_{15}$ plate were tested in a Shimadzu

Universal testing machine with the newly designed clamped fixture explained in Chapter II. The setup is shown in Figure 23. The samples were clamped in the fixture with 50 Nm torque on all bolts. Accurate measurements by a digital caliper were conducted to make sure that samples and the fixture are in perfect geometrical symmetry. The test rate was 10 mm/min.



Figure 23. Static test setup with clamped four-point bending fixture.

Figure 24 shows direct comparison of stress – strain values measured with two different four-point setups. Also, Table 7 summarizes the results of comparison between the two fixtures.

Table 7. Force, displacement and stress values for clamped and regular four-point bending fixture.

Fixture	Regular	Clamped	Increase
Maximum force	749 N	1063 N	42 %
Maximum Displacement	9.2 mm	11.2 mm	21 %
Maximum Stress	315 MPa	480 MPa	52 %

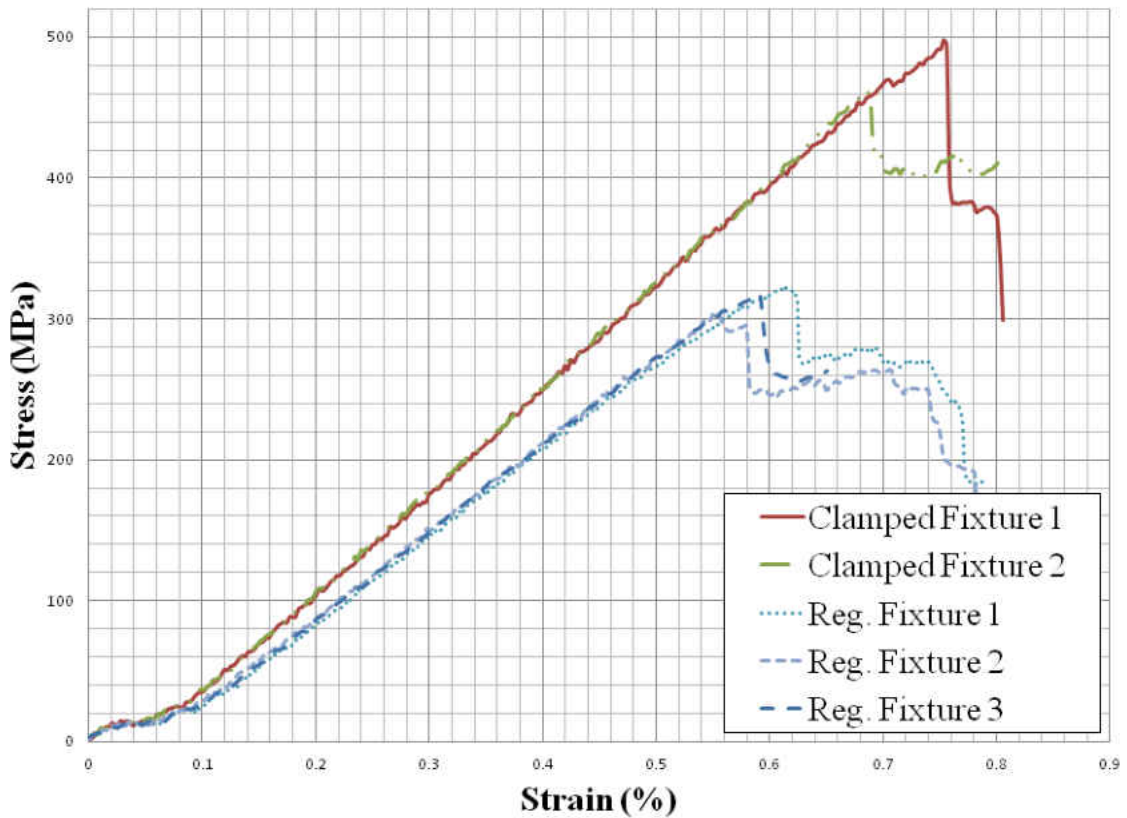


Figure 24. Comparison of stress-strain values measured with two types of four-point bending setup for $(0^\circ/90^\circ)_{15}$ samples.

De Baere *et al.*[47] compared clamped four-point and three-point bending setups with regular four-point and three-point fixtures with rotating supports. The clamped samples reached much higher forces than were reached in the current tests. Maximum stresses reached with the clamped fixture was 1830 MPa compared to 625 MPa for the regular fixture, an almost 300% increase [47]. De Baere *et al.* did the same comparison with a clamped three-point bending setup and a regular three-point bending fixture with rotating supports. Moreover, they simulated two fixtures using ABAQUS. Results of simulations and experimental tests with clamped fixture are shown in Figure 25.

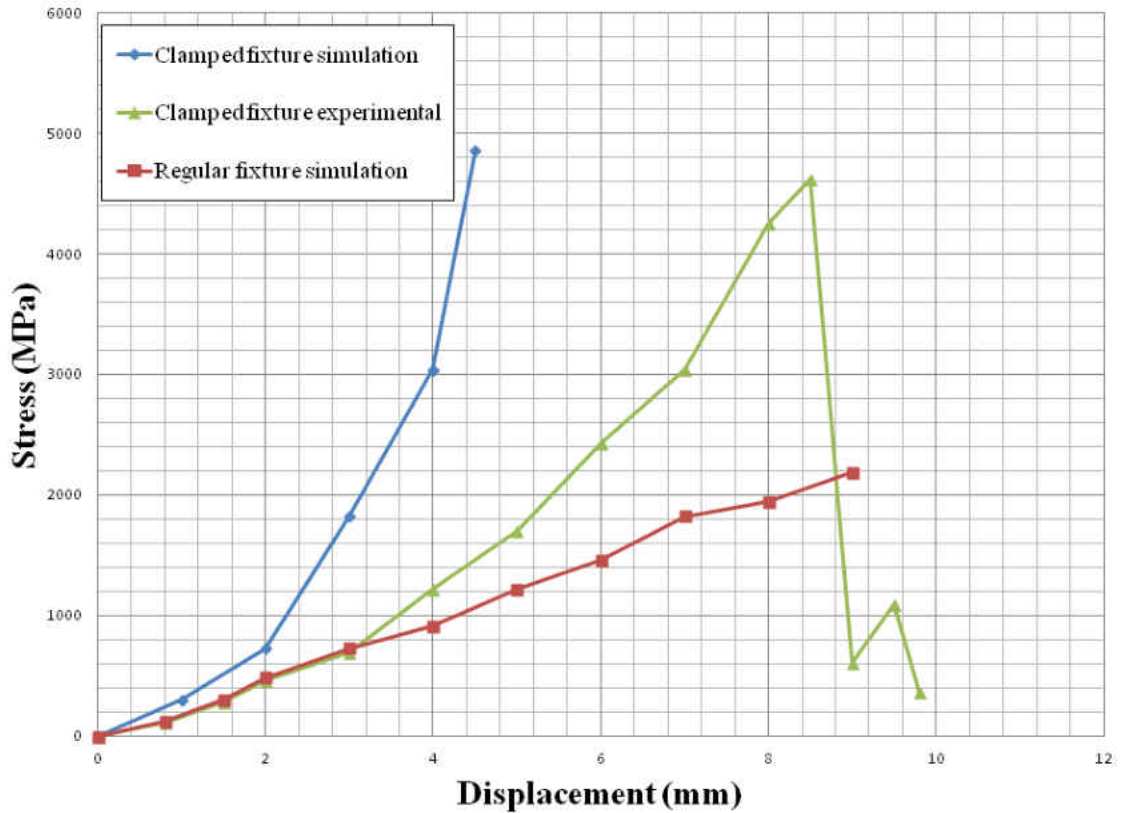


Figure 25. Different stress-displacement curves for the simulation of clamping and regular three-point bending fixtures in [47].

In the simulation of the clamped fixture, a maximum stress of 4860 MPa was measured; this value was 2180 MPa for the regular three-point bending fixture, an increase of 120% [47].

Static test Four-Point Bending – ($\pm 45^\circ$)₁₅ Fibers

Static four-point bending tests were carried out on three samples from the ($\pm 45^\circ$)₁₅ plate to measure mechanical properties of the CFRP. Tests were displacement-controlled at the rate of 10 mm/min. In all three tests, no visual fracture or failure of the samples was observed. The tests were stopped because of the geometrical limitation of the three-point bending fixture, shown in Figure 26. With the current setup, the test

machine's crosshead can move down 38.8 mm before the loading supports touch the sample. Beyond this point, the measured load won't be correct anymore; this value of deformation corresponds to 4.8% strain in the samples.

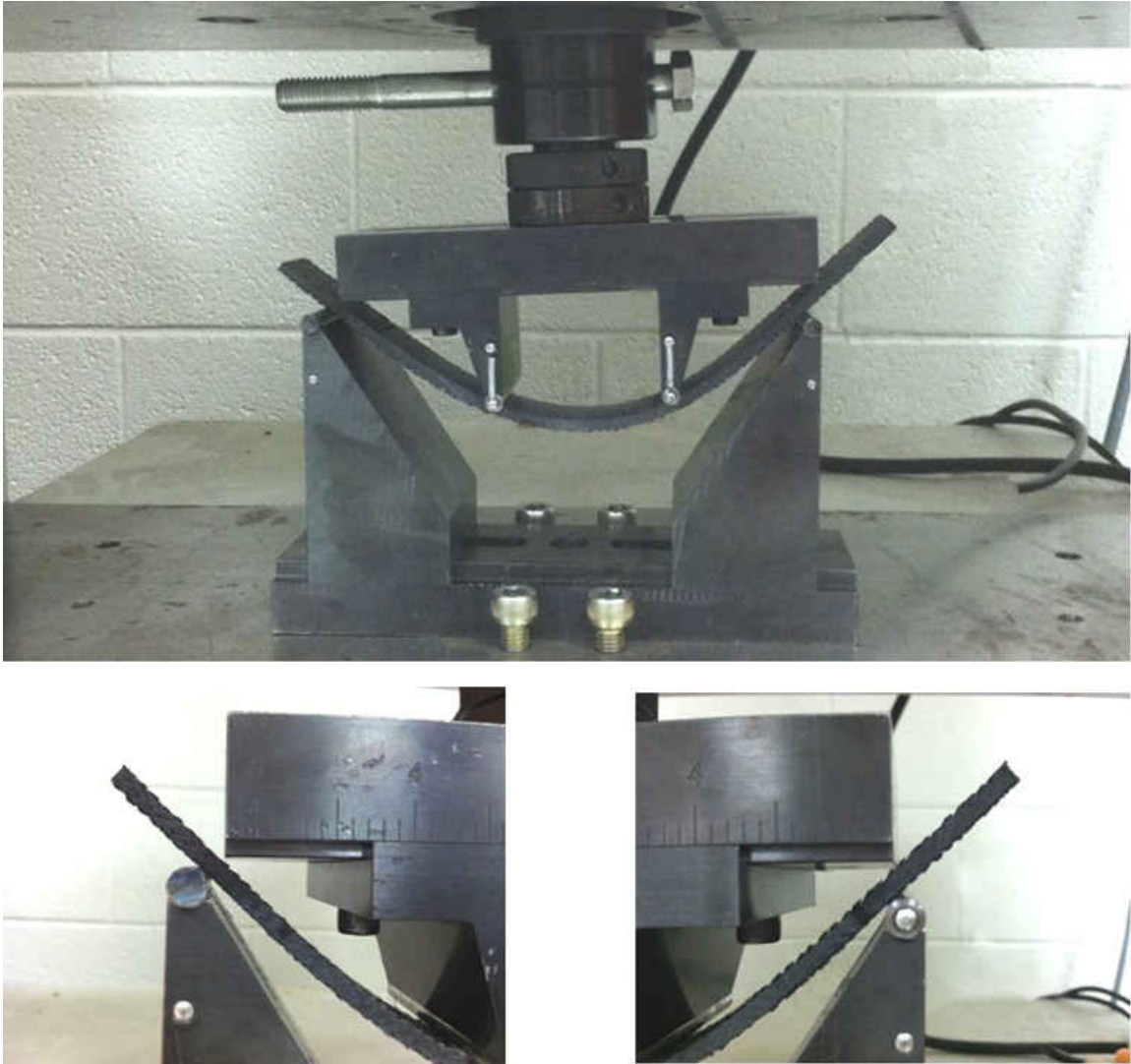


Figure 26. Geometrical limitation of four-point bending test fixture for $(\pm 45^\circ)_{15}$ samples.

Tables 8 shows the results of these tests and the calculated mechanical properties of $(\pm 45^\circ)_{15}$ samples based on these results. The modulus of elasticity is calculated from Equation 8. Stress – deformation curves for the three tested samples are plotted in Figure 27. Strain is calculated from Equation 9.

Table 8. Measured mechanical properties of $(\pm 45^\circ)_{15}$ samples.

Property	Measured average	CV ^a (%)
Maximum load (N)	192	7.5
Maximum stress (MPa)	92	1.6
Maximum strain (%)	2.3	3
Flexural Modulus (GPa)	12	1

^a CV = coefficient of variation = (standard deviation / average) x 100 %

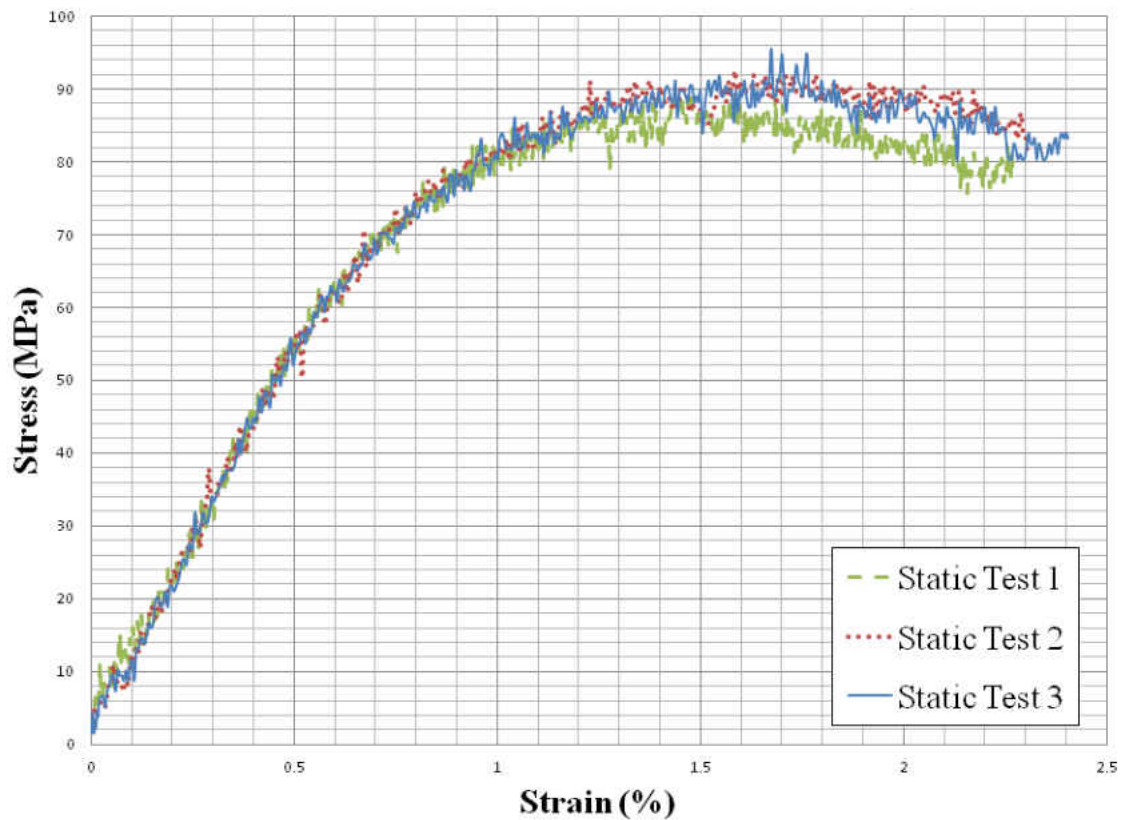


Figure 27. Stress-strain curves for four-point bending tests for $(\pm 45^\circ)_{15}$ samples.

Figure 28 shows a direct comparison between stress-strain curves for $(0^\circ/90^\circ)_{15}$ and $(\pm 45^\circ)_{15}$ samples. For cross-ply samples, the curve is linear up to failure, while for angle-ply samples the curve is non-linear and reaches a sort of “plateau” between strain

of 1.5% and 1.8%, where the displacement is increasing without hardly any increase in the load. Non-linearity of $(\pm 45^\circ)_{15}$ curves is due to the significant contribution of the polymer matrix [57]. Also, in literature [57], in four-point bending static tests, Theoretical predictions based on the Classical Laminate Theory showed that, for $(0/90)_s$ laminates, at the failure load, the transverse tensile strength of outer carbon fiber lamina is reached while for $(\pm 45^\circ)_{15}$ specimens the shear stress exceeds the shear strength of the matrix.

Herakovich *et al.* [80] studied the effect of fiber rotation on stiffness of $[(\pm 45^\circ)_3]_s$ carbon fiber/polyimide matrix composite laminates. They studied seven different laminates: $[0]_{12}$, $[90]_{12}$, $[(\pm 45)_3]_s$, $[(\pm 67.5)_3]_s$, $[(0/90)_3]_s$, $[(\pm 22.5)_3]_s$ and $[0/-45/90/45]_s$. By performing monotonic and cyclic tension tests, they determined the parameters in the mesoscale damage model developed by Ladeveze [81]. The results of their stress-strain tests are plotted in Figure 30. Only results of $[(0/90)_3]_s$ and $[(\pm 45)_3]_s$ laminates are shown.

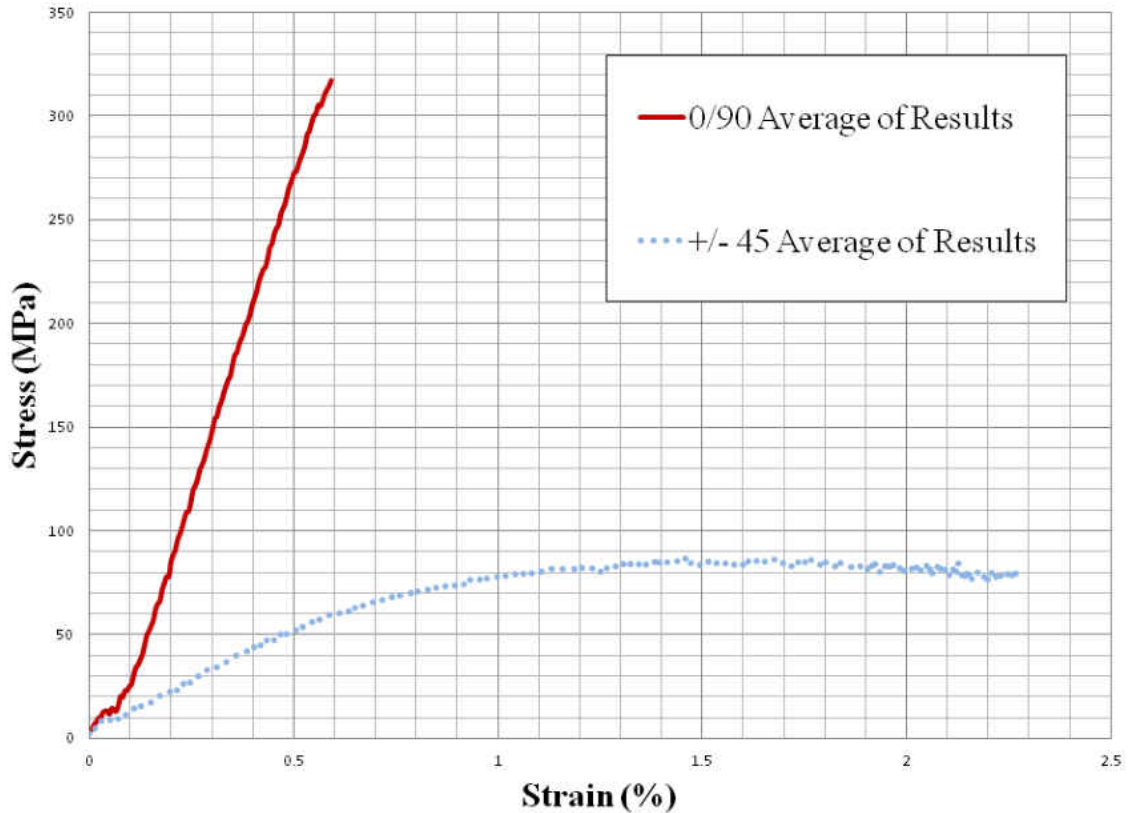


Figure 28. Average stress-strain curves for $(0/90)_{15}$ and $(\pm 45)_{15}$ samples.

Comparing Figures 28 and 29, it is observed that in both cases, higher stress was reached with lower amount of strain for $(0/90)$ laminates, while lower stresses in (± 45) laminates caused higher strains. Also, the slopes of the initial part of the graphs in Figure 28 correlate well with the results of Herakovich *et al.*. Herakovich *et al.* concluded that the orientation of fibers has a significant effect on the stiffness and lack of considering this effect in predicting large strain non-linear response and damage modeling prediction can result in significant errors [80]. The same conclusion can be derived based on the results of static four-point bending test shown in Figure 28.

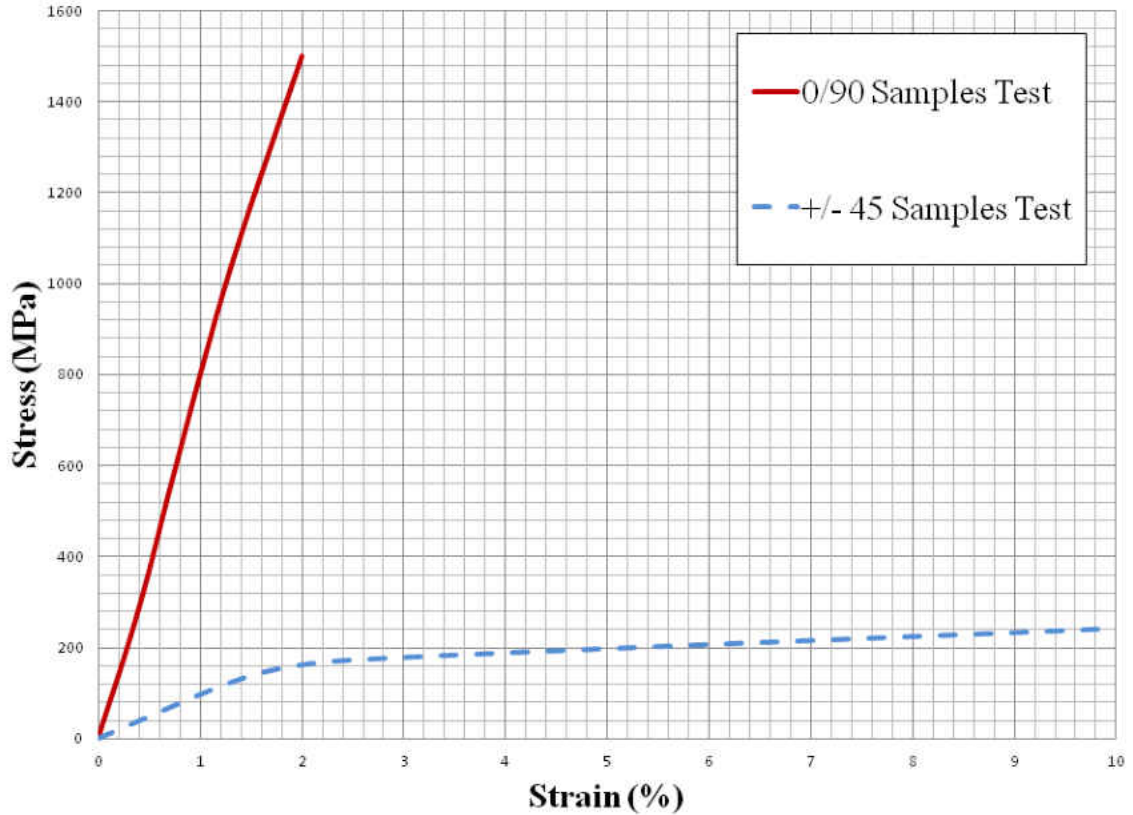


Figure 29. Stress-strain curves for (0/90) and (± 45) samples from [80].

In another study [57], Belingardi *et al.* studied static and fatigue behavior of two lay-ups, cross-ply (0/90)₁₀ and angle-ply (± 45)₁₀ carbon/glass hybrid composites. As part of their study, they compared static behavior of two different lay-ups as shown in Figure 30. Same trend is seen in current study. However, stresses are twice as higher as we observed in this study. As mentioned in literature, hybrid composites have higher static and fatigue strength [82-84]. Belingardi *et al.* measured mean ultimate flexural stress of 516 MPa and 145 MPa for cross-ply and angle-ply respectively. The mean stress values for cross ply were 3.5 times higher compared to angle-ply laminates. In current study, the mean values of maximum stresses are 314 MPa and 92 MPa for (0/90)₁₅ and (± 45)₁₅

respectively. Stresses for $(0/90)_{15}$ laminates are 3.4 times higher compared to $(\pm 45)_{15}$ laminates.

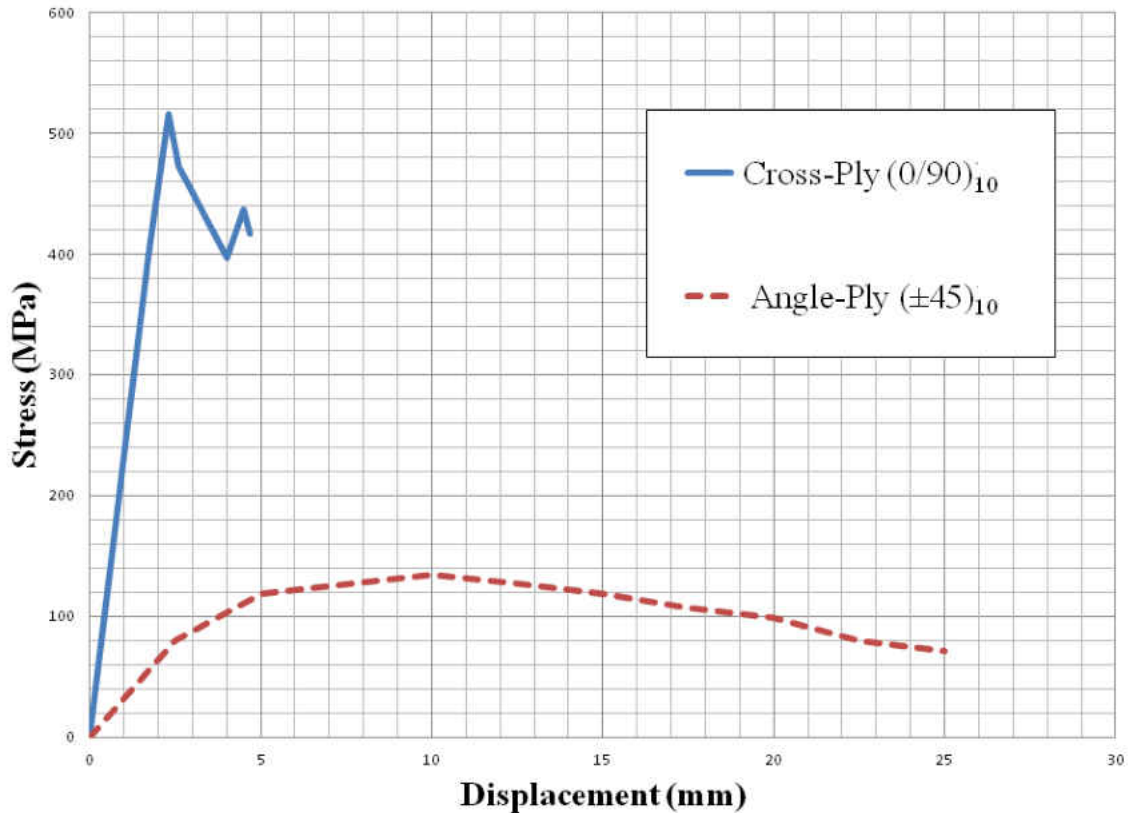


Figure 30. Stress – displacement curves for static flexural tests from [57].

Fatigue Test

Four-Point Fatigue Test – $(0^\circ/90^\circ)_{15}$ samples

Figure 31 shows four-point bending fixture. The frequency of the fatigue tests was 5 Hz. To make sure to record one complete cycle during each sampling, a scan time period of 0.3 seconds with total 30 scan points was chosen in Wintest[®]. Up to 3000 scans were made during each test. Figure 32(a) shows a characteristic loading sine wave. The maximum load applied for this sample was set to ± 340 N. the corresponding deformation of the mid-span of the beam was +3.22 mm and -3.26 mm as seen in Figure 32(b).

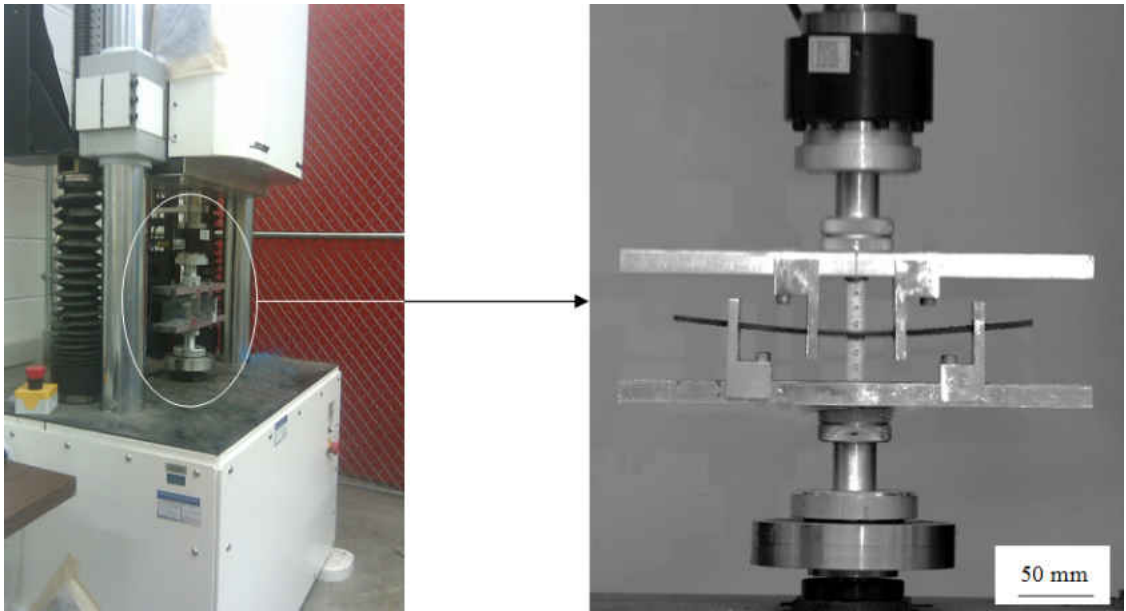
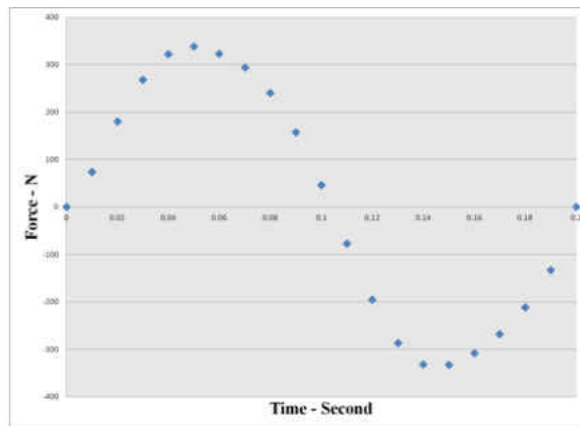
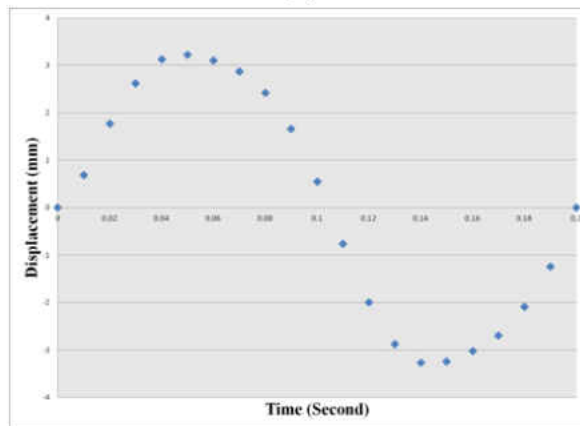


Figure 31. Fatigue test apparatus and four-point bending test fixture.



(a)



(b)

Figure 32. (a) Sample of sine wave applied (b) corresponding deformation at same cycle.

Four-point bending fatigue tests were carried out with maximum stresses of approximately 45%, 56%, 67%, 72% and 76% of the measured yield stress for $(0^\circ/90^\circ)_{15}$ samples. The resulting maximum stresses were nominally 140 MPa, 175 MPa, 210 MPa, 225 MPa and 240 MPa. The stopping limits on fatigue machine were set to ± 15 mm, so the tests were stopped automatically if the samples in the fixture broke apart resulting in the displacement of the crosshead exceeding 15 mm. For maximum stresses of 140 MPa and 175 MPa there were no failures detected and tests were stopped after 1.7×10^6 cycles. All other samples failed during cyclic loading. There was visible cracking through the thickness of the samples. Fatigue tests results are listed in Table 9.

Table 9. Fatigue lives for CFRP samples with $(0^\circ/90^\circ)_{15}$ layup.

Sample	Test Condition	R	σ_{\max}/σ_y	Number of Cycles
2	$\sigma_{\max} = 140$ MPa	-1	0.45	1.72×10^6
14				1.76×10^6
1	$\sigma_{\max} = 175$ MPa	-1	0.56	1.71×10^6
3				1.70×10^6
4				1.71×10^6
6	$\sigma_{\max} = 210$ MPa	-1	0.67	1.91×10^5
11				4.66×10^5
12				4.73×10^5
8	$\sigma_{\max} = 225$ MPa	-1	0.72	1.31×10^5
9				1.15×10^5
10				1.21×10^5
5	$\sigma_{\max} = 240$ MPa	-1	0.76	3.20×10^4
13				2.40×10^4
15				4.04×10^4

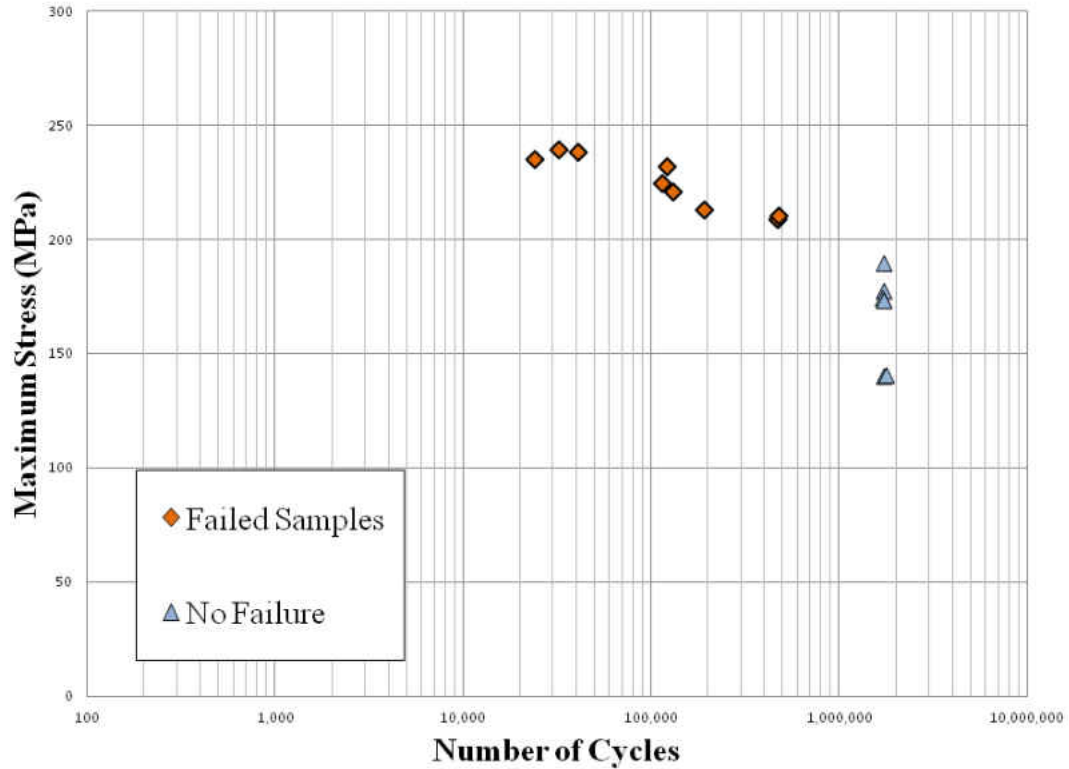


Figure 33. S-N data for CFRP samples with $(0^\circ/90^\circ)_{15}$ layup.

Discussion of Fatigue Results for $(0^\circ/90^\circ)_{15}$ Samples

The fatigue results shown in Table 9 and Figure 33 show the expected downward trend in fatigue life with increasing maximum applied stress. There appears to be a threshold for ‘infinite’ life, defined as 1.7 million cycles in the current work, at a maximum stress of about 200 MPa. No change in mechanism was observed for specimens that did exhibit failure.

Tomita *et al.* examined the bending fatigue behavior of a variety of different carbon fibers and layups in fully-reversed bending at a frequency of 30 Hz [55]. As shown in Figure 34 for a cross-ply specimens and fatigue life of 10,000 cycles, they found stress amplitudes ranging from 450-475 MPa could be applied. This would

correspond to maximum stresses of 230-240 MPa, very consistent with the values observed in the current work.

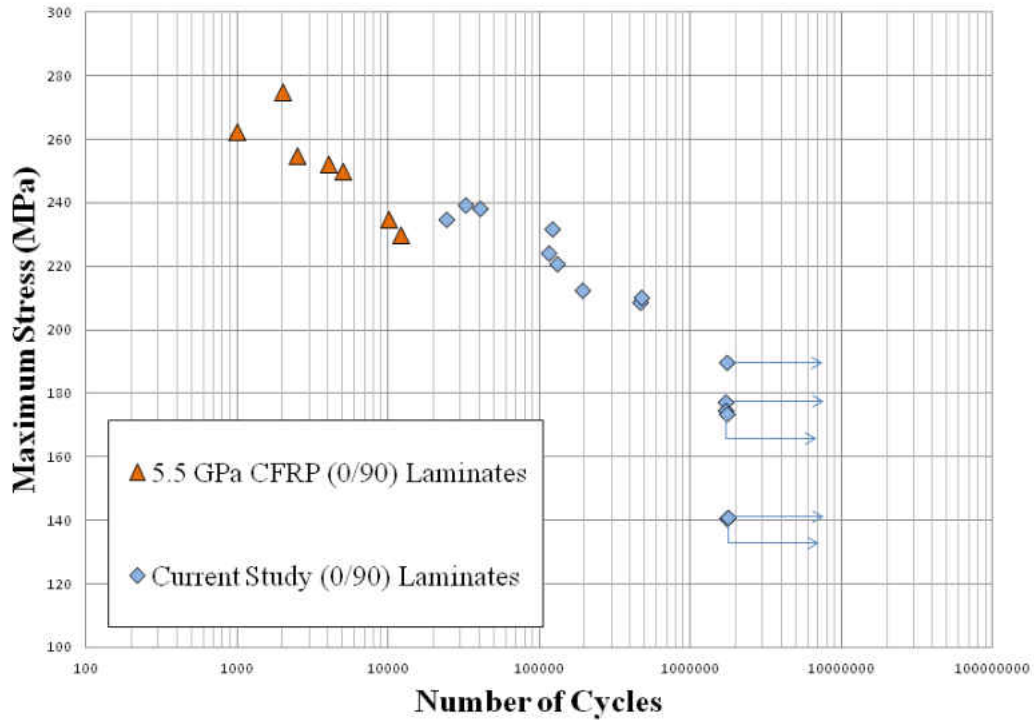


Figure 34. S-N diagram for (0/90) laminates with 5.0 GPa CFRP from [55].

Based on previous results in the literature, e.g. [85], fully-reversed fatigue loading is expected to significantly reduce the fatigue life of carbon composites compared to positive values of R between 0 and 1. Comparing the current results with those of Kawai and Maki [56], we see that this is indeed the case. Under room temperature bending fatigue at R = 0.1 and 10 Hz, those authors found that a maximum stress of about 700 MPa resulted in a fatigue life of 1 million cycles. In the current study, the maximum stress resulting in failure at 1 million cycles was only 200 MPa. For fatigue lives of 10,000 to 1,000,000 cycles, the allowable maximum stress in the work of Kawai and Maki decreased from about 1000 MPa to 700 MPa (a decrease of 30%). In the current work, for the same range of fatigue lives, the allowable maximum stress decreased from

about 250 MPa to about 200 MPa (a decrease of 20%), perhaps indicating a fundamental difference in the damage accumulation in the material during testing. Additional characterization work is needed to determine if this is the case. S-N diagram for $(0/90)_3$ CFRP at room temperature is shown in Figure 35.

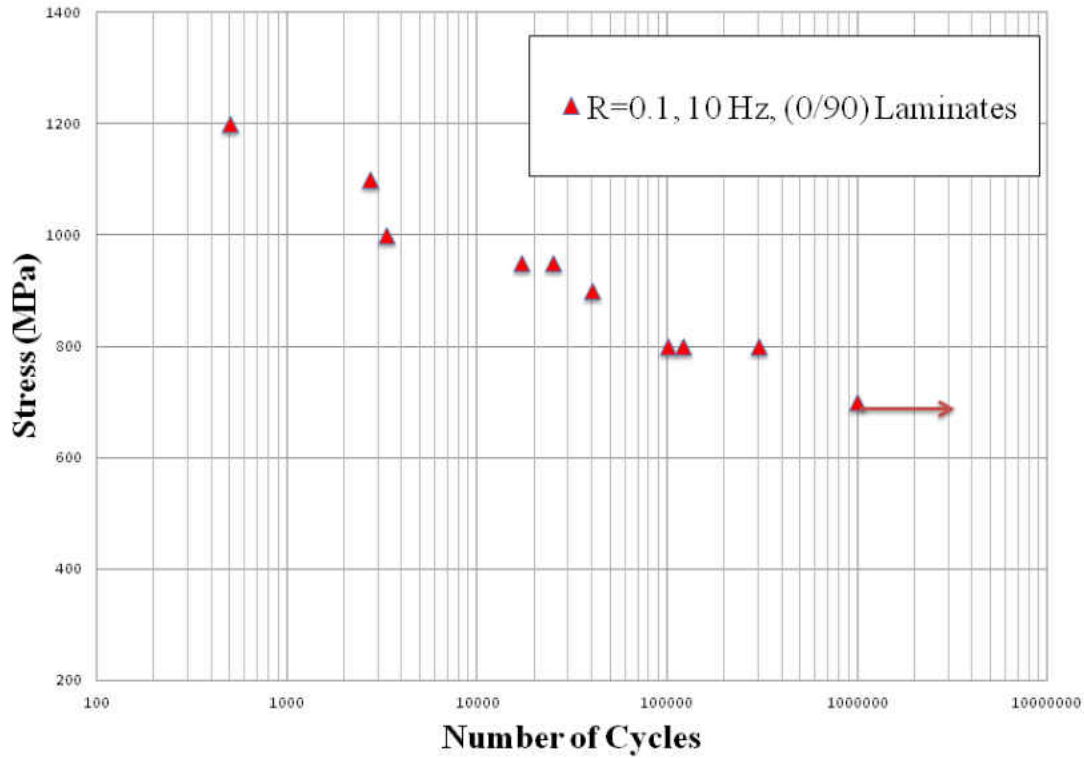


Figure 35. S-N diagram for $(0/90)_3$ at room temperature in [56].

Predicting Fatigue Life of Composite Samples

As reported in some bending fatigue studies [30, 86-88] , stiffness degradation is measured as reduction in relative bending moment (RBM) during fatigue loading. RBM is defined as the ratio between bending moment applied at first cycle and bending moment applied at N^{th} cycle.

As tests in this study were done as load-controlled, and as there is a direct relation between stiffness and flexural modulus of the beam, we will calculate the decay in

flexural modulus of the beam as it goes under cyclic loading. Stiffness of a beam can be defined as [89, 90]:

$$K = \frac{F}{D} \quad (12)$$

where K is the stiffness of the beam, F is the applied force and D is the mid-span deflection caused by force, F. Also for four-point bending we have [91, 92]:

$$D = \frac{Fa}{48EI} (4a^2 - 3L^2) \quad (13)$$

where a is 55 mm (see Figure 19), E is the flexural modulus of the beam, L is the length of the beam (170 mm) and I is the moment of inertia. After plugging in values of a and L and rearranging Equation 13 we have:

$$E = \frac{K}{I} (85.48 \times 10^3) \quad (14)$$

To find reduction in the flexural modulus, the load and mid-span deformation of the composite beams recorded by WinTest[®] were collected at different lives of each sample before failure. For each sample at each life, averages of 30 measurements were calculated. And flexural moduli at different lives were calculated using Equation 14. Figures 36 and 37 show flexural modulus plotted vs. lives of tested samples. In Figures 36 and 35 average measurements for all samples with same value of stress ratio are plotted.

As seen, during bending fatigue tests, samples showed a progressive decrease in stiffness which is result of damage accumulation in them. As the amount of applied stress goes higher, the amount of decay in stiffness is higher. Normalized flexural modulus vs. number of cycles for tested samples is represented in Figures 36 and 37 in linear and logarithmic scale respectively. Although samples with applied stress of 45% and 56% of

yield stress didn't failed during fatigue tests, in Figure 36 there is decay in flexural modulus. The amount of this decay is more in samples 1, 3 and 4 where the stress was 56% of yield stress.

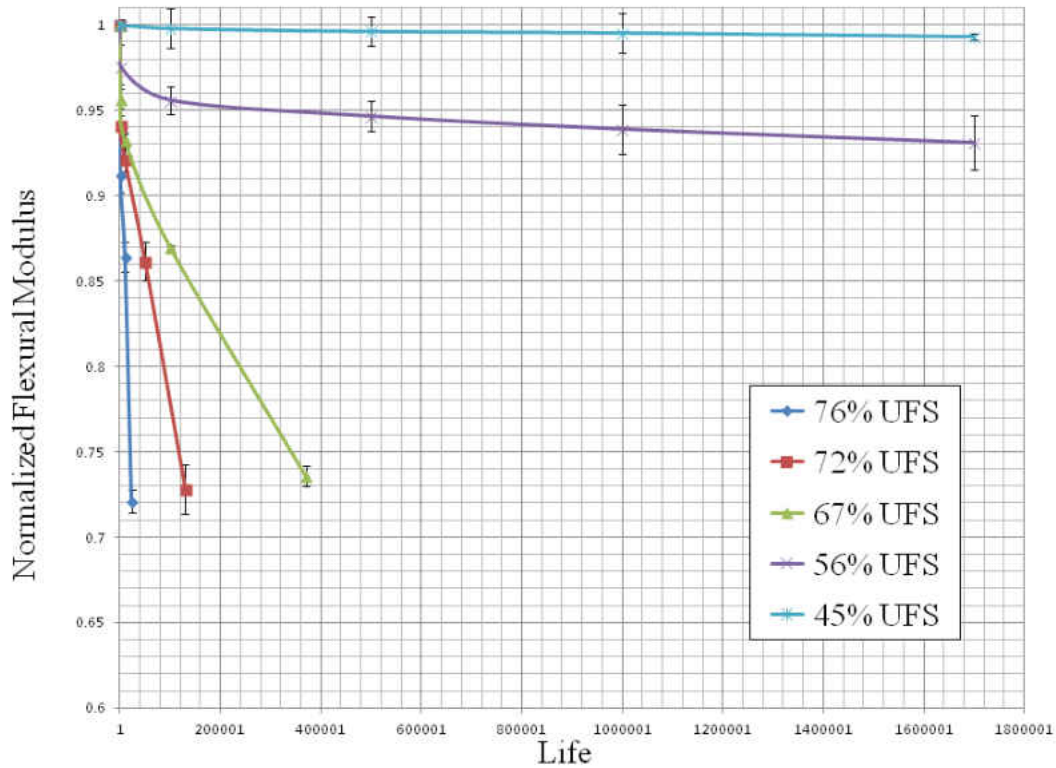


Figure 36. Loss in flexural modulus vs. lives of $(0^\circ/90^\circ)_{15}$ samples.

The linear curve shows at 76% and 72% of maximum stress, the loss of stiffness is almost linear while for 67% and 56% the loss of stiffness is initially greater and at 56% and 45% it will eventually level off. As Figure 37 shows, at failure, samples showed 25% decrease in flexural modulus.

When the loss in flexural modulus is plotted versus natural log of the number of cycles to failure, it is seen that flexural modulus shows an exponential decay which can be expressed as:

$$E = E_0 e^{AN} \quad (15)$$

where E is flexural modulus after N cycles of loading, E_0 is the flexural modulus at first cycle calculated from Equation 8 and A is a constant. Values of A for each sample can be calculated by using Figure 37, rearranging Equation 15 and solving for A . Table 10 shows the measured value of A for each sample.

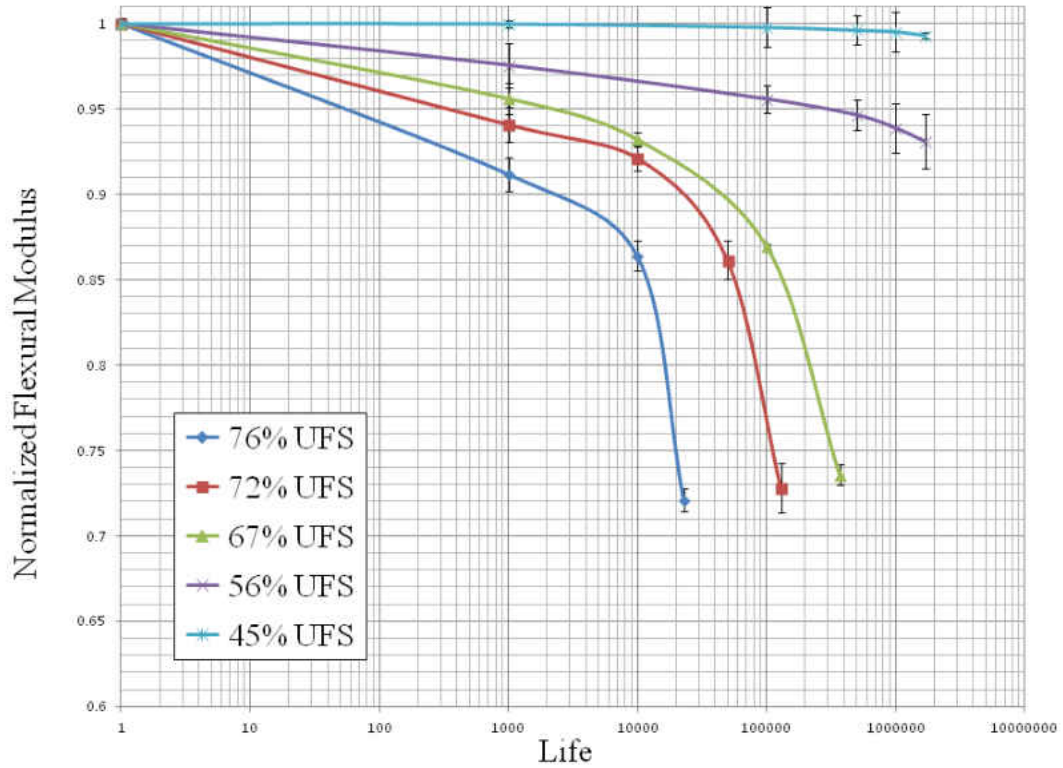


Figure 37. Loss in flexural modulus vs. lives of $(0^\circ/90^\circ)_{15}$ samples (log scale).

Table 10. Values of Constant A in Equation 15.

Sample	Test Condition	R	σ_{\max}/σ_y	A
6	$\sigma_{\max} = 210$ MPa	-1	0.67	-1×10^{-6}
11				-6×10^{-7}
12				-9×10^{-7}
8	$\sigma_{\max} = 225$ MPa	-1	0.72	-2×10^{-6}
9				-2×10^{-6}
10				-2×10^{-6}
5	$\sigma_{\max} = 240$ MPa	-1	0.76	-8×10^{-6}
13				-6×10^{-6}
15				-7×10^{-6}

As seen from Figures 36 and 37 and Table 10, if less stress is applied, less damage occurs. As a result, the magnitude of the slope (flexural modulus decay rate) decreases and the life of the composite will increase. The fatigue life of composite samples can be expressed as:

$$N_f = e^{\frac{E-E_0}{E_0 B}} \quad (16)$$

where N_f is the estimated fatigue life of the composite samples and B is decay constant which will be depending upon amount of stress applied. Solving Equation 16 for current results gives us $B = -0.002$.

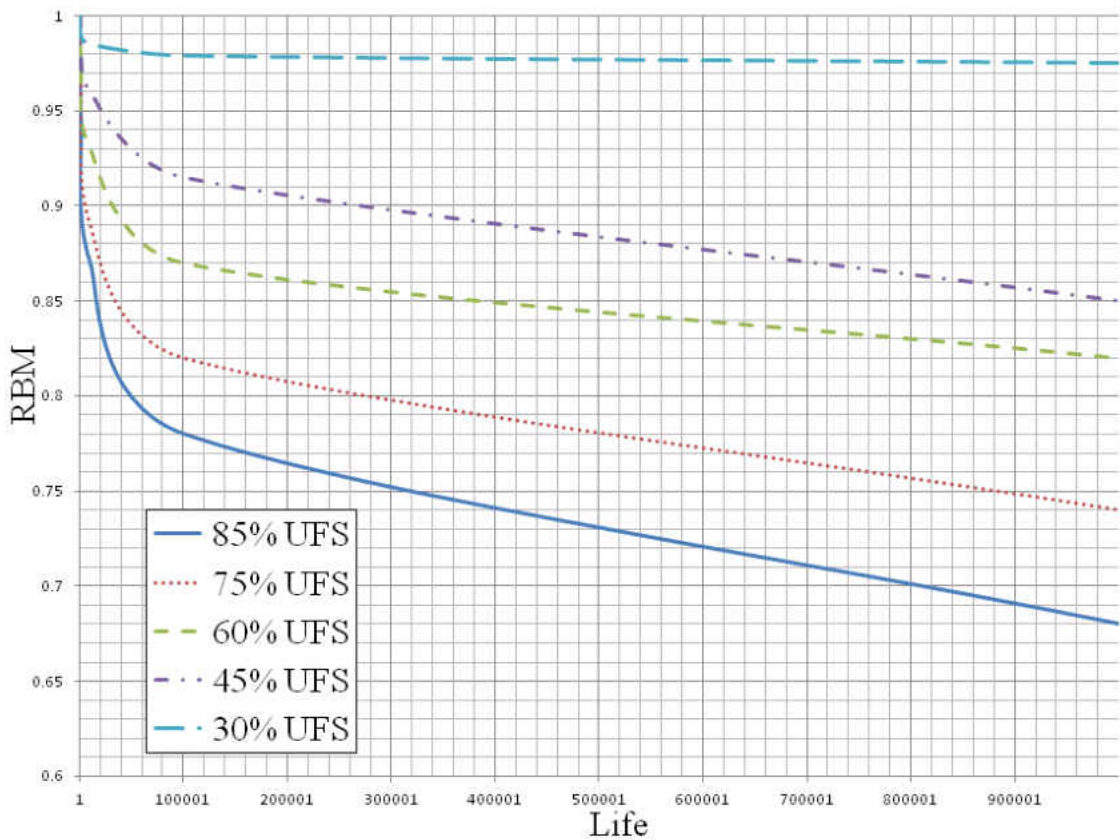


Figure 38. Loss of applied bending moment through 10^6 cycles versus number of cycles for $(0/90)_{15}$ samples (linear scale) in [57].

Belingardi *et al.* [27] evaluate the stiffness degradation by measuring reduction of RBM during fatigue tests. They plotted RBM vs fatigue life of their tested samples in linear and logarithmic scale as seen in Figures 38 and 39. They observed that in linear scale, loss of material stiffness was initially greater and as life went higher the curves leveled off. In logarithmic scale, they observed that at first couple of hundred of cycles, loss of stiffness was negligible and the stiffness drop was almost linear with logarithmic of number of cycles. They found the threshold for their fatigue tests at 30% of ultimate flexural stress [27].

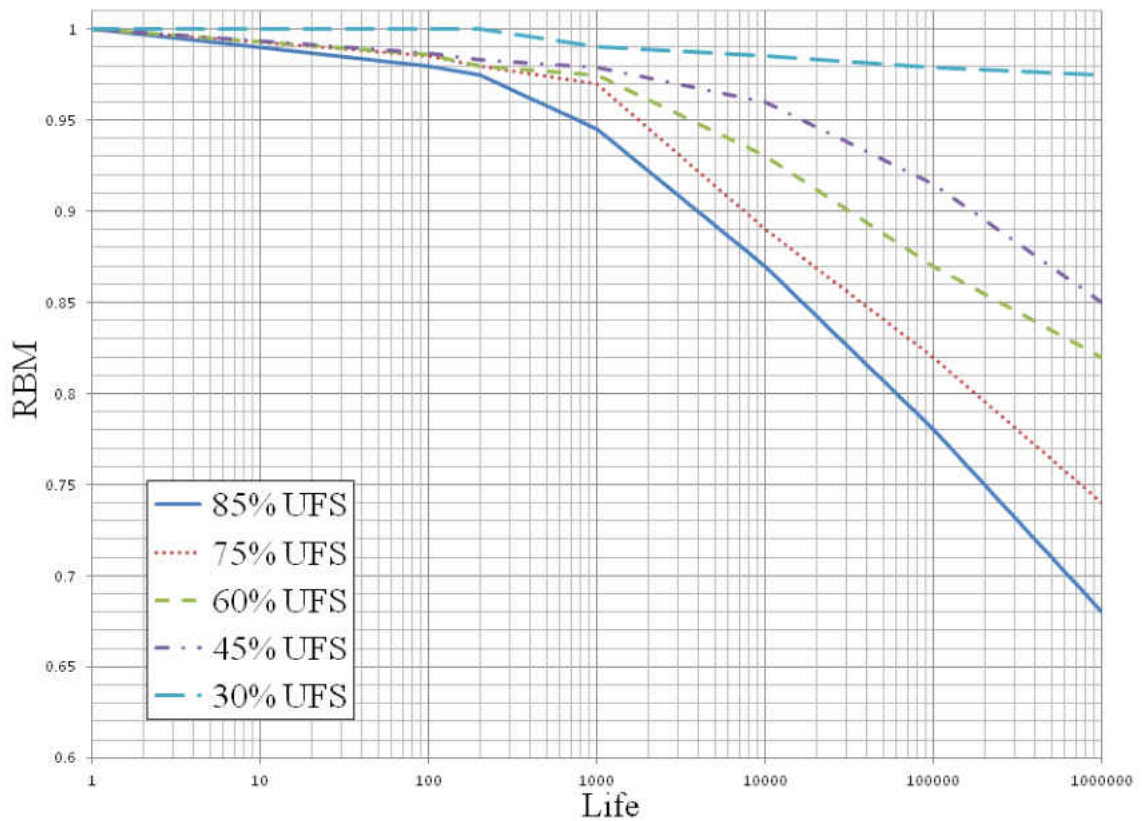


Figure 39. Loss of applied bending moment through 10^6 cycles versus number of cycles for $(0/90)_{15}$ samples (logarithmic scale) in [57].

Post-Fatigue Tests of $(0/90)_{15}$ Samples

To investigate more the mechanical properties of $(\pm 45^\circ)_{15}$ samples, static four-point bending tests were done on Samples 1, 3 and 4 after undergoing fatigue for 1.7×10^6 cycles with applied stress equal to 56% of the yield stress. The results of these static tests are shown in Figure 40. Also, the averages of three tests along with average of static tests before fatigue are plotted in Figure 41.

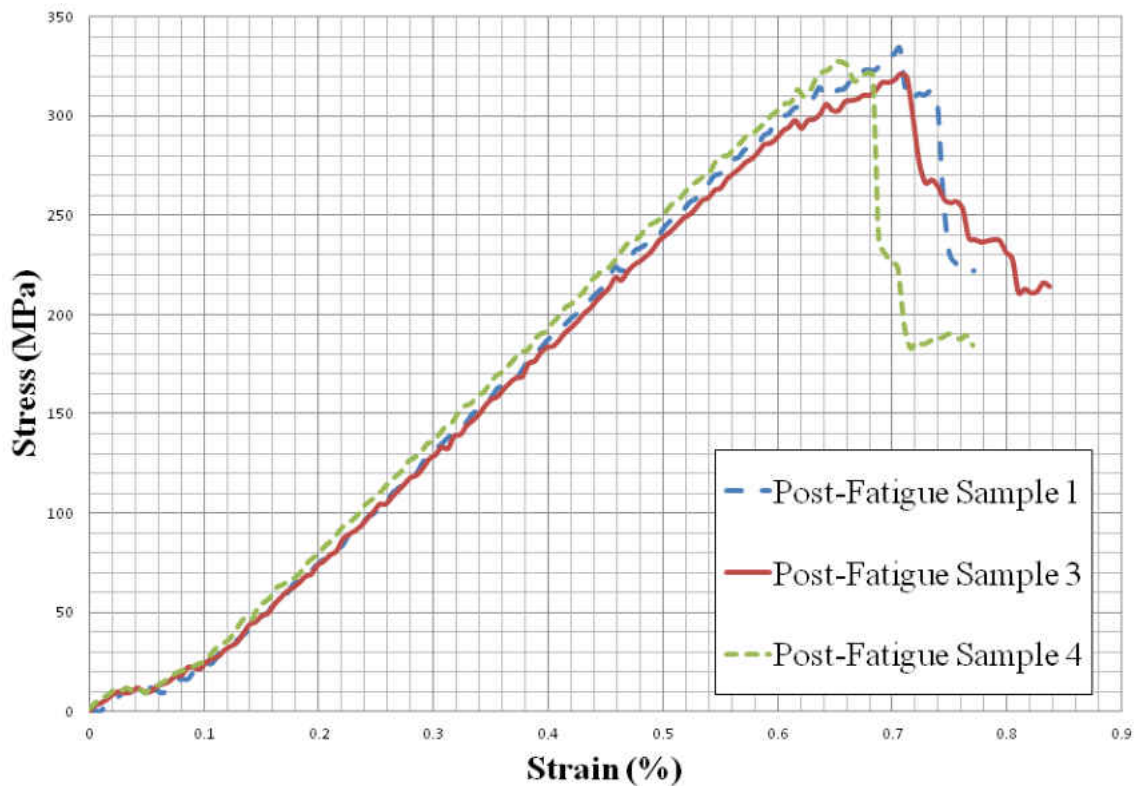


Figure 40. Post-fatigue results of static four-point bending test for $(0/90)_{15}$ Samples.

As observed in Figure 41, same amount of stress was reached by samples before failure. Same as before, the curve is linear up to yield point. However, the slope of the curve is less than the curve from samples before fatigue tests. For the same amount of stress, higher strains were reached. These results are consistent with the results from previous section. As seen in Figure 36 and 37, for samples with applied stress of 56% of yield stress, after 1.7×10^6 cycles, there is a loss in flexural modulus of 7%. As seen in

Figure 41, at yield stress of 314 MPa, there an increase of 8% in the amount of strain, which is due to decay in flexural modulus because of cyclic loading.

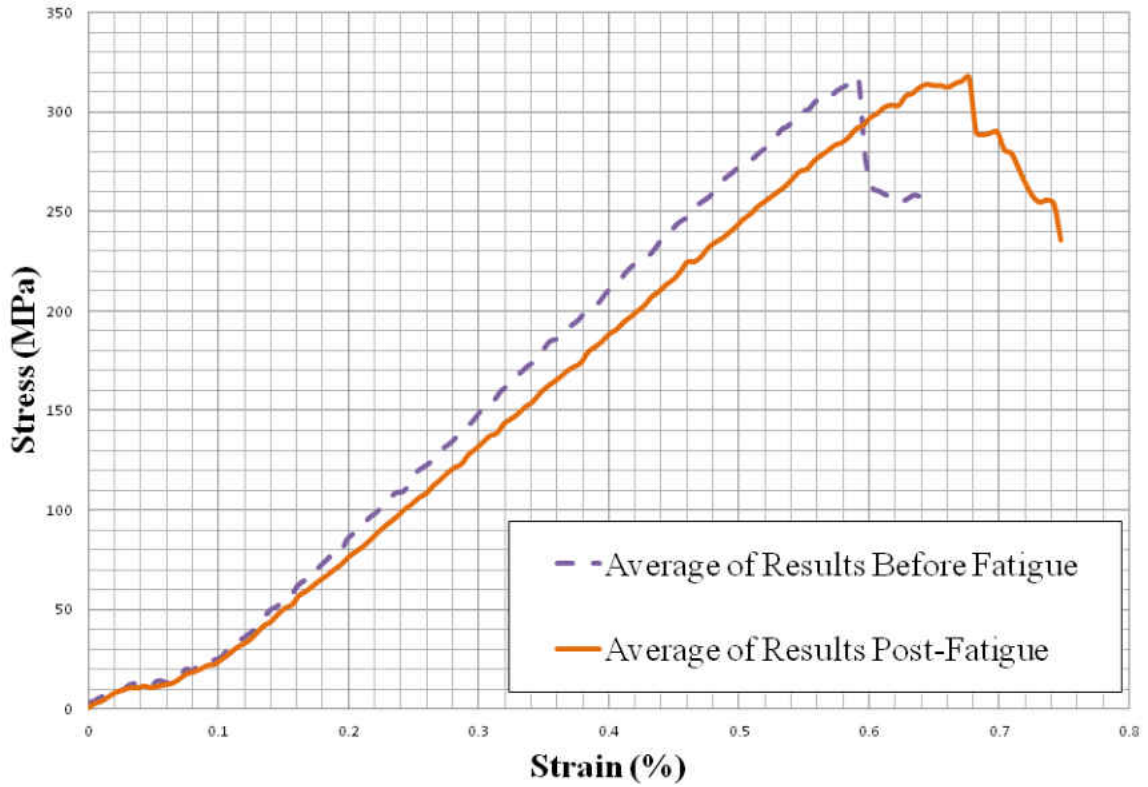


Figure 41. Average of results before fatigue tests and after fatigue tests for samples 1, 3 and 4 of $(0/90)_{15}$.

Four-Point Fatigue Test – $(\pm 45^\circ)_{15}$ samples

Four-point bending fatigue tests were carried out with a maximum stress of 80 MPa, approximately 85% of the measured yield stress for $(\pm 45^\circ)_{15}$ samples. Table 11 shows the results of these tests.

Table 11. Fatigue lives for CFRP samples with $(\pm 45^\circ)_{15}$ layup.

Sample	Test Condition	R	σ_{\max}/σ_y	Number of Cycles
8	$\sigma_{\max} = 80 \text{ MPa}$	-1	0.85	1.70×10^6
9				1.71×10^6
10				1.71×10^6

Although the applied stress was 85% of the measured yield stress, none of the samples failed, nor any sign of crack was seen. Tests were stopped once the number of cycles passed 1.7×10^6 .

As shown in Figure 27, the beam mid-span deformation for 80 MPa is about 16 mm. As mentioned in Table 4, the maximum deformation of the fatigue fixture is 17 mm. As a result, testing composite samples with higher ratio of stress was not possible.

Discussion of Fatigue Results for $(\pm 45^\circ)_{15}$ Samples

Based on similar studies in the literature e.g. [27], the lives of $(\pm 45^\circ)_{15}$ samples at 75% of the yield stress, were expected to be less than 1.7×10^6 cycles. But there were no signs of failure in $(\pm 45^\circ)_{15}$ samples. To investigate whether there was any degradation in stiffness of samples, a full analysis was performed on the recorded data on three samples to compare corresponding deformation of mid-span of the samples in different cycles. Same analysis as $(0/90)_{15}$ fibers were done using Equations 12, 13 and 14. Figures 42 and 43 show average normalized flexural modulus plotted versus lives of three tested samples in linear and logarithmic scale respectively. For each sample at each life, averages of 30 measurements were calculated. And flexural moduli at different lives were calculated using Equation 14.

As seen in figure 42, there is decay in flexural modulus till 100,000 cycles. After this point there is a slight increase in flexural modulus. The same trend is observed when flexural modulus is plotted versus life of samples in logarithmic scale. The minimum amount of flexural modulus observed during this period was 0.97 of the value, and then afterwards the value is gone up to 0.98 of the initial value of flexural modulus

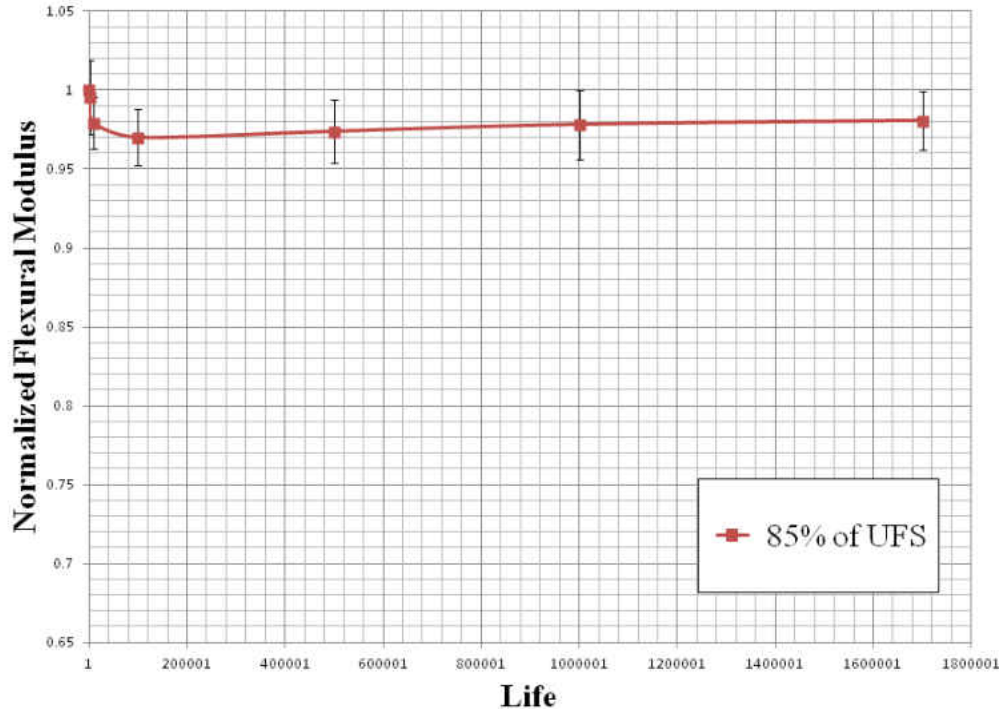


Figure 42. Variation in flexural modulus vs. lives of $(\pm 45^\circ)_{15}$ samples (linear scale).

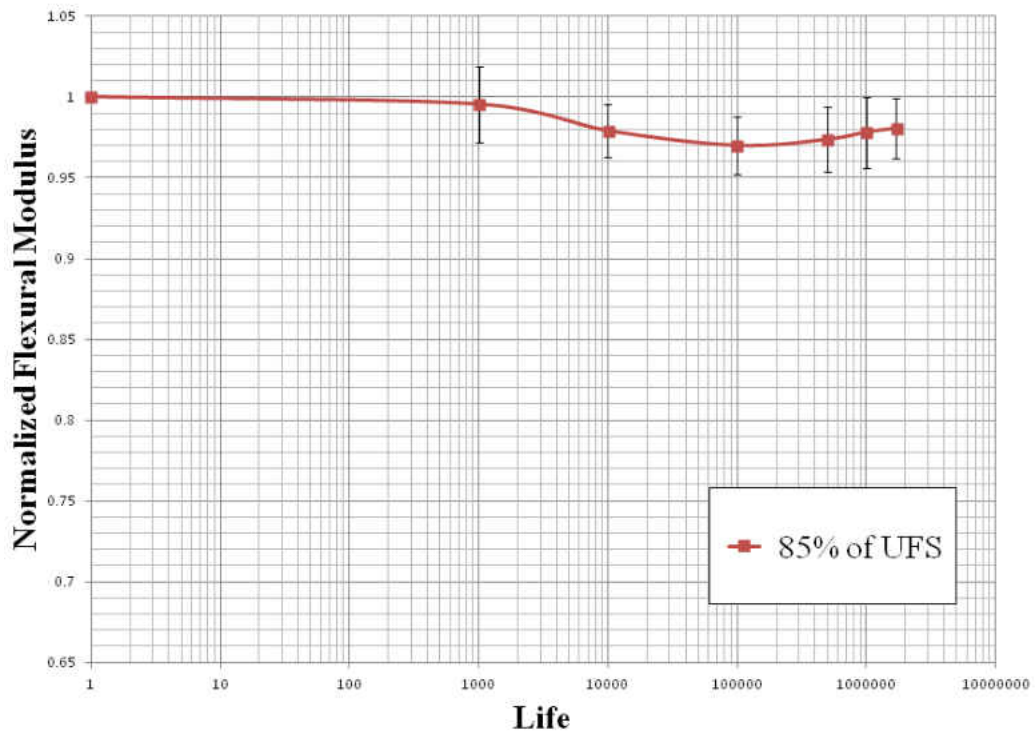


Figure 43. Variation in flexural modulus vs. lives of $(\pm 45^\circ)_{15}$ samples (Logarithmic scale).

Post-Fatigue Tests of $(\pm 45^\circ)_{15}$ Samples

Based on experimental results and the aforementioned analysis, to investigate more the mechanical properties of $(\pm 45^\circ)_{15}$ samples, static four-point bending tests were done on Samples 8, 9 and 10 after undergoing fatigue for 1.7×10^6 cycles. First, Sample 8 was put into four-point bending test and the first test was done. Compared to static test on other samples from the same plate, higher stresses were reached. As before, because of geometrical limitations of the four-point bending fixture, the test was stopped before any visible crack or failure. The same sample was put back into the fixture and the test was repeated. This procedure was repeated two more times (four total) and the stress-strain graphs were plotted in Figure 44. Figure 45 shows similar results for Sample 9 and results of similar tests are shown in Figure 46. As seen, the stresses reached on the first post-fatigue test are slightly higher than next three tests. Figure 47 shows direct comparison of the average values of stress vs. strain for samples tested before fatigue tests, and samples after 1.7×10^6 cycles of loading.

In Figures 44, 45 and 46, the graph is linear until about 0.5% strain, which corresponds to about 60 MPa of bending stress in the samples. After this point for the same percent of strain, stresses are higher for samples which have been through fatigue loading (Figure 47).

As observed in Figures 42 and 43, there is variation in flexural modulus of $(\pm 45^\circ)_{15}$ samples as they are exposed to cyclic loading. From 1 to 100,000 cycles, there is decay in flexural modulus of the beam. From this point there is a slight increase in stiffness of the beam. Since the tests were stopped at 1.7×10^7 cycles, there is no information after this point. As seen in Figure 47, for the stress of 80 MPa, the strain for

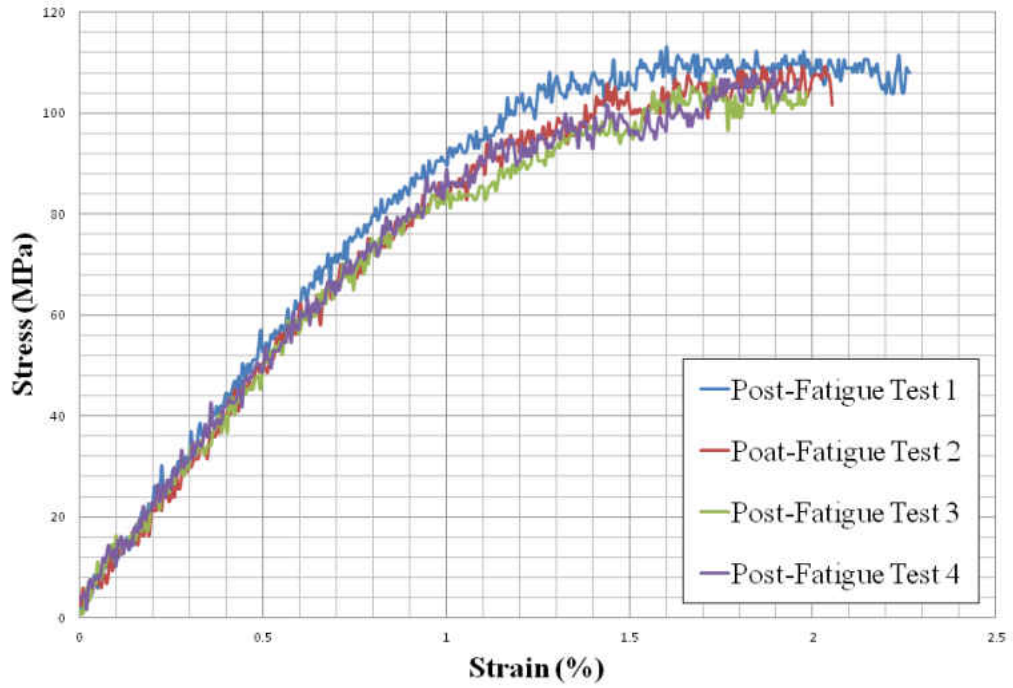


Figure 44. Post-fatigue results of static four-point bending test for Sample no. 8.

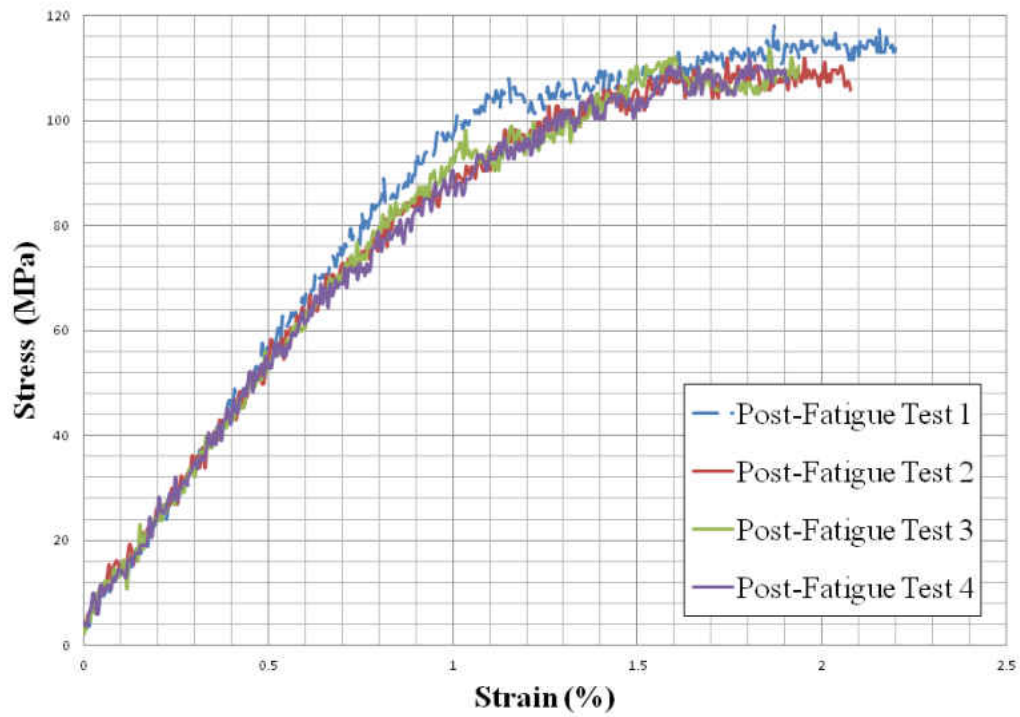


Figure 45. Post-fatigue results of static four-point bending test for Sample no. 9.

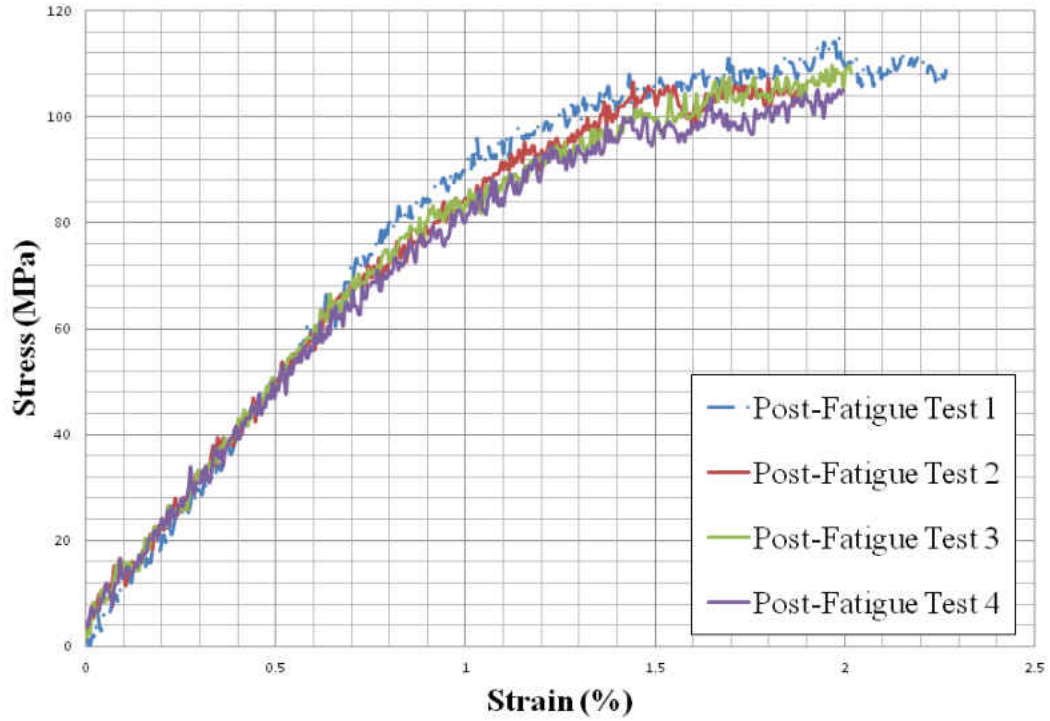


Figure 46. Post-fatigue results of static four-point bending test for Sample no. 10.

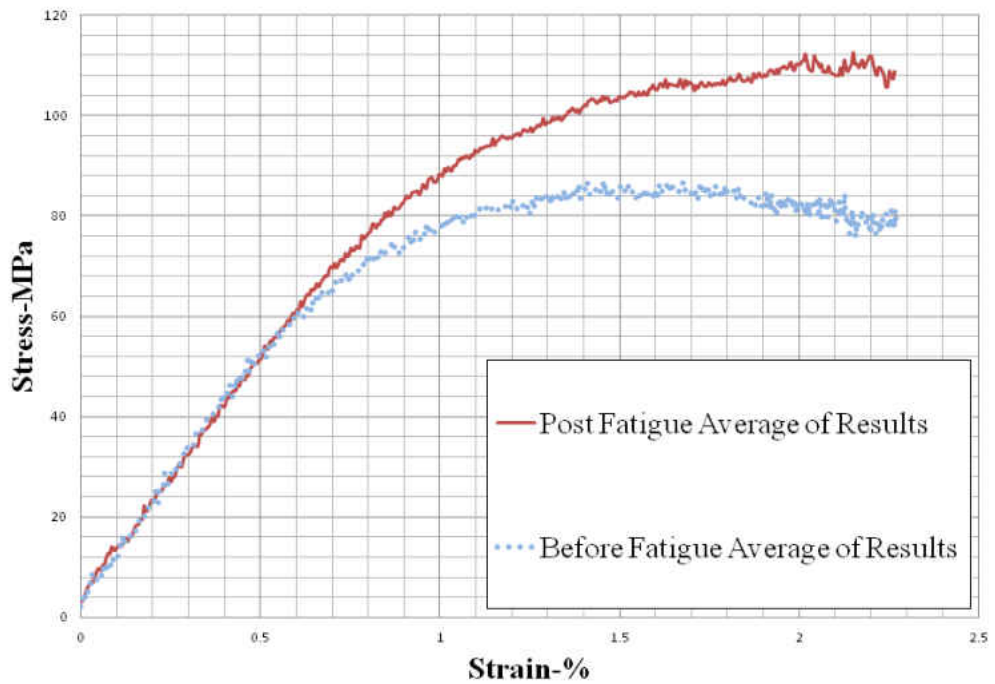


Figure 47. Direct comparison of the average values of stress-strain for samples tested before fatigue, and samples after 1.7×10^6 cycles of fatigue loading.

post-fatigue results, the strain reached is 40% less than the samples before fatigue tests. This can be result of aforementioned variations in the value of flexural modulus.

Bryan Harris in [19, 25] mentioned a phenomena in composites called “wear-in”. Most composites sustain damage at early life during fatigue loading. The damage is distributed over the stressed area and usually reduces the stiffness of the composite. Wear-in is usually accompanied by a slight increase in strength at early stages of cyclic loading. These increases are results of slight improvement in fiber alignment. Also, there are small stress-induced, viscoelastic or creep deformations in the matrix. As discussed in discussion of static test results, orientation of fibers has significant effect on stiffness and strength of laminates. Also, as mentioned, in angle-ply laminates matrix has great contribution to stiffness of the samples. Considering the fact that the resin used in this study was polyester resin which is an intermediate viscose resin with viscosity of 90 GPa (900 poise) and the orientation of the fibers as angle-ply, might have made a stronger case for “wear-in” phenomena in current study. Further investigations and longer fatigue tests, over 10^7 needed to see if this is the case.

CHAPTER IV

SUMMARY AND CONCLUSION

In this research, static and fatigue behavior of carbon fiber and polyester matrix were studied. The composite laminates used for this study were 15 layers of cross-ply, $(0/90)_{15}$, and angle-ply, $(\pm 45)_{15}$ carbon fibers.

- 1) Static four-point bending tests were carried out on three $(0^\circ/90^\circ)_{15}$ to measure the mechanical properties of CFRP. Testing was displacement-controlled at the rate of 10 mm/min until failure. In all cases, samples failed by cracking/buckling on the compressive side of the sample. Average stress of 314 MPa was reached at failure of samples. This stress correlates with average strain of 0.58% at failure.
- 2) Static four-point bending tests were carried out on three samples from the $(\pm 45^\circ)_{15}$ plate to measure mechanical properties of the CFRP. Tests were displacement-controlled at the rate of 10 mm/min. In all three tests, no visual fracture or failure of the samples was observed. Average maximum stress of 92 MPa was reached during the tests, which correlates with 2.3% average maximum strain.
- 3) For cross-ply samples, Stress-strain curve is linear up to failure, while for angle-ply samples the curve is non-linear and reaches a sort of “plateau” between strain of 1.5% and 1.8%, where the displacement is increasing without hardly any increase in the load. 3.4 times higher stresses were reached during four-point

static bending test of $(0^\circ/90^\circ)_{15}$ samples compared to $(\pm 45^\circ)_{15}$. Same trend was seen in literature for similar tests.

- 4) Four-point bending fatigue tests were carried out on $(0/90)_{15}$ sample with stress ratio, $R = -1$ and frequency of 5 Hz. Applied maximum stresses were approximately 45%, 56%, 67%, 72% and 76% of the measured yield stress for $(0^\circ/90^\circ)_{15}$ samples. The resulting maximum stresses were nominally 140 MPa, 175 MPa, 210 MPa, 225 MPa and 240 MPa. For maximum stresses of 140 MPa and 175 MPa there were no failures detected and tests were stopped after 1.7×10^6 cycles. All other samples failed during cyclic loading. There was visible cracking through the thickness of the samples. The expected downward trend in fatigue life with increasing maximum applied stress was observed in S-N curves of samples. There appears to be a threshold for 'infinite' life, defined as 1.7 million cycles in the current work, at a maximum stress of about 200 MPa.
- 5) The decay in flexural modulus of the beam as it goes under cyclic loading was calculated and plotted. It was seen that flexural modulus shows an exponential decay which can be expressed as: $E = E_0 e^{AN}$.
- 6) Post-fatigue static tests were done on $(0/90)_{15}$ samples which went under cyclic loading with applied stress of 56% of yield stress. Samples showed same yield stress with higher amount of strains. This can be result of decay in stiffness of the beam observed in 5.
- 7) Four-point bending fatigue tests were carried out on three $(\pm 45)_{15}$ samples with stress ratio, $R = -1$ and frequency of 5 Hz. Maximum applied stress was 80 MPa, approximately 85% of the measured yield stress of $(\pm 45^\circ)_{15}$ samples. None of the

samples failed, nor any sign of crack was seen. Tests were stopped once the number of cycles passed 1.7×10^6 .

- 8) Flexural moduli of the $(\pm 45)_{15}$ samples as they go under cyclic loading were calculated and plotted versus number of cycles. It was observed that there was decay in flexural modulus till 10,000 cycles. After this point there was a slight increase in flexural modulus.
- 9) Pre-cycled samples of $(\pm 45^\circ)_{15}$ were tested in four-point bending machine to measure the strength after fatigue tests. All three samples showed 15% increase in maximum stress after going through 1.7×10^6 cycles of fatigue loading.

APPENDICES

APPENDIX A. CAD Drawings of four-point bending fatigue fixture

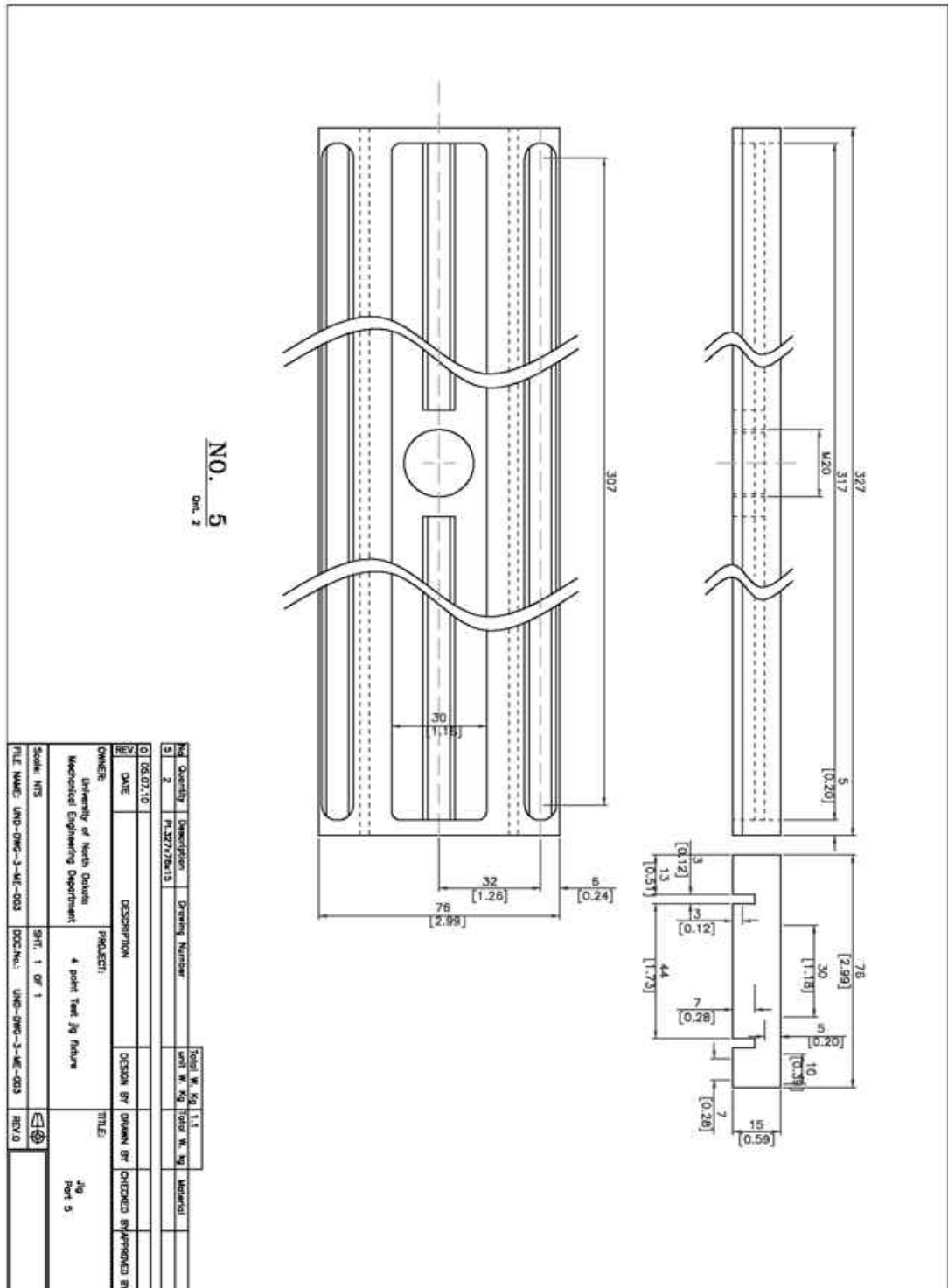


Figure 48. Fatigue fixture, drawing of part 5.

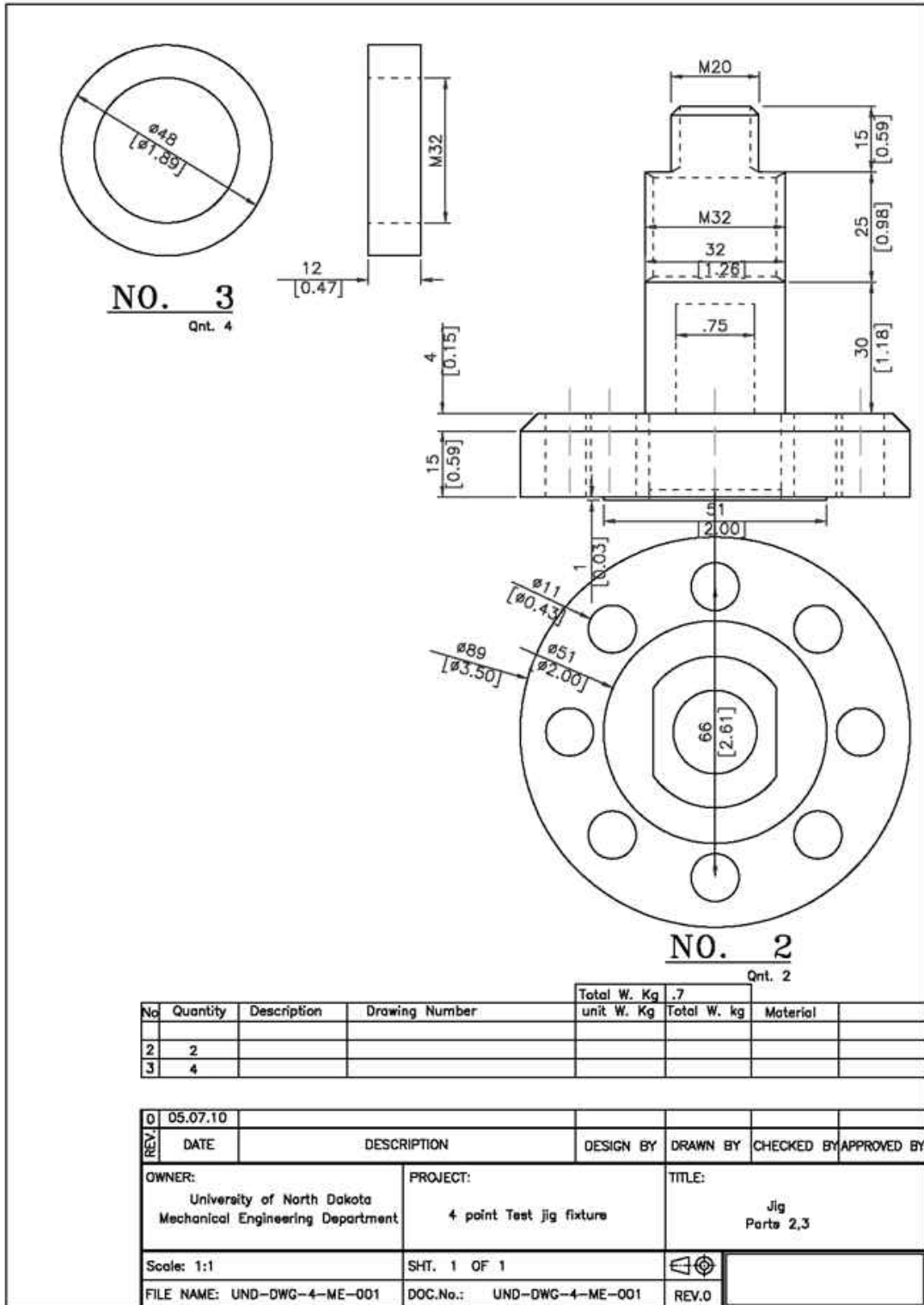
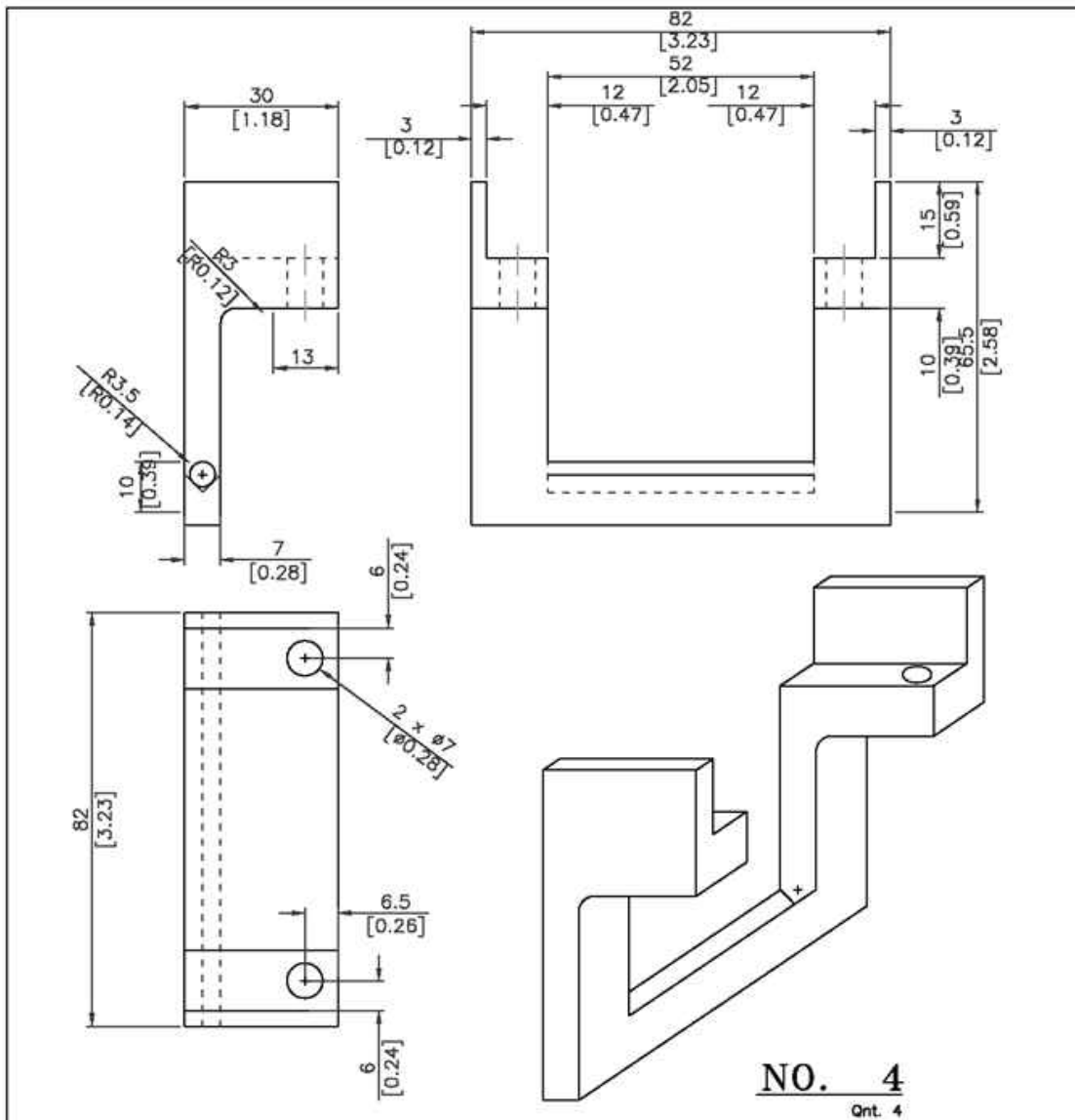


Figure 49. Fatigue fixture, drawing of parts 2 and 3.



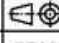
No	Quantity	Description	Drawing Number	Total W. Kg unit W. Kg	0.150 Total W. kg	Material
4	4					
REV	DATE	DESCRIPTION	DESIGN BY	DRAWN BY	CHECKED BY	APPROVED BY
0	05.07.10					
OWNER: University of North Dakota Mechanical Engineering Department			PROJECT: 4 point Test jig fixture		TITLE: Jig Part 4	
Scale: 1:1			SHT. 1 OF 1			
FILE NAME: UND-DWG-4-ME-002			DOC.No.: UND-DWG-4-ME-002		REV.0	

Figure 50. Fatigue fixture, drawing of part 4.

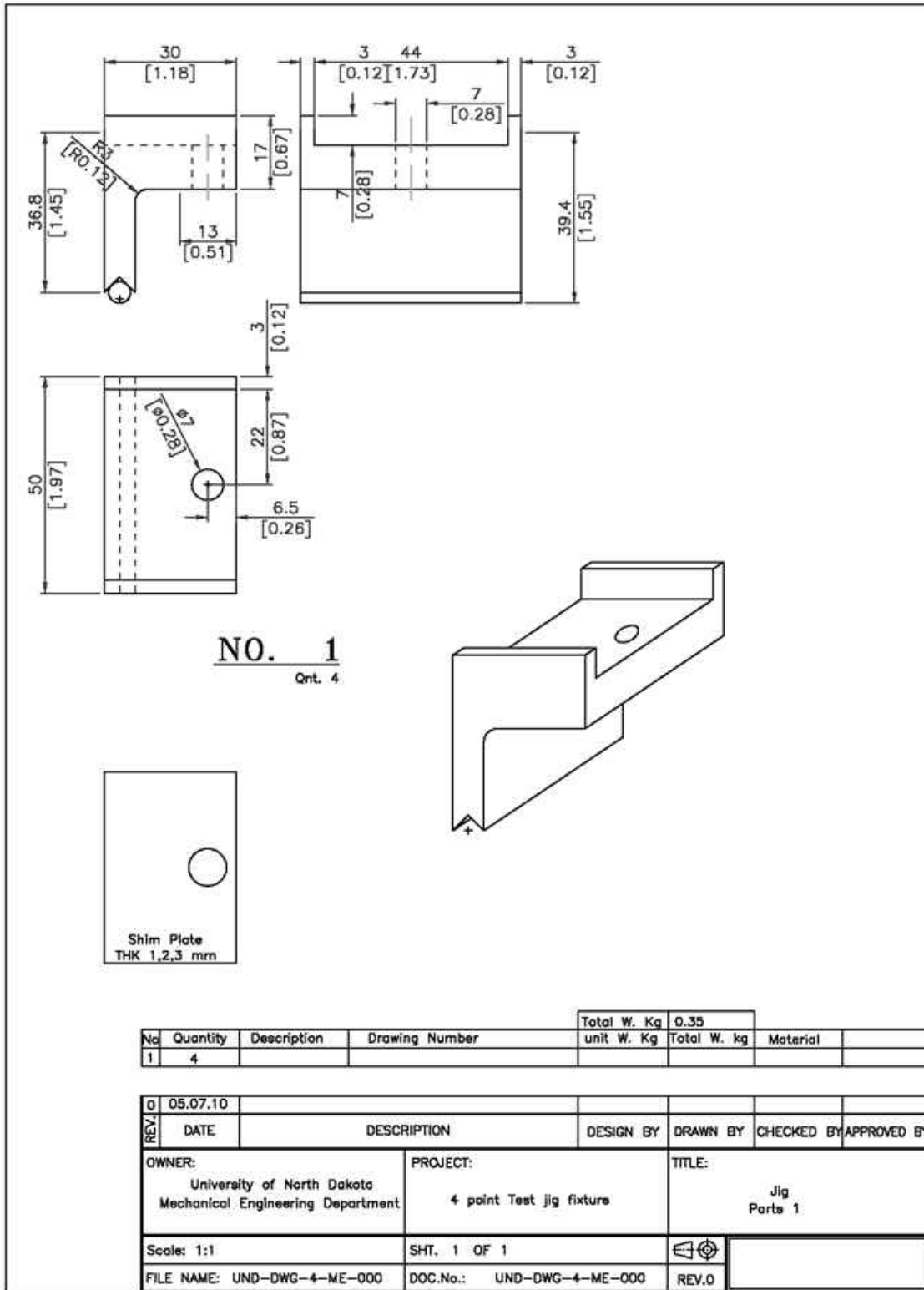


Figure 51. Fatigue fixture, drawing of part 1.

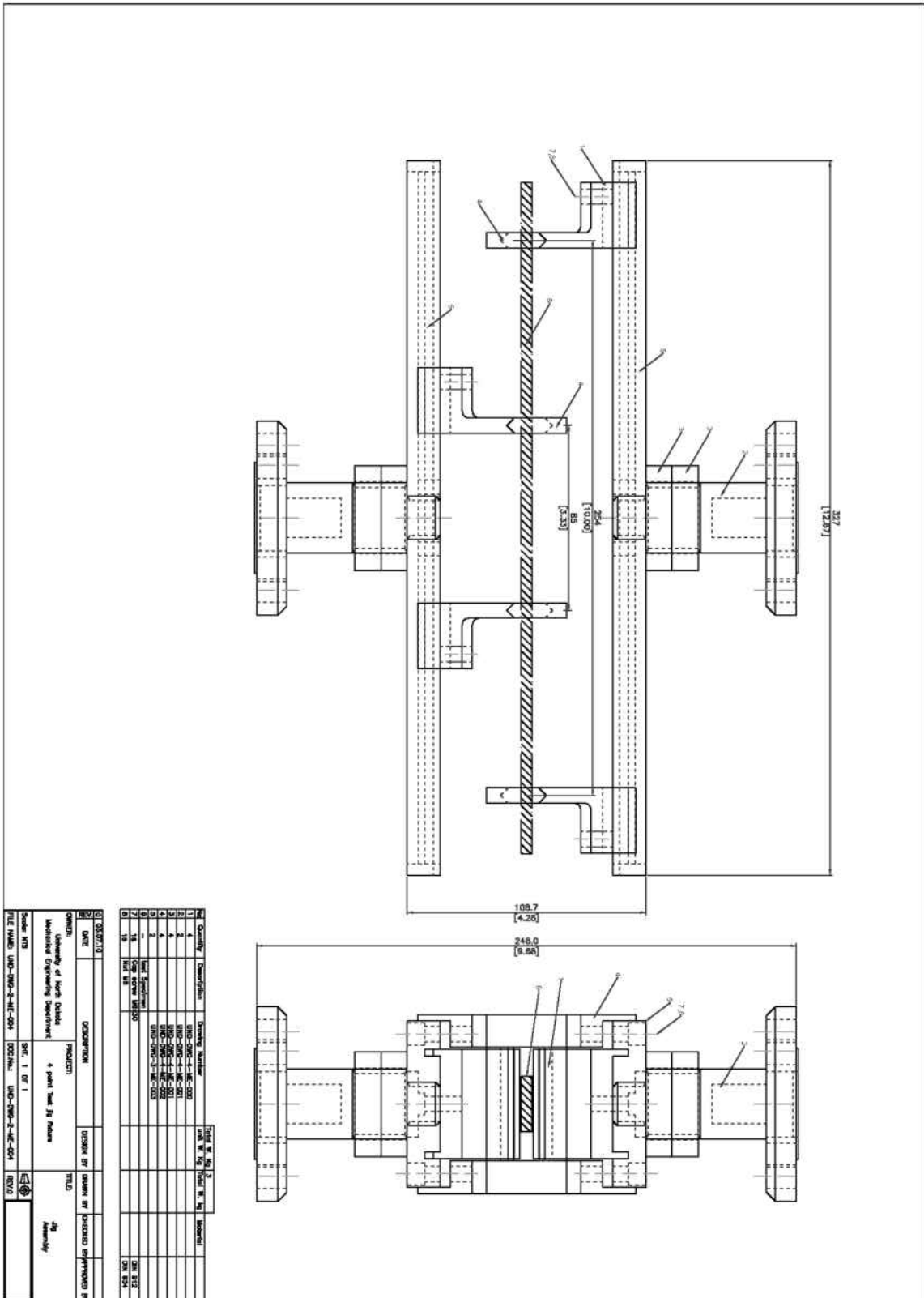


Figure 52. Fatigue fixture, assembly drawing.

REFERENCES

- [1] R. F. Gibson. *Principles of Composite Material Mechanics* 2011.
- [2] R. M. Jones. *Mechanics of Composite Materials* 1999.
- [3] I. M. Daniel and O. Ishai. *Engineering mechanics of composite materials*. New York, USA 1994.
- [4] A. A. Griffith. The phenomena of rupture and flow in solids. *Philosophical Transactions of the Royal Society of London. Series A, Containing Papers of a Mathematical Or Physical Character* 221pp. 163-198. 1921.
- [5] E. T. Thostenson, Z. Ren and T. W. Chou. Advances in the science and technology of carbon nanotubes and their composites: A review. *Composites Sci. Technol.* 61(13), pp. 1899-1912. 2001.
- [6] A. Dry, "The development of the carbon fiber industry," *Evolving Technologies for the Competitive Edge*, pp. 979-988, 1997.
- [7] C. Soutis, "Carbon fiber reinforced plastics in aircraft construction," *Materials Science and Engineering: A*, vol. 412, pp. 171-176, 2005.
- [8] M. Bruderick, D. Denton, M. Shinedling and M. Kiesel, "Carbon fiber composite body structures for the 2003 Dodge Viper," in *Proc. 2nd SPE Automotive Compo. Conf.*, Troy, MI, USA, 2002.
- [9] G. Wolbring, "Oscar Pistorius and the future nature of Olympic, Paralympic and other sports," *SCRIPTed—A Journal of Law, Technology & Society*, vol. 5, pp. 139-160, 2008.
- [10] "The Flex-Foot Cheetah blade," Osurr, vol. 2012, <http://www.ossur.com/?PageID=13462>.
- [11] M. Hojo, K. Nakashima, T. Kusaka, M. Tanaka, T. Adachi, T. Fukuoka and M. Ishibashi, "Mode I fatigue delamination of Zanchor-reinforced CF/epoxy laminates," *Int. J. Fatigue*, vol. 32, pp. 37-45, 2010.
- [12] W. G. Roeseler, B. Sarh and M. Kismarton, "Composite structures—the first 100 years," in *16th International Conference on Composite Materials*, Kyoto, 2007.

- [13] B. Glover, "History of development of commercial aircraft and 7E7 dreamliner," *Aviat Eng*, vol. 592, pp. 16-21, 2004.
- [14] W. B. Hwang and K. S. Han, "Fatigue of composite materials-damage model and life prediction," *American Society for Testing and Materials STP*, vol. 1012, pp. 87-102, 1989.
- [15] M. Beheshty and B. Harris, "A constant-life model of fatigue behaviour for carbon-fibre composites: the effect of impact damage," *Composites Sci. Technol.*, vol. 58, pp. 9-18, 1998.
- [16] W. Yao and N. Himmel, "A new cumulative fatigue damage model for fibre-reinforced plastics," *Composites Sci. Technol.*, vol. 60, pp. 59-64, 2000.
- [17] M. Quaresimin, L. Susmel and R. Talreja, "Fatigue behaviour and life assessment of composite laminates under multiaxial loadings," *Int. J. Fatigue*, vol. 32, pp. 2-16, 2010.
- [18] S. U. Khan, A. Munir, R. Hussain and J. K. Kim, "Fatigue damage behaviors of carbon fiber-reinforced epoxy composites containing nanoclay," *Composites Sci. Technol.*, vol. 70, pp. 2077-2085, 2010.
- [19] B. Harris, N. Gathercole, J. Lee, H. Reiter and T. Adam, "Life-prediction for constant-stress fatigue in carbon-fibre composites," *Philosophical Transactions of the Royal Society of London. Series A: Mathematical, Physical and Engineering Sciences*, vol. 355, pp. 1259-1294, 1997.
- [20] J. Lee, D. Almond and B. Harris, "The use of neural networks for the prediction of fatigue lives of composite materials," *Composites Part A: Applied Science and Manufacturing*, vol. 30, pp. 1159-1169, 1999.
- [21] T. Adam, N. Gathercole, H. Reiter and B. Harris, "Life prediction for fatigue of T800/5245 carbon-fibre composites: II. Variable-amplitude loading," *Int. J. Fatigue*, vol. 16, pp. 533-547, 1994.
- [22] N. Gathercole, H. Reiter, T. Adam and B. Harris, "Life prediction for fatigue of T800/5245 carbon-fibre composites: I. Constant-amplitude loading," *Int. J. Fatigue*, vol. 16, pp. 523-532, 1994.
- [23] J. R. Schaff and B. D. Davidson, "Life prediction methodology for composite structures. Part I—Constant amplitude and two-stress level fatigue," *J. Composite Mater.*, vol. 31, pp. 128-157, 1997.
- [24] Y. Al-Assaf and H. El Kadi, "Fatigue life prediction of unidirectional glass fiber/epoxy composite laminae using neural networks," *Composite Structures*, vol. 53, pp. 65-71, 2001.

- [25] B. Harris, *Fatigue in Composites: Science and Technology of the Fatigue Response of Fibre-Reinforced Plastics*. Woodhead Publishing, 2003.
- [26] A. S. Chen and F. L. Matthews, "Static and cyclic biaxial bending of CFRP panels," *Composites Science and Technology*, vol. 52, pp. 267-273, 1994.
- [27] G. Belingardi, M. Cavatorta and C. Frasca, "Bending fatigue behavior of glass-carbon/epoxy hybrid composites," *Composites Sci. Technol.*, vol. 66, pp. 222-232, 2006.
- [28] M. Amiri and M. Khonsari, "Rapid determination of fatigue failure based on temperature evolution: Fully reversed bending load," *Int. J. Fatigue*, vol. 32, pp. 382-389, 2010.
- [29] T. Smith and M. Owen, "The progressive nature of fatigue damage in glass reinforced plastics," *J. Composite Materials*, vol. 9, pp. 380-390, 1968.
- [30] R. A. A. Couillard and P. Schwartz, "Bending fatigue of carbon-fiber-reinforced epoxy composite strands," *Composites Sci. Technol.*, vol. 57, pp. 229-235, 1997.
- [31] J. F. Shackelford, *Introduction to Materials Science for Engineers*. {Prentice Hall}, 2004.
- [32] S. Timoshenko and G. H. MacCullough. *Elements of Strength of Materials* 1935.
- [33] M. Owen and R. Howe, "The accumulation of damage in a glass-reinforced plastic under tensile and fatigue loading," *J. Phys. D*, vol. 5, pp. 1637, 1972.
- [34] A. Chen and B. Harris, "Fatigue-induced damage mechanisms in carbon fibre-reinforced plastic composites," *J. Mater. Sci.*, vol. 28, pp. 2013-2027, 1993.
- [35] A. Poursartip, M. Ashby and P. Beaumont, "The fatigue damage mechanics of a carbon fibre composite laminate: I--development of the model," *Composites Sci. Technol.*, vol. 25, pp. 193-218, 1986.
- [36] A. Poursartip and P. Beaumont, "The fatigue damage mechanics of a carbon fibre composite laminate: II—life prediction," *Composites Sci. Technol.*, vol. 25, pp. 283-299, 1986.
- [37] T. O'brien, "Characterization of delamination onset and growth in a composite laminate," *Damage in Composite Materials, ASTM STP*, vol. 775, pp. 140-167, 1982.
- [38] A. Sedrakian, T. Ben Zineb, J. Billoet, N. Sicot and P. Lardeur, "A numerical model of fatigue behaviour for composite plates: Application to a three point

- bending test," in *International Conference on Fatigue of Composites. Proceedings*, 1997, .
- [39] G. Caprino and A. D'Amore, "Flexural fatigue behaviour of random continuous-fibre-reinforced thermoplastic composites," *Composites Sci. Technol.*, vol. 58, pp. 957-965, 1998.
- [40] A. Chemami, K. Bey, J. Gilgert and Z. Azari, "Behaviour of composite sandwich foam-laminated glass/epoxy under solicitation static and fatigue," *Composites Part B: Engineering*, 2011.
- [41] K. Nip, L. Gardner, C. Davies and A. Elghazouli, "Extremely low cycle fatigue tests on structural carbon steel and stainless steel," *Journal of Constructional Steel Research*, vol. 66, pp. 96-110, 2010.
- [42] A. Brunner, S. Stelzer, G. Pinter and G. Terrasi, "Mode II fatigue delamination resistance of advanced fiber-reinforced polymer–matrix laminates: Towards the development of a standardized test procedure," *Int. J. Fatigue*, 2012.
- [43] B. Sun, R. Liu and B. Gu, "Numerical simulation of three-point bending fatigue of four-step 3-D braided rectangular composite under different stress levels from unit-cell approach," *Computational Materials Science*, vol. 65, pp. 239-246, 2012.
- [44] O. Coskun and H. S. Turkmen, "Bending Fatigue Behaviour of Laminated Sandwich Beams," *Advanced Materials Research*, vol. 445, pp. 548-553, 2012.
- [45] A. Abbadi, Z. Azari, S. Belouettar, J. Gilgert and P. Freres, "Modelling the fatigue behaviour of composites honeycomb materials (aluminium/aramide fibre core) using four-point bending tests," *Int. J. Fatigue*, vol. 32, pp. 1739-1747, 2010.
- [46] P. Theocaris, S. Paipetis and S. Paolinelis, "Three-point bending at large deflections," *Journal of Testing and Evaluation*, vol. 5, pp. 427-436, 1977.
- [47] I. De Baere, W. Van Paepegem and J. Degrieck, "Comparison of different setups for fatigue testing of thin composite laminates in bending," *Int. J. Fatigue*, vol. 31, pp. 1095-1101, 2009.
- [48] S. Joseph and M. Charles. *Standard Handbook of Machine Design* 2004.
- [49] I. De Baere, W. Van Paepegem and J. Degrieck, "On the feasibility of a three-point bending setup for the validation of (fatigue) damage models for thin composite laminates," *Polymer Composites*, vol. 29, pp. 1067-1076, 2008.
- [50] W. C. Young and R. G. Budynas. *Roark's formulas for stress and strain* 2002.

- [51] W. Van Paepegem, K. De Geyter, P. Vanhooymissen and J. Degrieck, "Effect of friction on the hysteresis loops from three-point bending fatigue tests of fibre-reinforced composites," *Composite Structures*, vol. 72, pp. 212-217, 2006.
- [52] M. Matthewson, C. R. Kurkjian and S. T. Gulati, "Strength measurement of optical fibers by bending," *J. Am Ceram Soc*, vol. 69, pp. 815-821, 1986.
- [53] G. J. Nelson, M. J. Matthewson and B. Lin, "A novel four-point bend test for strength measurement of optical fibers and thin beams. I. Bending analysis," *J. Lightwave Technology*, vol. 14, pp. 555-563, 1996.
- [54] L. Ferry, D. Perreux, D. Varchon and N. Sicot, "Fatigue behaviour of composite bars subjected to bending and torsion," *Composites Sci. Technol.*, vol. 59, pp. 575-582, 1999.
- [55] Y. Tomita, K. Morioka and M. Iwasa, "Bending fatigue of long carbon fiber-reinforced epoxy composites," *Materials Science and Engineering: A*, vol. 319, pp. 679-682, 2001.
- [56] M. Kawai and N. Maki, "Fatigue strengths of cross-ply CFRP laminates at room and high temperatures and its phenomenological modeling," *Int. J. Fatigue*, vol. 28, pp. 1297-1306, 2006.
- [57] G. Belingardi and M. Cavatorta, "Bending fatigue stiffness and strength degradation in carbon-glass/epoxy hybrid laminates: Cross-ply vs. angle-ply specimens," *Int. J. Fatigue*, vol. 28, pp. 815-825, 2006.
- [58] N. AMSC and A. A. CMPS. *Composite Materials Handbook 2002*.
- [59] N. Correia, F. Robitaille, A. Long, C. Rudd, P. Šimáček and S. G. Advani, "Use of resin transfer molding simulation to predict flow, saturation, and compaction in the VARTM process," *J. Fluids Engineering*, vol. 126, pp. 210, 2004.
- [60] M. Kang, W. Lee and H. Hahn, "Analysis of vacuum bag resin transfer molding process," *Composites Part A: Applied Science and Manufacturing*, vol. 32, pp. 1553-1560, 2001.
- [61] T. S. Lundström and B. R. Gebart, "Influence from process parameters on void formation in resin transfer molding," *Polymer Composites*, vol. 15, pp. 25-33, 1994.
- [62] A. T. Standard, "D6272-02," *Standard Test Method for Flexural Properties of Unreinforced and Reinforced Plastics and Electrical Insulating Materials by Four-Point Bending*, ASTM International, West Conshohocken, PA, 2002.

- [63] F. Abdalla, M. Megat and M. Sapuan, "Determination of volume fraction values of filament wound glass and carbon fiber-reinforced composites," *APRN J. Engineering and Applied Science*, vol. 3, pp. 7-11, 2008.
- [64] M. W. Hyer and S. R. White, *Stress Analysis of Fiber-Reinforced Composite Materials*. WCB McGraw-Hill, 1998.
- [65] D. Hull, M. Legg and B. Spencer, "Failure of glass/polyester filament wound pipe," *Composites*, vol. 9, pp. 17-24, 1978.
- [66] International Standard, "ISO 14127:2008, carbon-fibre-reinforced composites. determination of the resin, fibre and void contents," in *International Standard ISO BSI*, 2008.
- [67] ASTM Designation, "D2584-68 standard test method for ignition loss of cured Reinforced Resins'," in *Annual Book of ASTM Standards*, Vol. 8.01 ed. Anonymous Philadelphia, PA: American Society for Testing and Materials, 1985, pp. pp. 328–329.
- [68] B. S. Ye, A. L. Svenson and L. C. Bank, "Mass and volume fraction properties of pultruded glass fibre-reinforced composites," *Composites*, vol. 26, pp. 725-731, 1995.
- [69] E. J. Barbero, *Introduction to Composite Materials Design*. CRC, 2010.
- [70] U. Khashaba and M. Seif, "Effect of different loading conditions on the mechanical behavior of $[0/\pm 45/90]_s$ woven composites," *Composite Structures*, vol. 74, pp. 440-448, 2006.
- [71] L. Lagunegrand, T. Lorriot, R. Harry and H. Wargnier, "Design of an improved four point bending test on a sandwich beam for free edge delamination studies," *Composites Part B: Engineering*, vol. 37, pp. 127-136, 2006.
- [72] P. Qiao, L. Zhang, F. Chen, Y. Chen and L. Shan, "Fracture characterization of Carbon fiber-reinforced polymer-concrete bonded interfaces under four-point bending," *Eng. Fract. Mech.*, vol. 78, pp. 1247-1263, 2011.
- [73] P. Feraboli and K. Kedward, "Four-point bend interlaminar shear testing of uni- and multi-directional carbon/epoxy composite systems," *Composites Part A: Applied Science and Manufacturing*, vol. 34, pp. 1265-1271, 2003.
- [74] H. R. Sobuz, E. Ahmed, N. M. Sutan, N. M. Sadiqul Hasan, M. Alhaz Uddin, M. Jahir Uddin, "Bending and time-dependent responses of RC beams strengthened with bonded carbon fiber composite laminates," *Construction Building Material.*, vol. 29, pp. 597-611, 2012.

- [75] M. R. Kharrazi and S. Sarkani, "Frequency-dependent fatigue damage accumulation in fiber-reinforced plastics," *J. Composite Mater.*, vol. 35, pp. 1924-1953, 2001.
- [76] A. Rotem, "Load frequency effect on the fatigue strength of isotropic laminates," *Composites Sci. Technol.*, vol. 46, pp. 129-138, 1993.
- [77] K. Reifsnider, W. Stinchcomb and T. O'Brien, "Frequency effects on a stiffness-based fatigue failure criterion in flawed composite specimens," *Fatigue of Filamentary Composite Materials, ASTM STP*, vol. 636, pp. 171-184, 1977.
- [78] G. Sims and D. Gladman, "Effect of test conditions on the fatigue strength of a glass±fabric laminate: Part A±frequency," *Plastics and Rubber: Materials and Applications*, vol. 3, pp. 41-48, 1978.
- [79] G. Sims and D. Gladman, "Effect of test conditions on the fatigue strength of a glass±fabric laminate: Part B±specimen condition," *Plastics and Rubber: Materials and Applications*, vol. 122, pp. 128, 1980.
- [80] C. T. Herakovich, R. D. Schroedter, A. Gasser and L. Guitard, "Damage evolution in $[\pm 45]_s$ laminates with fiber rotation," *Composites Sci. Technol.*, vol. 60, pp. 2781-2789, 2000.
- [81] P. Ladevèze. *Sur Une Théorie De L'Endommagement Anisotrope* 1983.
- [82] G. Marom, H. Harel, S. Neumann, K. Friedrich, K. Schulte and H. Wagner, "Fatigue behaviour and rate-dependent properties of aramid fibre/carbon fibre hybrid composites," *Composites*, vol. 20, pp. 537-544, 1989.
- [83] G. Fernando, R. Dickson, T. Adam, H. Reiter and B. Harris, "Fatigue behaviour of hybrid composites," *J. Mater. Sci.*, vol. 23, pp. 3732-3743, 1988.
- [84] R. Dickson, G. Fernando, T. Adam, H. Reiter and B. Harris, "Fatigue behaviour of hybrid composites," *J. Mater. Sci.*, vol. 24, pp. 227-233, 1989.
- [85] N. Himmel and C. Bach, "Cyclic fatigue behavior of carbon fiber reinforced vinylester resin composites manufactured by RTM and VARI," *Int. J. Fatigue*, vol. 28, pp. 1263-1269, 2006.
- [86] W. Van Paepegem and J. Degrieck, "Coupled residual stiffness and strength model for fatigue of fibre-reinforced composite materials," *Composites Science and Technology*, vol. 62, pp. 687-696, 2002.
- [87] Y. Shan and K. Liao, "Environmental fatigue behavior and life prediction of unidirectional glass-carbon/epoxy hybrid composites," *Int. J. Fatigue*, vol. 24, pp. 847-859, 2002.

- [88] W. Van Paepegem and J. Degrieck, "Experimental set-up for and numerical modelling of bending fatigue experiments on plain woven glass/epoxy composites," *Composite Structures*, vol. 51, pp. 1-8, 2001.
- [89] R. C. Hibbeler, "Mechanics Of Materials Author: Russell C. Hibbeler, Publisher: Prentice Hall Pages: 896 Published: 2004-07," 2004.
- [90] F. Baumgart, "Stiffness-An unknown world of mechanical science?" *Injury-International Journal for the Care of the Injured*, vol. 31, pp. 14-23, 2000.
- [91] R. G. Budynas and J. K. Nisbett. *Shigley's Mechanical Engineering Design*. McGraw-Hill, 2008.
- [92] U. Fischer, M. Heinzler, F. Näher, H. Paetzold, R. Gomeringer, R. Kilgus, S. Oesterle and A. Stephan. *Mechanical and Metal Trades Handbook 2010*.